A New Coating Method for Semiconductor Lithography: Fluid Layer Overlap in Extrusion-Spin Coating

by

James Stephen Derksen

Bachelor of Science in Mechanical Engineering
Massachusetts Institute of Technology, 1994

Submitted to the Department of Mechanical Engineering
in partial fulfillment of the requirements for the degree of

Master of Science in Mechanical Engineering

at the

MASSACHUSETTS INSTITUTE OF TECHNOLOGY

June 1997

Author .....
Department of Mechanical Engineering
May 9, 1997

Certified by .....
Jung-Hoon Chun
Edgerton Associate Professor of Mechanical Engineering
Thesis Supervisor

Accepted by .....
Professor Ain A. Sonin
Chairman, Department Committee on Graduate Students

A New Coating Method for Semiconductor Lithography: Fluid Layer Overlap in Extrusion-Spin Coating

by

James Stephen Derksen

Submitted to the Department of Mechanical Engineering
on May 9, 1997, in partial fulfillment of the
requirements for the degree of
Master of Science in Mechanical Engineering

Abstract

Current methods of manufacturing microelectronic chips use microlithography to transfer a pattern from a photographic image of circuit geometry to the surface of a semiconductor wafer. An important step in this process is the deposition of a thin coating of photoresist from which the lithographic mask is made. The photoresist layer is typically 1 μm thick with a thickness variation of less than 25 Å(within 3 σ). In addition, coating defects greater than 0.2 microns must be kept to a minimum. Although the current coating method – spin coating – can achieve these demanding specifications, it wastes over 95% of the photoresist applied. Therefore, the semiconductor industry is looking for ways to reduce the amount of photoresist used. This thesis discusses extrusion-spin coating, a new coating method which has the potential to waste as little as 50% of the photoresist applied. Before extrusion-spin coating can be used effectively, however, solvent evaporation must be reduced and fluid deposition in the wafer center must be improved.

Thesis Supervisor: Jung-Hoon Chun
Title: Edgerton Associate Professor of Mechanical Engineering

Acknowledgments

I would first like to thank Professor Chun for cultivating a positive research environment. His guidance was instrumental in completing this thesis, and his advice has provided many valuable insights into becoming an effective engineer—both technically and in other ways.

I would also like to thank Sangjun Han for his encouragement as we have worked together during the past two years. His patience and humor helped make the long hours in the lab much more enjoyable.

Thanks to Professor Frank Feng, Professor Anthony Patera, Dr. Nannaji Saka, Dr. Andre Sharon, and Professor David Trumper whose valuable assistance helped advance the research more quickly.

Thanks to Kevin Ellwood, Michael Joos, and Charles Szmanda for the helpful references they provided.

Thanks to Marc Hodes, Andy Pfahnl, and Mike Quintana in the Heat Transfer Lab who gave valuable feedback. Gregg Duthaler, Barbara Hamer Ressler, and Stefano Schiaffino in the Fluid Mechanics Lab contributed good ideas as well as help with instrumentation.

Thanks to the many people who helped facilitate construction of the prototype coater. In the machine shop, Fred Cote and Gerry Wentworth helped with the machining of the prototype coater. Fred's patient instruction and careful evaluation of the prototype design were invaluable. Tom Lynch from the Industrial Hygiene Office helped facilitate safety. Donna Wallington was always helpful in getting administrative tasks done quickly.

Thanks to Julie Drennan who proofread the final thesis and gave many helpful suggestions.

Thanks to Tim Booher, Daniel Derksen, and Tony Eng for the hours they put in typing or recording data. Special thanks to Tony and Daniel who made me many meals and gave lots of encouragement as I was working to finish this thesis.

Thanks to our sponsors for their support. Silicon Valley Group provided most of the funding for this research. Special thanks go to Bill Gadson and Bette Mullen for teaching me the practical aspects of spin coating. George Wong and Sophia Sia provided valuable information on the coater module donated by SVG. Jim Azzola, Emir Gürer, Bob Mandel, Rich Savage, and Ed Ward also helped facilitate the research. FAS Technologies provided a photoresist pump and an extrusion die.

Thanks also to the other graduate students working under Professor Chun who have been encouraging and supportive. They are Chen-An Chen, Jeanie Cherng, Sukyoung Chey, Mark Hytros, Dongsik Kim, Ho-Young Kim, Jiun-Yu Lai, Juan-Carlos Rocha, and Pyongwon Yim.

Many others have made my stay at MIT an enjoyable experience and thus have contributed indirectly to this thesis. Thanks to Daniel, Eric, Ien, Tony and Jack for the encouragement each week in our cooking group. Thanks to the many people in UCF whose friendship I will always remember, especially those in my small group—Bridgette, Elliott, Eric, Mike, Tony, and Weslynne. Thanks to Pastor Reid, Alex, Jim, Ed, Elsa, Lisa, Ericka, Sean and so many others at church. Thanks also to those who made Ashdown 5th Floor an enjoyable place—Adam, Agno, Alice, Alok, Bin, Ching-Yi, Chris, Edward, Elliott, Guoling, Ioanid, Min-Ha, Niranjan, Payman, Ramses, Sanjay, Tan, Tony, Victor, and many others. Thanks also to Joe, Steve, Tara, Jeanie, and many others with whom I have worked together in the many classes taken at MIT.

Thanks also to my parents (Stan and Irene) and my brothers (Tim and Daniel) whose unconditional love and support have helped me become the person I am today. I will always cherish the memory of the past several years together with both my brothers. It is to my parents and my brothers that this thesis is dedicated.

Most of all, I would like to thank the Almighty God who created me and sustains me each day. To Him all of the credit is untimately due.

Contents

List of Figures

Nomenclature

a	Characteristic length for spreading models (half-width of fluid bump)
A	Cross-sectional area of a fluid bump
B_s	Mass transfer driving force
G	Gap between extrusion slot and substrate
c	Solids fraction
d	Slot gap width
D	Solvent diffusivity (diffusion coefficient)
e	Fraction of solvent evaporated
g	Mass transfer coefficient
G	Coating gap between extrusion slot lips and substrate
h	Wet coating thickness
K	Temperature dependent diffusivity parameter
l	Fluid bump thickness
L	Extrusion die lip width
m''	Mass of solvent evaporated per unit area
$m_{s,e}$	Mass fraction of solvent in the air away from the surface of a fluid film
$m_{s,s}$	Mass fraction of solvent at the surface of a fluid film
p	Pressure
Q	Photoresist flow rate
r	Radial distance from the center of a disk (wafer)
r'	Actual position of extrusion die after initial position misalignment
Δr_0	Initial extrusion die position misalignment
R	Wafer radius
t	Time
T	Coating time
u	Extrusion head speed along the diameter of the wafer
U	Characteristic velocity

V	Volume of photoresist
ΔV	Excess photoresist
v	Relative tangential velocity between wafer and extrusion head
w	Extrusion width
Δw	Extrusion overlap
w'	Effective extrusion width ($=w - \Delta w$)
x	Horizontal position from the center of a 2-D fluid bump
z	Vertical coordinate

Greek

α	Misalignment angle: extrusion die lips not parallel to substrate
β	Misalignment angle: between spinner axis and substrate axis
γ	Misalignment angle: die motion not perpendicular to spinner rotation
ε	Efficiency
η	Non-dimensional kinematic viscosity
θ	Dynamic contact angle between photoresist and moving substrate
κ	Fluid curvature
μ	Dynamic viscosity
ν	Kinematic viscosity
ρ	Density
σ	Standard deviation, surface tension
Ω	Wafer rotation speed

Superscripts and Subscripts

$*$	Critical
$^-$	Average
avg	Average
as	Air-solvent
c	Critical
$center$	Center part of spiral
dry	Dry state of resist
$excess$	Excess time required to coat the wafer center
f	Final
l	Liquid (solvent)
max	Maximum
min	Minimum
mod	Modified spiral
o	Initial
r	At radius r
$r - w$	At radius $r - w$
s	Solid
ϕ	Gap error caused by angle ϕ

Dimensionless Numbers

Bo	Bond number
Ca	Capillary number
Ca*	Critical Capillary number
Nu	Nusselt number
Pr	Prandtl number
Re	Reynolds number
Sc	Schmidt number
Sh	Sherwood number
We	Weber number

Chapter 1

Introduction

The use of electronic equipment has expanded tremendously in the past several decades. The invention of the transistor has led to an intense competition among device manufacturers to make the smallest, fastest, cheapest microelectronic chips. The rate of this technological advancement is often limited by particular manufacturing processes. One such process is microlithography, the method used to transfer a chip design onto a semiconductor substrate.

1.1 Microlithography

Microlithography is the process used to construct three-dimensional microelectronic devices using a sequence of planar processes[34]. Each planar process adds one layer to the microelectronic circuit geometry. Twenty or more layers are needed to complete complex circuit geometries. Figure 1-1[37] shows the steps required to complete each layer. First, a thin layer of photoresist, on the order of one micron thick, is applied to a semiconductor substrate. Second, the photoresist is irradiated through a mask which contains the pattern to be reproduced on the substrate. The source of irradiation can be photons (photolithography), electrons (e-beam lithography), or x-rays (x-ray lithography)[34]. Third, the photoresist film is developed, removing photoresist which is not a part of the pattern transferred through the mask. For negative photoresists, the unexposed region is removed, while for positive photoresists the exposed region is removed. Fourth, the photoresist is baked to harden it onto the substrate. Fifth, one specific process (etching, deposition, oxidation, doping, etc.) is used to add to

or remove material from the exposed parts of the substrate. Sixth, the photoresist is stripped from the substrate in preparation for the next layer.

1.2 Coating Requirements

Producing a defect-free, uniform photoresist film is critical to the microlithography process because the film affects the quality of every layer of the microelectronic device. Other constraints on the application of photoresist film include coating time requirements and efficiency requirements.

1.2.1 Coating Materials

Much research has been focused on the discovery and characterization of the photoresists needed to construct microelectronic devices. New coating methods must be able to use currently-available photoresists as well as have the flexibility to be used with new developments.

Photoresist Properties

Photoresist (often called resist) is usually composed of three elements: a polymer base; photosensitizer; and solvent [37, 44]. The composition is roughly 15-30% base, 1-5% photosensitizer, and 65-85% solvent by mass[1]. The solvent serves as a carrier for the rest of the photoresist and evaporates almost entirely during the coating process. The polymer base material (also called resin) provides the mechanical properties of the final film. The photosensitizer (a photoactive compound) is activated in response to a particular wavelength of light, making the photoresist sensitive or resistant to a developer solution (for a positive or negative photoresist respectively).

The properties of photoresist which are important for modeling the coating process are viscosity, density, surface tension, mass fraction of solids, and solvent diffusivity. Some of these properties for several typical photoresists are shown in Table 1.1, along with the properties of water for comparison. These physical properties of photoresist change dramatically during the coating process. In the liquid state the solvent properties are dominant, while in the final film, the base polymer properties are dominant.

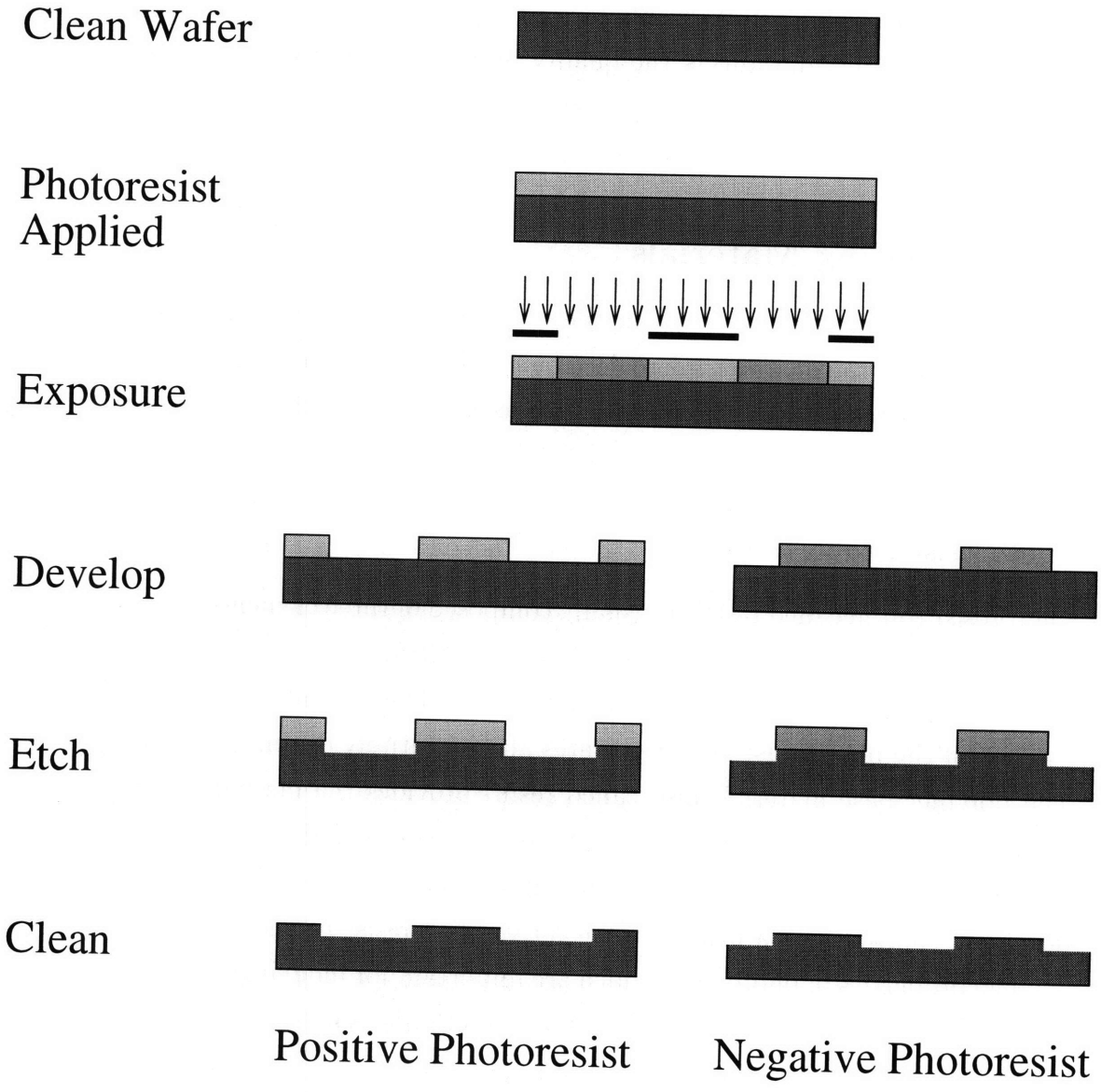

Figure 1-1: Microlithography.

Photoresist	Viscosity	Solids Fraction	Density	Surface Tension
	(mPa-sec)		(g/cm^3)	(dyne/cm)
Shipley SPR2	19-46	22-29	1.06	
Shipley SPR500-A	0.53-5.1	16-32	1.05	
Shipley 510A	26.5	23	1.06	22
Shipley XP-90236	5.2-15.6	18-22	1.04	
AZ 1512	19.4	26	1.04	32
AZ 1518	36.1	30	1.06	32
AZ DX 1200 P	11	20	1.00	30
Water (at 70°F)	1.0	0	1.00	74

Table 1.1: Typical photoresist properties.

Viscosity Meyerhofer[33] modeled photoresist viscosity, ν, for Newtonian fluids as a function of solid (base + photosensitizer) concentration. Sukanek[42] later used a non-dimensional form:

$$\eta = \frac{\nu}{\nu_0} = \frac{\nu_l}{\nu_0} + \left(1 - \frac{\nu_l}{\nu_0}\right)\left(\frac{c}{c_0}\right)^n \tag{1.1}$$

where η is non-dimensional viscosity, ν_0 is the initial viscosity, ν_l is the liquid (solvent) viscosity, c is the mass fraction of solids, c_0 is the initial mass fraction of solids, and n is a constant. Sukanek found that the ratio ν_l/ν_0 did not significantly change his calculations. He used ν_l/ν_0=0.01 and n=4. Flack et al. modeled photoresist viscosity for non-Newtonian fluids[22].

Diffusivity Flack[22] modeled solvent diffusivity as a function of solids concentration as:

$$D = D_0 \exp\left(\frac{c}{K_1 + K_2 c}\right) \tag{1.2}$$

where D_0 is the initial diffusivity and K_1 and K_2 are temperature-dependent parameters. Bornside[10, 11] and others have modeled diffusion using finite element formulations.

Density The density of the polymer mixture can be modeled as:

$$\rho = \rho_l(1 - c) + \rho_s c \tag{1.3}$$

where ρ_l is the liquid density and ρ_s is the solid density.

Surface Tension Surface tension is much more difficult than the other properties to model. In this thesis, surface tension will only be used for theoretical calculations involving liquid photoresist. Therefore, it is assumed that surface tension remains constant even when a small amount of solvent evaporates from the photoresist.

Coating Substrates

Thin photoresist films must be applied to a variety of materials and topographies during semiconductor processing. The base substrate is normally a flat, polished silicon or GaAs wafer. These wafers are typically 10-20 cm in diameter and approximately 1 mm in thickness. Wafers 30 cm in diameter are now being used in research facilities. Materials typically applied to the surface of a semiconductor wafer include semiconductor materials, metal films, and insulators [44]. As semiconductor devices are layered on the wafer, the surface properties and surface topography of the wafer are modified by thin film deposition, oxidation, and diffusion[37]. Consequently, the photoresist coating process must produce a consistent film for a range of surface properties and topographies. Sometimes, when the underlying topography is very rough, an extra coating must be applied or chemical-mechanical polishing must be used to planarize the surface before subsequent lithographic steps[41].

Before coating, the surface must be cleaned thoroughly to remove defect-causing particles and films. Next, the wafer is baked to remove moisture, and the wafer surface is primed with a chemical vapor to promote adhesion of the photoresist. Finally the wafer is cooled to the desired temperature immediately before coating[37].

1.2.2 Film Thickness

The photoresist film thickness required depends on the desired defect protection, step coverage, and resolution[44]. Thicker films provide better adhesion, greater protection for reactive ion erosion, and improved defect protection. However, thicker films also result in lower resolution because they take longer to expose and develop. Photoresist film thicknesses used in current semiconductor manufacturing are typically 0.5–4 μm thick[37].

1.2.3 Film Thickness Uniformity

Excellent photoresist film thickness uniformity is required to maintain good transfer of the mask pattern to the photoresist. Uniformity is important to maintain a constant exposure level across the surface of the wafer. Nonuniformities cause position overlay errors when optical steppers attempt to sense alignment marks beneath the photoresist film[37]. Nonuniformities also change the reflectivity of a photoresist deposited over an oxide.

Uniformity measurements can be classified into two categories: film thickness variation across a single wafer and mean film thickness variation among wafers in a production run. Usually good wafer-to-wafer uniformity is more difficult to achieve than good uniformity on a single wafer.

The small critical dimensions of microelectronic devices require photoresist coating thickness to be uniform to within 25 Å (3 σ). As the critical dimension decreases further, even better uniformities will be required.

1.2.4 Defect Limits

Defects in photoresist films must be eliminated since they can lead to failure of microelectronic devices. These defects develop in several ways. Wafers can be contaminated with particles or surface films when a wafer is not properly cleaned before coating. Airborne particles can contaminate photoresist films—especially before they are dried. Photoresist composition can change due to freezing, high temperatures, or aging. Thin photoresist films may lead to high pinhole density and increased problems with small particles in the photoresist[18].

Even a small number of defects in each layer of a complex microelectronic circuit can lead to a large number of defective chips when the defects of all layers are con-

sidered. In 1986 a typical chip had an area of 0.25 cm^2 and a defect density of 5 defects/cm^2 per layer. These defects led to a yield of only 30% good chips[37]. During more complex manufacturing procedures, the number of process steps increases, and the number of defects must be even lower to maintain the same chip yield. Any decrease in chip yield for a new coating process would cost far more than the savings from a reduction in photoresist usage. Therefore, new coating methods must at least maintain the defect levels of spin coating.

1.2.5 Coating Time Limits

The cycle time for coating a wafer must be short enough to meet the production rate requirements. Cycle time includes loading a wafer into the coating module, applying photoresist to the wafer, spinning the wafer, and removing the wafer from the coating module. Typical coating times for spin coating range from 30 to 45 seconds.

1.2.6 Photoresist Use Efficiency

Photoresist use efficiency is defined as the fraction of photoresist solids applied to a wafer which remain on the wafer after the coating process is complete:

$$\varepsilon = \frac{V_{dry}}{V_0\ c} \tag{1.4}$$

where V_{dry} is the volume of dry photoresist on a wafer after coating, V_0 is the initial (wet) photoresist volume applied to a wafer, and c is the solids concentration in V_0. The amount of photoresist that must be used at 100% efficiency is:

$$V_{min} = \frac{V_{dry}}{c} = \frac{\pi R^2 h_{dry}}{c} \tag{1.5}$$

where R is the radius of the wafer and h_{dry} is the desired final dry coating thickness. The minimum average wet coating thickness (before the solvent is evaporated) is:

$$h_{min} = \frac{V_{min}}{\pi R^2} = \frac{h_{dry}}{c} \tag{1.6}$$

For a typical photoresist with 23% solids, only 0.14 mL is needed to coat a 20-cm wafer to a final dry thickness of 1 μm. Such a coating requires a 4.34-μm wet coating thickness. Any excess resist is wasted. Figure 1-2 shows the progressive increase in photoresist coating efficiency assuming 25% solids fraction[37, 36].

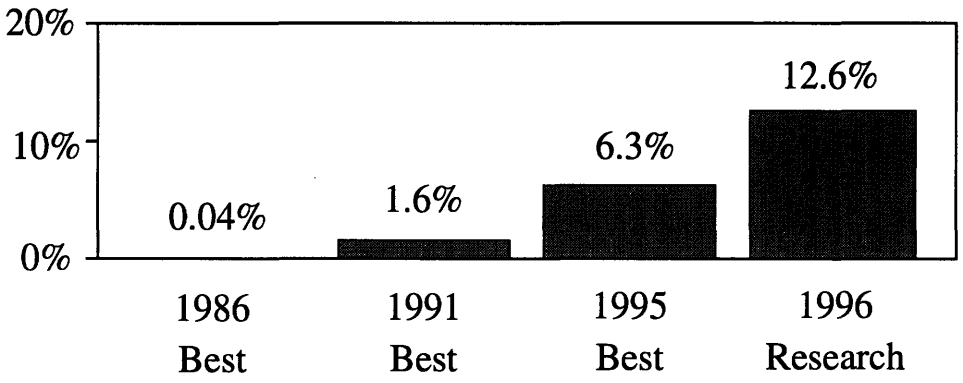

Figure 1-2: Photoresist use efficiency history.

1.3 A New Coating Method

Many methods which have been proposed for coating wafers include dip coating, meniscus coating, spray coating, patch coating, bubble coating, chemical vapor deposition, and spin coating. Only a few of these methods produce films with the thicknesses and uniformities required for semiconductor production. Of these, only spin coating has a production rate fast enough to meet the demands of chip manufacturers. One major shortcoming of spin coating, however, is that it wastes over 90% of the photoresist applied to the wafer surface. About one million gallons of photoresist are consumed each year at a cost of $400 million. This represents approximately 3% of the material costs of the lithography process[36]. As the critical dimension of semiconductor devices becomes smaller, new deep UV photoresists will be used. These new photoresists can cost five or more times the cost of the i-line photoresists used currently. Therefore, a new coating method is needed which wastes less photoresist while producing uniform, defect-free coatings at a rate comparable to that of spin coating.

The objective of this thesis is to develop a new coating method which meets the following criteria:

- uses existing photoresists
- produces photoresist films approximately 1 μm thick
- produces thickness uniformities equal to or better than those attained by spin coating
- produces the same number or fewer defects than those produced by spin coating
- produces a complete coating in less than one minute
- has a photoresist use efficiency between 25 and 50% or greater

1.4 Overview of Thesis

The remainder of this thesis describes a new method for coating wafers more efficiently than traditional spin coating. In Chapter 2, an inefficiency in spin coating is identified, and an approach to eliminating this inefficiency is proposed. Chapter 3 describes the extrusion slot coating process, a partial solution to spin-coating inefficiencies. In Chapter 4, spin coating and extrusion coating are combined to obtain extrusion-spin coating, an efficient coating method which is described in detail. Chapter 5 investigates in detail the effects of extrusion ring overlap, one potential problem with extrusion-spin coating. Chapter 6 describes the design of an extrusion-spin coater prototype. In Chapter 7, the results of extrusion-spin coating experiments are presented, and the strengths and weaknesses of extrusion-spin coating are discussed. In Chapter 8, conclusions about the extrusion-spin coating process are made, and future developments are described.

Chapter 2

More Efficient Spin Coating

A number of coating methods were examined in the search for a coating process to replace spin coating. Although a few of these methods could meet one or more of the coating requirements, none could meet all of them. Consequently, spin coating was examined to determine if any modifications could improve its efficiency.

2.1 Spin Coating Description

Spin coating uses centrifugal force to spread photoresist over the surface of a semiconductor wafer and produce a thin film of photoresist. The process has three phases: photoresist is dispensed onto a wafer, the photoresist is spread across the wafer, and the wafer is spun at a high angular speed to decrease the thickness of the photoresist to the final film thickness and uniformity.

2.1.1 Dispensing Photoresist onto Wafer Surface

During the first phase, a small volume of photoresist is dispensed onto the wafer surface. The amount of photoresist dispensed does not affect the final film thickness as long as there is sufficient photoresist[16]. In practice, the minimum volume which results in consistent uniformity is used[18]. Figure 2-1 shows the three primary ways photoresist is dispensed. For the first method, called static dispense, the photoresist is dispensed directly into the center of a stationary wafer, producing a circular pool of photoresist, or the entire surface of the wafer is flooded with photoresist[44]. Often the wafer is rotated slowly after a static dispense to begin spreading the photoresist over the wafer surface. The second and third methods are called dynamic dispenses

because the wafer is rotating slowly while the photoresist is dispensed. During forward radial dispense, the dispense nozzle is initially located at the center of the wafer and moves radially outward as the photoresist is deposited. For reverse radial dispense, the dispense nozzle begins at the edge of the wafer and moves radially inward. Both forward and reverse radial dispenses produce a spiral pattern of photoresist. The geometry of the spiral (number of turns and volume of photoresist per unit length along the spiral) is determined by the angular rotation of the wafer, the radial velocity of the nozzle with respect to the wafer, and the volumetric flow rate of the photoresist during the dispense. Dynamic dispenses use less photoresist[37], but static dispenses produce a more uniform film[44, 16].

2.1.2 Establishing Initial Coating Layer

In the second phase of spin coating the wafer is accelerated to create a centrifugal force which spreads the photoresist toward the edge of the wafer. Sometimes the wafer is spun at an intermediate speed for a few seconds before being accelerated to the final high-speed spin. For both fast and slow spin speeds the interface between the photoresist and the wafer surface is unstable. Daughton and Givens[16] used high-speed photography to capture rotating "arms" of photoresist which flow quickly off the wafer when the wafer is accelerated rapidly. These arms of photoresist have narrow areas of uncoated wafer between them which are covered as the arms advance. When the wafer is accelerated slowly, the photoresist tends to flow outward along narrow paths called *rivulets* as shown in Figure 2-2. These rivulets are much narrower than the arms described by Daughton and Givens. Fraysse and Homsey[23] found that rivulet formation for a spinning drop begins after a critical radius is reached. The critical radius, as well as the number of rivulets formed, are highly dependent on the surface tension and contact angle. The photoresist front between the rivulets advances at a slower rate than the rivulets until the entire surface of the wafer is covered. High-speed photography shows that it takes only a few tenths of a second to spread the photoresist over the entire wafer surface [16]. When the bulk of the photoresist reaches the edge of the wafer, most of it is flung off in many tiny droplets [10].

Flack et al.[22], Daughton and Givens[16], and Sukanek[42] shows that higher acceleration rates do no affect the final film thickness. Flack, however, shows that higher acceleration rates do tend to produce more uniform films.

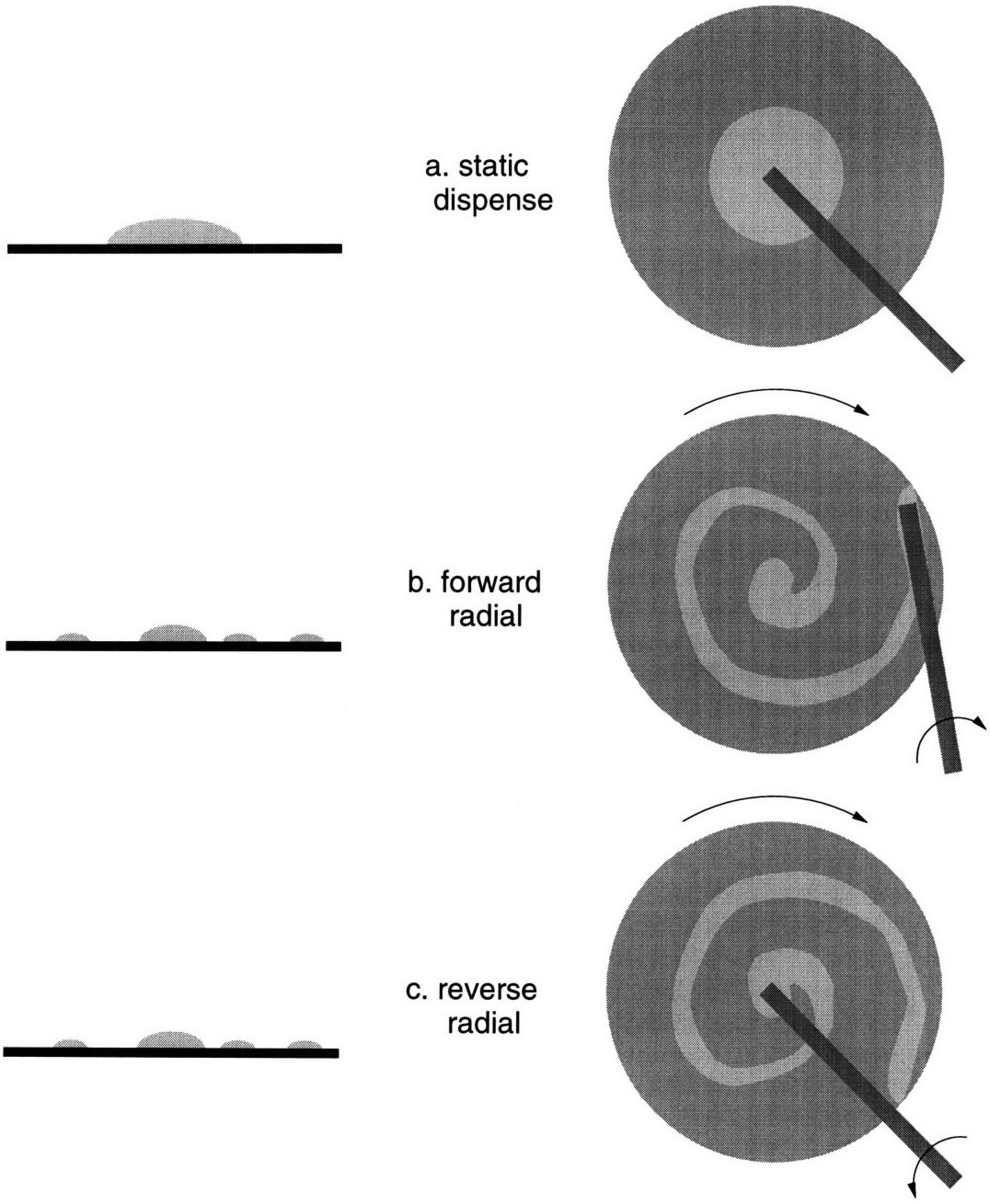

Figure 2-1: Methods of photoresist dispense. (a) Static dispense, (b) Forward radial dispense, (c) Reverse radial dispense.

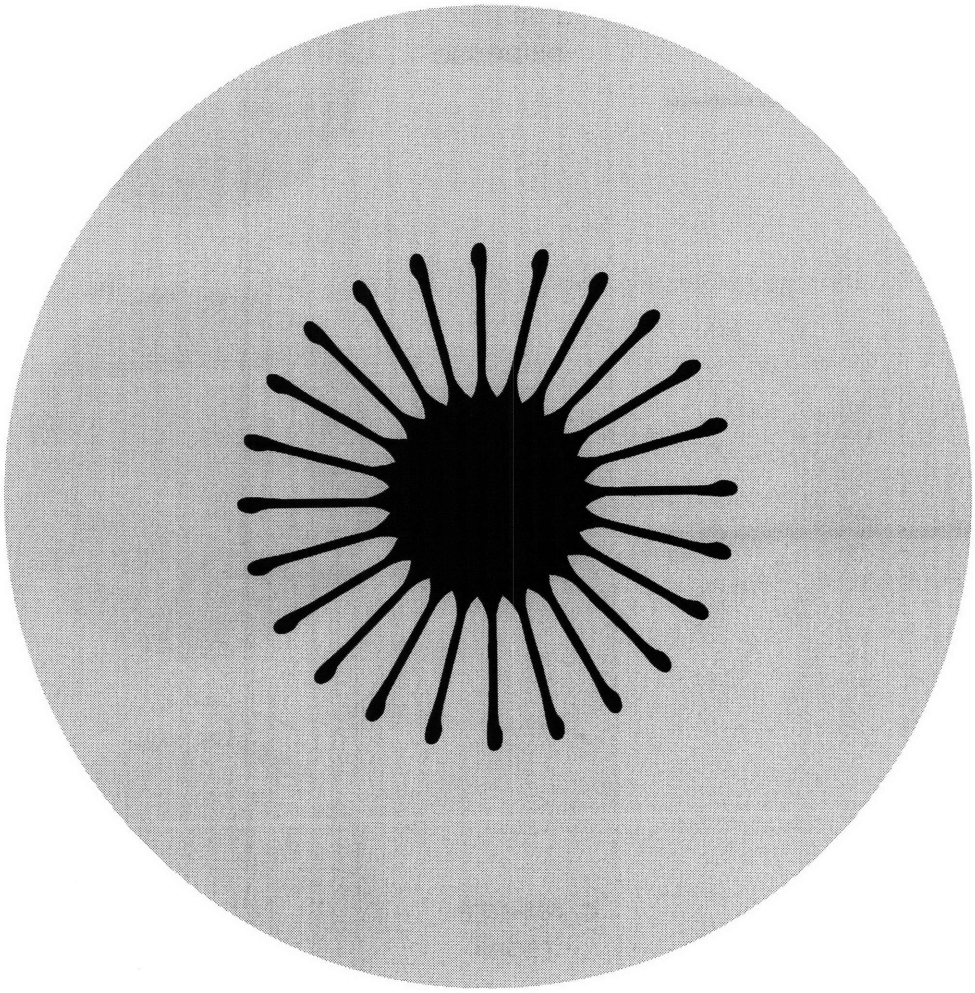

Figure 2-2: Rivulet formation in spinning fluid.

2.1.3 Thinning of Photoresist Layer

In the third phase of spin coating the wafer continues to spin at the final high speed. During this phase there are two mechanisms by which the photoresist film thins to its final thickness. At first the photoresist continues to flow outward and off the wafer in concentric "waves" which can be observed using polarized light. Simultaneously the solvent in the photoresist evaporates quickly because of the high convection over the wafer surface. As the solvent fraction in the photoresist decreases, the viscosity of the photoresist gradually increases (see Equation 1.1), causing the outward flow of photoresist to diminish until it almost ceases. Subsequent thinning of the photoresist comes almost entirely from solvent evaporation[11, 42]. When the solvent is mostly evaporated (typically after 30 seconds), spinning is stopped and the wafer is soft baked at a high temperature to evaporate the remaining solvent from the photoresist.

Non-uniform evaporation leads to variations in the photoresist viscosity which in turn reduce the final film thickness uniformity. The primary cause of non-uniform evaporation is uneven air flow over the wafer surface. This can arise from poorly designed exhaust systems or from turbulence which develops at the outer edges of spinning wafers[8].

2.1.4 Empirical Spin Coating Results

Empirical investigations have found that the final thickness of the photoresist layer depends primarily on initial solvent concentration, initial photoresist viscosity, final spin speed, total spin time, and solvent evaporation. It does not depend on dispense volume, dispense speed, or spin acceleration[30, 16].

Spin coating final thickness uniformity is determined largely by spin speed, spin time, spin acceleration, dispense quantity, dispense technique, type of solvent, photoresist viscosity, photoresist temperature, exhaust flow rate, and non-uniform evaporation due to turbulent flow over the wafer[9].

2.2 Spin Coating Models

Emslie et al.[19] developed the first model of spin coating which most subsequent models have followed. Their model, based on the axisymmetric lubrication approximation of the Navier-Stokes equations, assumes the following:

- an infinite rotating plane
- no radial gravitation component (because the plane is horizontal)
- an initial radially symmetric liquid layer so thin that differences in gravitational potential are negligible when compared to centrifugal forces
- Newtonian fluids
- negligible Coriolis forces
- no evaporation
- no surface tension effects

Based on these assumptions, a partial differential equation is derived to describe fluid motion on the spinning disk:

$$\frac{\partial h}{\partial t} = -\frac{\Omega^2}{3\nu}\frac{1}{r}\frac{\partial}{\partial r}(r^2 h^2) \tag{2.1}$$

where h is the thickness of the fluid, r is the radial distance from the center of the spinning disk, t is time, Ω is angular spin speed, and ν is the kinematic viscosity of the fluid. The solution is a set of two equations which define the surface contour of the fluid surface with time:

$$h = h_0\left(1 + \frac{4\Omega^2 h_0^2 t}{3\nu}\right)^{-1/2} \tag{2.2}$$

$$r = r_0\left(1 + \frac{4\Omega^2 h_0^2 t}{3\nu}\right)^{3/4} \tag{2.3}$$

where h_0 is the initial fluid thickness at a radial distance r_0 from the center of the disk. This model predicts that uniform fluid coatings will stay uniform and non-uniform coatings will tend to become more uniform during spinning.

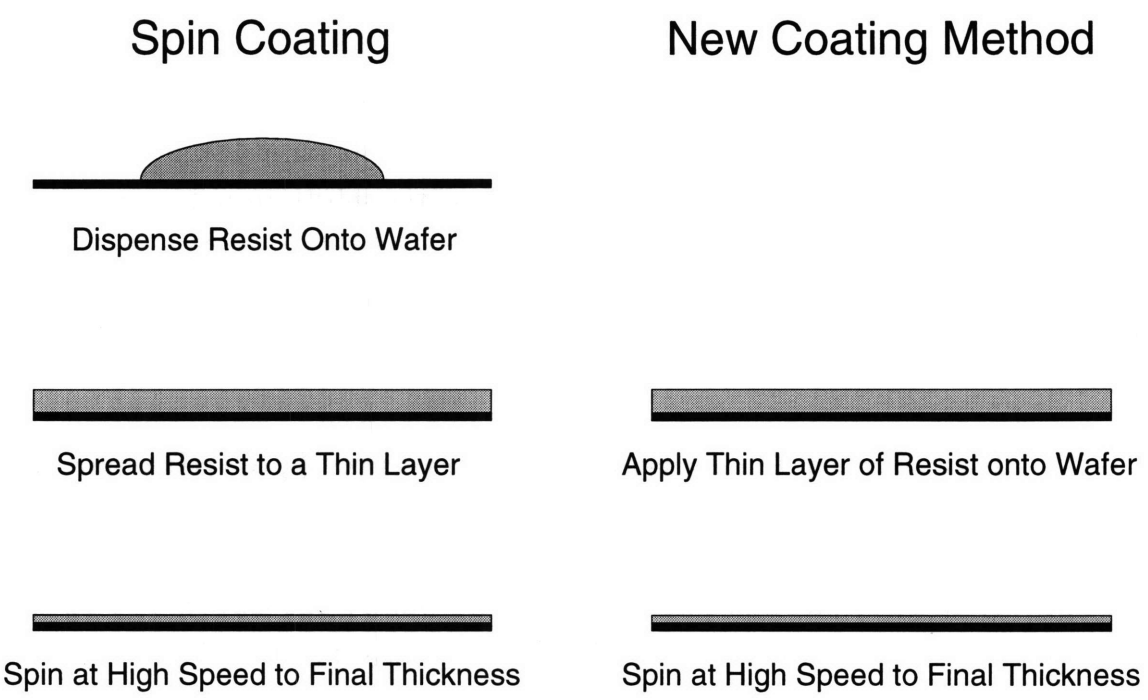

Figure 2-3: Comparison of new coating method with spin coating.

Other investigators have used the Emslie model as the basis for improved spin coating models. Acrivos et al.[2] investigated non-Newtonian fluids. Meyerhofer [33] investigated the effects of evaporation. Many other models improve on early developments by modeling other phenomena such as fluid and gas-phase resistance to solvent diffusion[8], the effects of topography[41], and the effects of relative humidity in the air flowing over the wafer[7, 13].

2.3 Spin Coating Inefficiencies

The efficiency of spin coating can be improved by isolating and eliminating the aspects of the process which waste photoresist. As discussed in Section 2.1, most of the photoresist is spun off the substrate during the second phase of the spin coating process when the photoresist is spread from the dispensed shape into an initial thick coat. Therefore, any method which applies this initial coat while using less photoresist eliminates the worst inefficiency. Figure 2-3 compares this new approach with spin coating.

None of the available spin coating models effectively addresses the inefficiencies of the spreading phase of spin coating. Modeling the spreading phase is very difficult because of the unsteady, dynamic spreading of photoresist. Instead, current models assume that an initial thick coating of photoresist exists on a disk before spinning begins. Any excess photoresist is simply thrown off the substrate and has no effect on the final coating thickness[16]. Because they do not model the spreading of photoresist from deposition until an initial thick layer is established on the disk, these models cannot predict the minimum amount of photoresist needed to coat a wafer.

2.4 Pre-Spin Coating Uniformity Requirements

A second limitation of the current models is their inability to predict coating uniformity. As before, this limitation arises from assuming the existence of an initial coating. Since the non-uniformities of an assumed coating are unknown, the models cannot predict how these non-uniformities will evolve during the final high-speed spin or what the final uniformity will be. If, however, the initial coating uniformity were known, the final uniformity could be predicted. Within its limitations, the Emslie model could be used to predict the evolution of the thickness of a thin film at various points on a spinning disk. From these thickness predictions the minimum initial uniformities which lead to the final required uniformities can be estimated. The minimum initial uniformities can then be used to evaluate whether potential coating methods are sufficiently uniform to replace the deposition and spreading phases of spin coating.

Based on the Emslie model, Figure 2-4 shows the initial uniformities required to achieve thickness variations less than 20 Å in a final coat with a thickness between 1 μm and 5 μm. Since the Emslie model does not include the effects of evaporation, the actual results are probably somewhere between the 5 μm final coating thickness (which assumes no evaporation) and the 1 μm final coating thickness (which assumes complete evaporation and no viscosity change for a photoresist with 0.2 solids content). The figure shows that the allowable variations in the initial thickness decrease for thinner initial coats. An initial coating thickness of 10 μm, for example, requires thickness variations less than 0.02–2 μm (depending on the effects of evaporation). Because the Emslie model assumes nearly uniform initial coatings, it will produce inaccurate results when used with coatings that have large initial thickness variations. Wang and Yen[43] also investigated the effects of non-uniformities in the initial

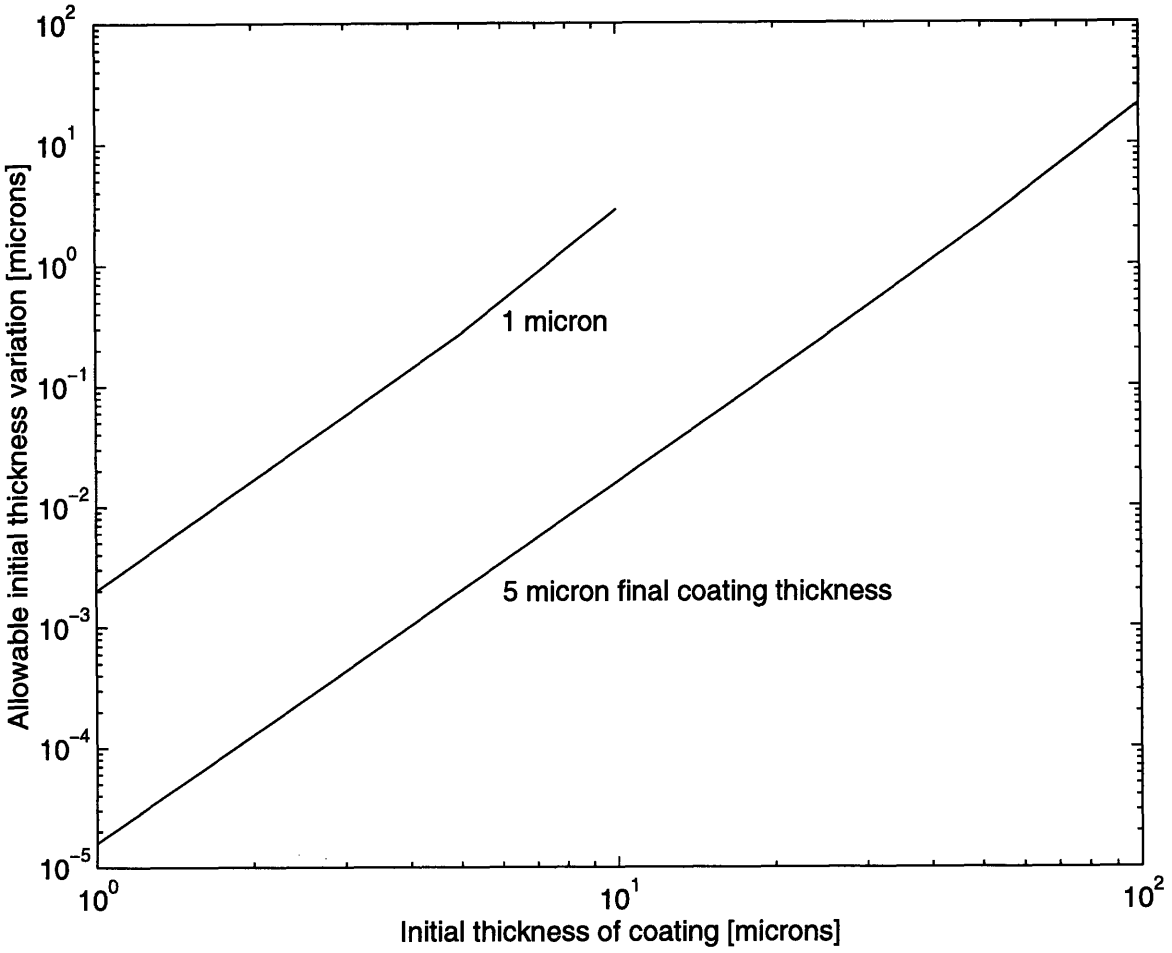

Figure 2-4: Allowable thickness variation before final high-speed spin to achieve less than 20-Å variation in the final coating thickness.

coating thickness. The results of their study are similar to the results of Emslie and indicate that small evaporation effects do not change the basic mechanism of spin coating which causes non-uniform films to become more uniform.

2.5 Pre-Spin Coating Requirements

Because of the inherent inefficiency of the current spin coating method, a new method must be developed to replace the dispense and spread phases of spin coating. This new method, in conjuction with a final high-speed spin, must satisfy all the requirements in

Section 1.2 at least as well as spin coating. To satisfy the uniformity requirement, the new method must produce initial coatings so sufficiently uniform that the smoothing mechanism of spin coating will produce the final required uniformities.

A number of coating methods were investigated to determine if they were suitable to produce the desired initial coatings. Of all the methods investigated, extrusion slot coating was most promising.

Chapter 3

Extrusion Slot Coating

Extrusion slot coating is one member of the class of pre-metered coating methods. For each of these coating methods, all of the fluid delivered to the coating head becomes a part of the final coating[25]. Consequently, the coating thickness is controlled by the fluid dispense rate, the efficiency is near 100%, and the thickness uniformity is very good.

3.1 Description of Extrusion Slot Coating

In extrusion slot coating (also known as slot or bead coating), fluid is forced (extruded) onto a substrate through a narrow slot, as shown by the cross-sectional view in Figure 3-1. The sides of the slot are made of two parallel plates which become narrow at the end of the slot, forming two narrow "lips" which direct the fluid onto a substrate. The gap between the lips and the substrate (the coating gap) is filled with a bead of coating fluid coming from the slot. When the substrate is moved perpendicular to the slot, keeping the coating gap constant, fluid is drawn out of the bead and remains as a thin film on the substrate. The width of the extruded film, w is approximately equal to the length of the extrusion slot. The thickness of the extruded film, h, is:

$$h = \frac{Q}{wv} \tag{3.1}$$

where v is the coating speed and Q is the fluid dispense rate. The menisci at the leading and trailing edges of the coating bead are pinned to the corners of the extrusion die lips[25]. According to Fahrni and Zimmermann[21], these corners must have

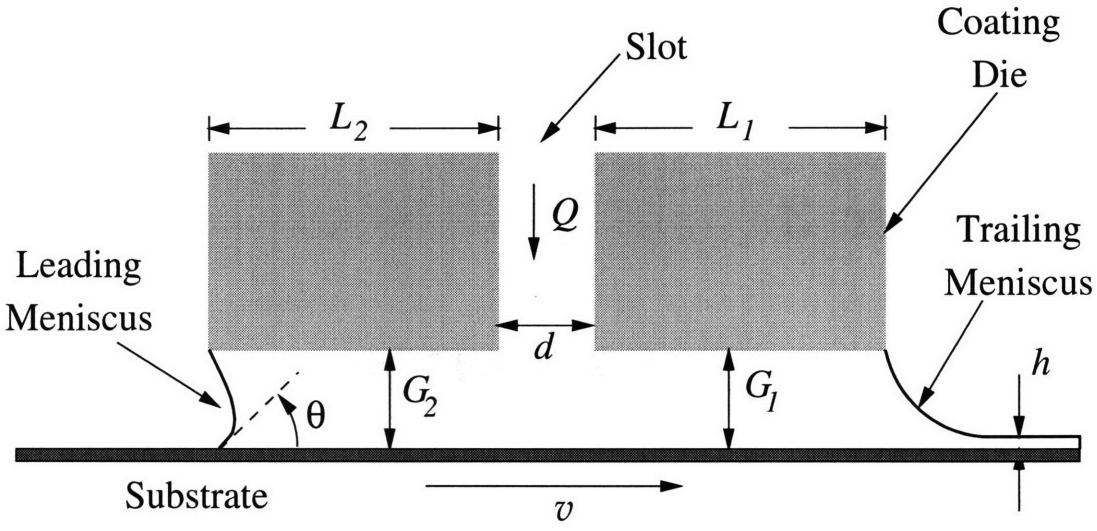

Figure 3-1: Cross-section of the lips of an extrusion slot coating die with a substrate moving beneath them.

a radius of curvature less than approximately 50 μm to keep the menisci pinned. The capillary, viscous, and inlet pressures in the coating bead must balance the external pressure to maintain stability in the coating bead[27]. A slight vacuum at the leading edge of the coating bead can be used to stabilize it when coating thinner films or at higher coating speeds[5]. Usually the coating lips are of equal length ($G_1 = G_2$) and the extrusion slot is perpendicular to the substrate. For very thin coatings, however, it is sometimes beneficial to have one of the lips extend beyond the other ($G_1 \neq G_2$) or to have the extrusion slot slightly tilted from perpendicular to the substrate[25].

3.2 Extrusion Die

Figure 3-2 shows an extrusion die, constructed of a U-shaped shim sandwiched between two flat plates[24]. Photoresist enters the extrusion die through a hole in the top of the back plate. The hole directs the photoresist to a cavity which is open to the inner surfaces of the plates and is as wide as the inner width of the shim. The void created by the U-shape of the shim leaves a narrow gap (the slot) between the two plates through which photoresist can flow. This gap (the slot gap) has a width equal to the thickness, d, of the shim. At the base of the extrusion die, the plates narrow to form two lips on each side of the slot gap, as shown in Figure 3-1. Photoresist is

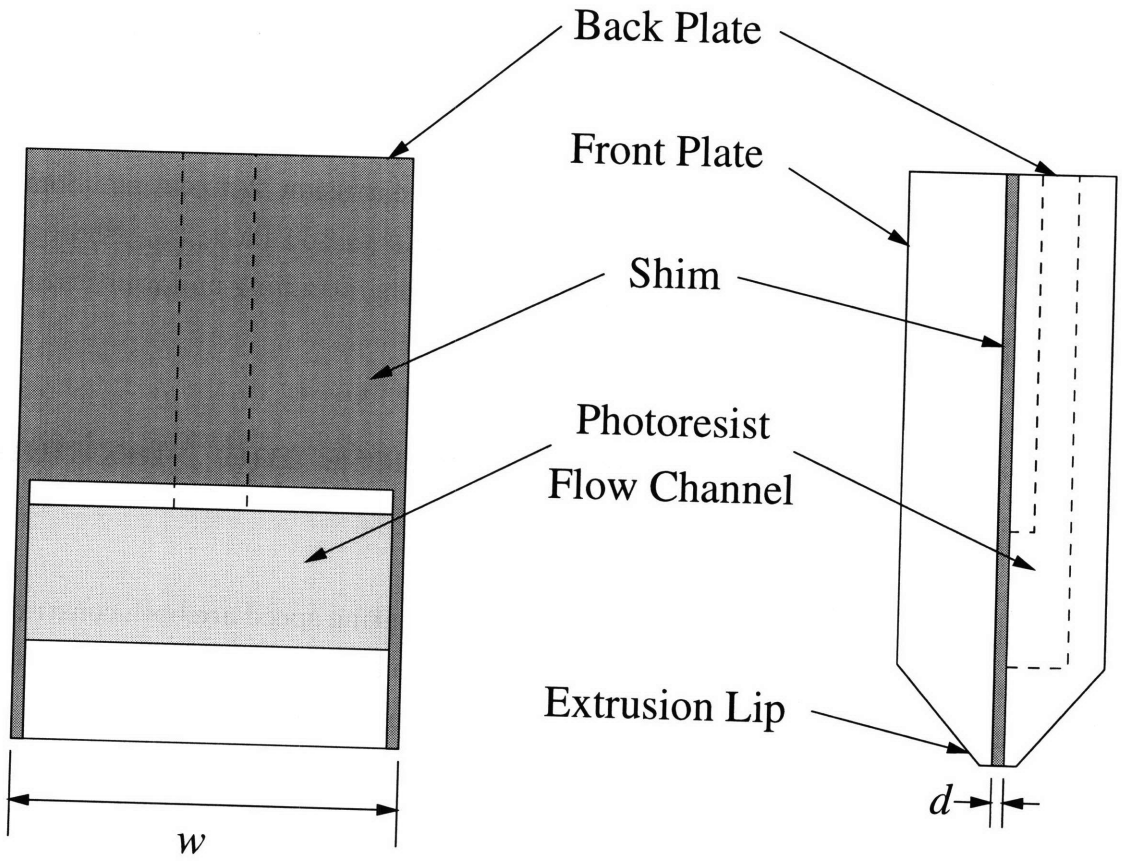

Figure 3-2: Extrusion die.

extruded out of the slot gap into the coating gap, G, between the extrusion die lips and the substrate.

3.3 Coating Materials for Extrusion Slot Coating

Extrusion slot coating has been used with a variety of fluids and substrates. Much of the experimental work has been done using a spinning roller. The coating fluid is applied on one side and removed on the other to maintain a continuous coating process[31]. A common application of extrusion slot coating is applying thin films to flat panel displays using a coating die the width of the display[3]. The substrate must be very flat to produce thin coatings using this method.

A wide range of viscosities have been used with extrusion slot coating. Some of the experiments have ranged from 10 mPa-sec[31] up to 130 Pa-sec[3]. Photoresist has been found to work well with extrusion slot coating, attaining uniformities of less than 2%[3].

3.4 Minimum Coating Thickness and Maximum Coating Speed

The minimum coating thickness and the maximum coating speed are both constrained by the same phenomenon, the low-flow limit of coatability[15]. Coating defects appear when higher coating speeds or smaller coating thicknesses are attempted.

3.4.1 Effect of Coating Gap

Lee et al.[31] found that at high coating speeds, the minimum coating thickness (and maximum coating speed) is very sensitive to the coating gap, but at low coating speeds the gap has little influence on the minimum coating thickness. The boundary between these two regimes is defined by a critical Capillary number ($\mathrm{Ca} = \mu v/\sigma$). By correlating the data from Lee's experiments, the critical Capillary number, Ca^* can be determined approximately as:

$$\mathrm{Ca}^* = 0.78G - 0.08 \tag{3.2}$$

where $G = G_1 = G_2$. Lee et al. showed that above the critical Capillary number,

the minimum coating thickness was approximately proportional to the gap, except at low viscosities. Below the critical Capillary number, the minimum coating thickness decreases as the Capillary number decreases.

3.4.2 Effect of Fluid Viscosity

Lee et al. found that the minimum coating thickness can be reduced or the maximum coating speed increased with lower fluid viscosities, especially at larger coating gaps.

3.4.3 Effect of Slot Gap

Lee et al. found that the slot gap, d, has little effect on the minimum coating thickness because viscosity forces in the coating gap are much greater than the forces from the momentum change of fluid coming out of the slot gap.

3.4.4 Models

Ruschak[39] modeled the minimum coating thickness for extrusion slot coating. According to his analysis, the minimum coating thickness depends primarily on the surface tension forces in the coating bead. With no bead vacuum present, the minimum coating thickness is:

$$h_{min} = \frac{1.338}{2}\mathrm{Ca}^{2/3}\left(\frac{G_1}{1+\cos\theta}\right) \tag{3.3}$$

where σ is the dynamic surface tension, θ is the dynamic contact angle between the upstream meniscus and the substrate, and $G = G_1 = G_2$ is the gap. Lee *et al*[31] showed by experiment that Rushak's model was valid for Capillary numbers below the critical Capillary number when the coating gap was 1 mm and the dynamic contact angle was between 0 and 90°.

Higgins and Scriven[27] derived an improved model for extrusion coating by including viscous forces. They identified two primary flows within the coating bead. First, a Couette flow is created by the motion of the substrate relative to the extrusion die. Second, a Poiseuille flow is driven by the pressure drop between the inlet slot and the edges of the coating bead. To maintain a constant coating bead the Poiseuille and Couette flows must exactly cancel each other in the leading edge of the coating bead. In the trailing edge of the coating bead, the difference between the Poiseuille and Couette flow rates equals the total flow rate.

The minimum coating thickness predicted by the Higgins and Scriven model for a flat coating surface with no bead vacuum present is:

$$h_{min} = h^0_{min}\left(1 + \frac{6\ \mathrm{Ca}}{1+\cos\theta}\left(\frac{L_1}{G_1}\right)\left(\frac{G_2}{G_1}\right)\left[1 + \left(\frac{L_2}{L_1}\right)\left(\frac{G_1}{G_2}\right)^2 - \frac{2h^0_{min}}{G_1}\right]\right) \tag{3.4}$$

where:

$$h^0_{min} = 1.34\mathrm{Ca}^{2/3}\frac{G_1}{1+\cos\theta} \tag{3.5}$$

and G_1,G_2,L_1, and L_2 are defined in Figure 3-1. The predicted minimum wet thickness from Equations 3.4 and 3.5 is shown in Figure 3-3 for two coating gaps and two dynamic contact angles. The experiments by Lee et al. verified this model for Capillary numbers below the critical Capillary number when the gap was 0.2 mm and dynamic contact angle was near 45°.

3.4.5 Coating Bead Vacuum

When small gaps and high coating speeds are used, the coating bead becomes unstable unless a vacuum is imposed at the leading edge of the coating bead. The vacuum creates a pressure drop across the coating bead which helps balance the viscous forces in the coating bead. The actual magnitudes of the gaps and coating speeds are dependent on the viscosity. The model of Higgins and Scriven[27] predicted the minimum and maximum operating pressures across a coating bead on a flat coating surface to be:

$$\Delta p_{min} = 1.34\mathrm{Ca}^{2/3}\frac{\sigma}{h} - \frac{\sigma(1+\cos\theta)}{G_2} + \frac{6\mu v L_1}{G_1^2}\left[1 + \left(\frac{L_2}{L_1}\right)\left(\frac{G_1}{G_2}\right)^2 - \frac{2h}{G_1}\right] \tag{3.6}$$

and:

$$\Delta p_{max} = 1.34\mathrm{Ca}^{2/3}\frac{\sigma}{h} + \frac{\sigma(1-\cos\theta)}{G_2} + \frac{6\mu v L_1}{G_1^2}\left[1 + \left(\frac{L_2}{L_1}\right)\left(\frac{G_1}{G_2}\right)^2 - \frac{2h}{G_1}\right] \tag{3.7}$$

where h is defined in Figure 3-1. Sartor[40] experimentally validated the model of Higgins and Scriven, developing a "window of coatability" which shows the pressure

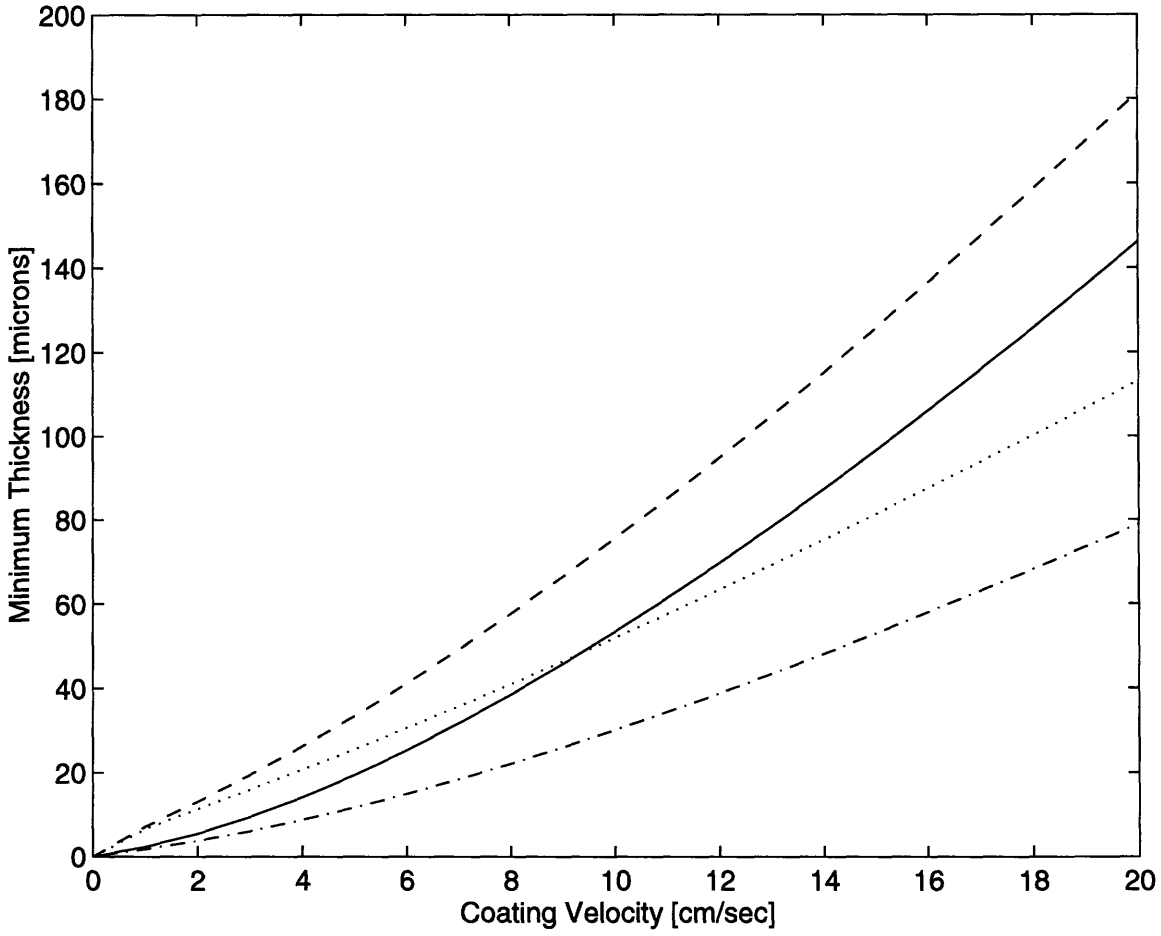

Figure 3-3: Theoretical minimum coating thickness for $G = 40$ μm and θ=90° (—), $G = 200$ μm and θ=90° (– –), $G = 40$ μm and θ=0° (– · – ·), $G = 200$ μm and θ=0° (· · ·). $\mu = 10$ mPa-sec, $\sigma = 30$ dyne/cm, $G_1 = G_2 = G$.

limits for stable coating beads. If the upper bead vacuum limit is exceeded, fluid is sucked out of the bead. Below the lower bead vacuum limit, ribbing and rivulets develop.

Most of the pressure drop across the bead comes from the viscous forces. With a small gap and a high coating speed, the allowable pressure range is very small. For a 14 mPa-sec fluid coated to 10 μm at 50 cm/sec the allowable pressure drop is 26.2 - 29.1 kPa.

The dynamic contact angle, θ, between the substrate and the upstream meniscus is an important parameter for these models that is difficult to predict or measure[40]. Sartor showed apparent dynamic contact angles between 110° and 140° for glycerin-water mixtures. Hens and Mues[26] found that the dynamic contact angle was less than 120° for the case of low Capillary number with no bead vacuum. Cohen and Gutoff[15] found that the dynamic contact angle should be a function of the Capillary number, the Physical Properties number (Pp $= \rho\sigma^3/g\mu^4$), and the dimensionless ratios of any important properties (such as ρ/ρ_{air} or μ/μ_{air}).

3.4.6 Experimental Thicknesses and Speeds

The maximum coating speed found in the literature for coatings on the order of 50μm is 5 cm/sec[14], with speeds up to 12.7 cm/sec cited as being possible. At these coating speeds, the Capillary number is generally below the critical Capillary number, and the minimum coating thickness depends only slightly on the gap.

3.5 Coating Uniformity

The uniformity of extrusion slot coatings has been the work of experimental investigation. Gutoff[24] stated that extrusion slot coaters were used extensively with coating thickness variations under 2%. Bagen and Newquist[3] obtained coating thickness variations between 1.3 and 1.7% for individual coatings of a 0.019 mPa-sec viscosity fluid. The overall coating thickness variation for all of their coatings was 2.04%.

3.6 Coating Time

The coating time for extrusion slot coating depends on the area to be covered and the width of the extrusion die. If the extrusion die is wide, large areas can be coated very quickly. If the extrusion die is small, however, the coating time would be higher.

3.7 Coating Efficiency

The coating efficiency of extrusion slot coating approaches 100%. The only wasted fluid is the fluid needed to flush the air bubbles from the extrusion die and the fluid dispensed off the coating substrate.

3.8 Coating Defects

Gutoff and Cohen[25] describe a number of coating defects that occur in extrusion slot coatings. The following list of coating defects follows their summary.

Chatter is the appearance of evenly-spaced thickness variations oriented perpendicular to the coating direction. It can be caused by fluctuations in the fluid flow rate, mechanical disturbances, vacuum fluctuations, or system hydrodynamics[40].

Ribbing is evenly-spaced thickness variations oriented in the coating direction, caused by system hydrodynamics. Bixler's mathematical analysis of ribbing[6] shows that ribbing can be reduced by using lower viscosity fluids, lower coating speeds, greater coating thicknesses, and smaller coating gaps. Ribbing is more likely to occur when the extrusion die lips are at an angle such that the upstream lip is closer to the substrate than the downstream lip. Ribbing can also occur when the upstream or downstream lip is too rounded. This creates the same problem as the extrusion die angle described above.

Neck-in arises when surface tension draws the edges of the coating bead together, causing the width of the coating bead to decrease. It is most pronounced at wide coating gaps, high surface tension, high viscosities, and in highly viscoelastic liquids. Neck-in is most severe near the limits of coatability. Edge guides are often used to reduce its effect.

Scalloped edges occur when the edge of the coating bead moves in and out from the edge of the extrusion die. This defect is more common for thin coatings, high coating speeds, and wide coating gaps. It is more common in viscoelastic fluids, such as photoresist.

Rivulets occur when the coating bead splits into two or more segments, resulting in two or more stripes of photoresist separated by dry regions. This defect occurs at high coating speeds and large coating gaps.

Edge Beads cause the edge of the extruded coating to be thicker than the center of the coated area. Gutoff shows that surface tension is the source of edge beads primarily at low viscosities, low coating speeds, low coating thicknesses, and wide coating gaps.

Air Entrainment beneath the coating bead is an important limit to the maximum coating speed[25]. Joos et al.[28], and Mues et al.[20] predict that air entrainment begins when the dynamic contact angle reaches 180°. They found the critical air entrainment velocity, v^*, to be:

$$v^* = \frac{\sigma}{4\mu} \tag{3.8}$$

where σ is the surface tension and μ is the viscosity.

3.9 Evaluation of Extrusion Slot Coating

Extrusion slot coating meets all the criteria of Section 1.2. It can be used with photoresist on flat substrates. It can produce uniform, thin coatings very efficiently. If the extremes of the coating limits are avoided, very few defects are formed. One problem it has, however, is the inability to coat substrates that vary in width. If this problem is solved, extrusion slot coating can replace the dispense and spread phases of spin coating.

Chapter 4

Extrusion-Spin Coating

Extrusion-spin coating combines the efficiency of extrusion-slot coating with the uniformities of spin coating. The extrusion coating method is used to apply an initial fluid coating on a wafer, which is then spun at high speeds to reduce the thickness of the fluid layer and improve the thickness uniformity.

4.1 Description of Extrusion-Spin Coating

Coating a flat disk using extrusion coating is difficult because the substrate does not have a constant coating width. To solve this problem, we can use a small extrusion slot coating die with a coating width much less than the disk radius, R. The extrusion slot is oriented along the diameter of the disk as shown in Figure 4-1. The disk is rotated at angular speed Ω, creating a relative velocity, v, between the extrusion head and the disk surface. As the disk is rotated, the extrusion head is moved along the diameter of the disk at a velocity, u. Rotating the disk at a rate proportional to the extrusion head speed creates a spiral-shaped coating, as shown in Figure 4-2. Coating geometries other than a spiral can be created by using other disk rotation rates and extrusion head speeds. Once the entire surface of the disk is coated with fluid, the disk is spun at high speed (as in the usual spin-coat method) to attain the final coating thickness.

4.1.1 Spiral Motion

To coat a disk using extrusion-spin coating, a geometric pattern which covers the whole surface of the disk must be used. A spiral is perhaps the simplest method of

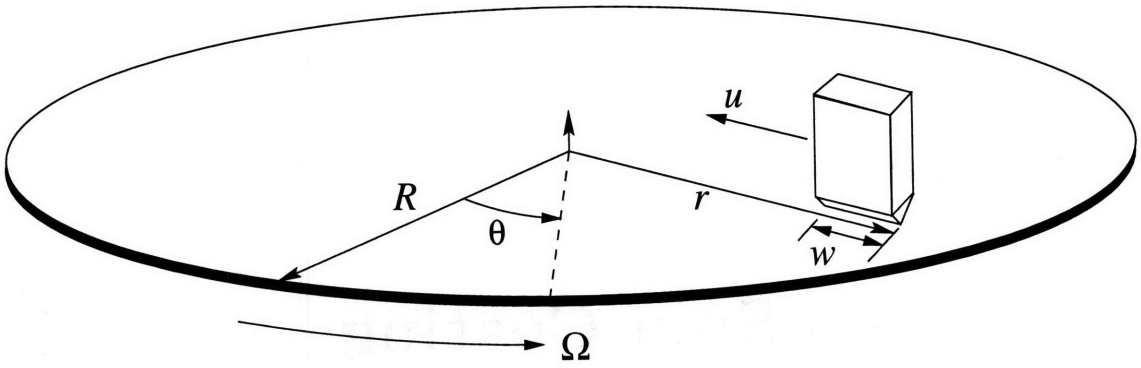

Figure 4-1: Extrusion-spin coating motion.

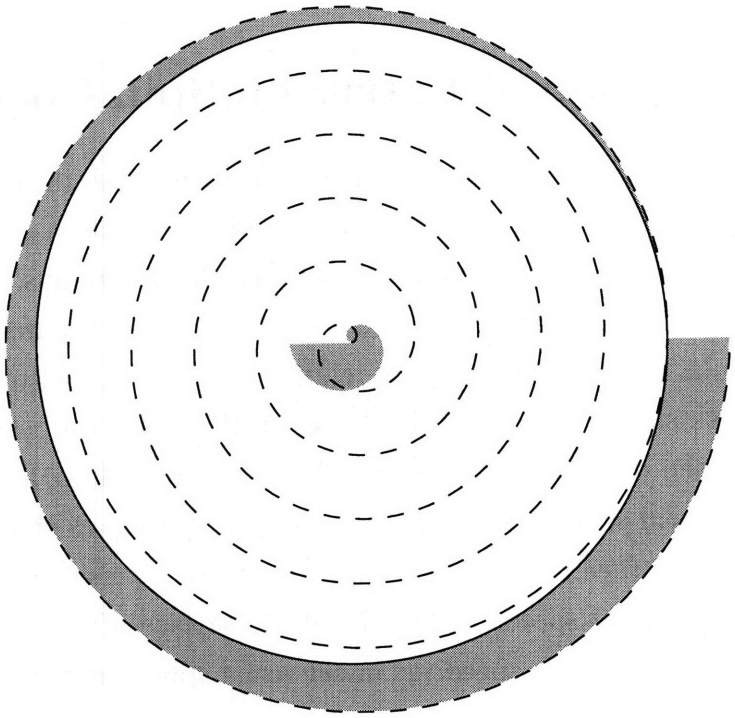

Figure 4-2: Extrusion-spin coating spiral pattern. Outline of disk (—), edge of spiral rings (– –). Shaded regions show wasted photoresist at outer edge and double photoresist thickness at center.

of doing so with an extrusion die that has a width between one tenth and one third of the disk diameter.

Spiral-shaped coatings are made by moving an extrusion head radially along the diameter of a turning disk. In this section all the equations developed are for radially inward motion of the extrusion head (from the edge of the disk toward the center), although radially outward motion is equally applicable.

Only small dispense volumes (between 0.1 and 0.2 mL) are required to produce thin coatings. The dispense rate of fluid is correspondingly small. Because precise, variable-rate pumps with low flow rates are not available, it is better to use a constant fluid dispense rate. To obtain a uniform-thickness coating using a constant dispense rate, the tangential velocity between the extrusion head and the disk must also remain constant. The tangential velocity of any point on the surface of a disk, at a distance r from the axis of rotation shown in Figure 4-1 is:

$$v = \Omega r \tag{4.1}$$

where Ω is the rotational speed of the disk (in radians per second). If we locate the outer edge of an extrusion die slot at a position r, we can make a spiral shape by moving the extrusion die inward one length of the extrusion slot for each revolution of the disk. The extrusion die speed along the diameter of the disk is then:

$$u = \frac{\Omega w}{2\pi} \tag{4.2}$$

where w is the width of the extruded coating. Solving for Ω from Equation 4.1 and substituting it into Equation 4.2 yields:

$$u = \frac{wv}{2\pi r} \tag{4.3}$$

For radially inward motion, $u = -dr/dt$, and a differential equation for the position of the extrusion head can be obtained as:

$$\frac{dr}{dt} = -\frac{wv}{2\pi r} \tag{4.4}$$

Integrating this equation using the initial condition $r = r_0$ at time t=0 yields:

$$r = \sqrt{r_0^2 - \frac{wv}{\pi}t} \tag{4.5}$$

where r_0 is the initial position of the outer edge of the extrusion die. (In order to make the spiral in Figure 4-2, the extrusion die must begin off the edge of the disk at an initial position $r_0 = R + w$.)

Substituting Equation 4.5 for r in Equations 4.1 and 4.3, the disk rotation speed and the extrusion die speed can be derived as a function of time as:

$$\Omega = \frac{v}{\sqrt{r_0^2 - \frac{wv}{\pi}t}} \tag{4.6}$$

and:

$$u = \frac{wv}{2\pi\sqrt{r_0^2 - \frac{wv}{\pi}t}}. \tag{4.7}$$

The angle of the wafer, θ, (in radians where $\Omega = d\theta/dt$) can be determined by integrating Equation 4.6 using the initial condition $\theta = 0$ at time $t = 0$ as:

$$\theta = \frac{2\pi r_0}{w}\left(1 - \sqrt{1 - \frac{wv}{\pi r_0^2}t}\right) \qquad \left(t < \frac{\pi r_0^2}{wv}\right) \tag{4.8}$$

4.1.2 Center Adaptation to Spiral Motion

The equations describing spiral motion (4.5 – 4.8) have a singularity at the center of the disk. As the outer edge of the slot approaches the center of the disk, both the disk rotation rate and the extrusion head speed should increase without limit to maintain a constant tangential coating speed. Because this is impossible, the spiral motion must be modified to stay within reasonable velocities. One method of accommodating the center singularity is to maintain a constant disk rotational speed after the speed reaches a critical maximum, or when the extrusion die reaches a critical radius. The constant disk rotation rate and extrusion die speed after reaching a critical radius r_c are:

$$u_c = \frac{wv}{2\pi r_c} \tag{4.9}$$

and:

$$\Omega_c = \frac{v}{r_c} \tag{4.10}$$

One logical position at which to fix the maximum rotation rate is when the inner edge of the extrusion slot reaches the center of the disk. At this position, the outer edge of the extrusion die is at a radius $r = w$, and the corresponding extrusion head speed and disk rotation rate, shown in Figure 4-3, are respectively:

$$u = \frac{v}{2\pi} \tag{4.11}$$

and:

$$\Omega = \frac{v}{w} \tag{4.12}$$

4.2 Coating Time

Solving Equation 4.5 for t, the coating time, T, can be computed as:

$$T = \frac{\pi(r_0^2 - r_f^2)}{wv} \tag{4.13}$$

where r_f is the final radial position of the outer edge of the extrusion slot.

When the modified spiral discussed in Section 4.1.2 is used, the coating time increases. The time required to complete the exact spiral from the critical radius $r = r_c$ to the center is:

$$T_{center} = \frac{\pi r_c^2}{wv} \tag{4.14}$$

The time required to complete the modified spiral from the critical radius $r = r_c$ to the center is:

$$T_{center,mod} = \frac{r_c}{u_c} = \frac{r_c}{\frac{wv}{2\pi r_c}} = \frac{2\pi r_c^2}{wv} \tag{4.15}$$

The excess time required to complete the modified spiral can by found by subtracting T_{center} from $T_{center,mod}$:

$$T_{center,excess} = \frac{2\pi r_c^2}{wv} - \frac{\pi r_c^2}{wv} = \frac{\pi r_c^2}{wv} \tag{4.16}$$

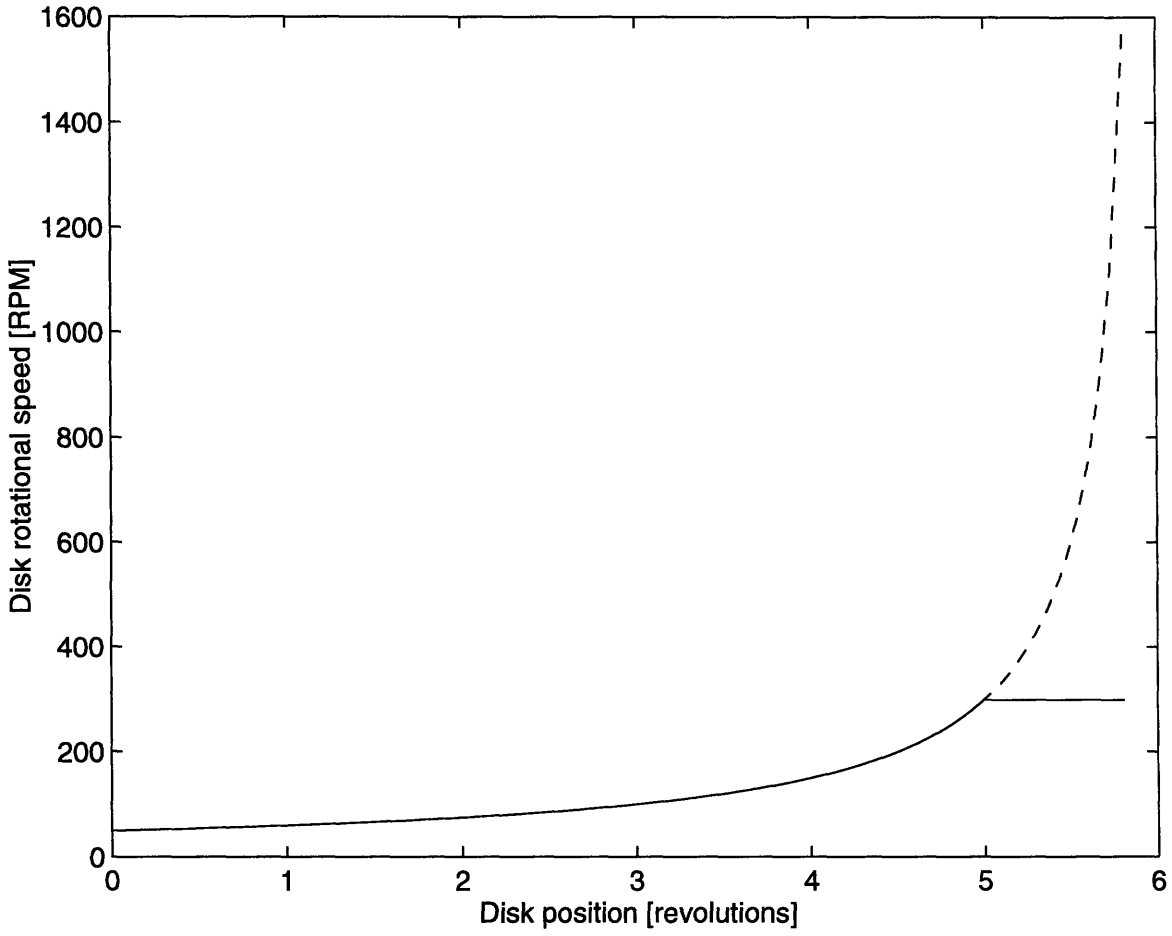

Figure 4-3: Disk rotational speed during extrusion-spin coating. Exact spiral (– –), modified spiral (—). $v = 10$ cm/sec, $w = 2$ cm.

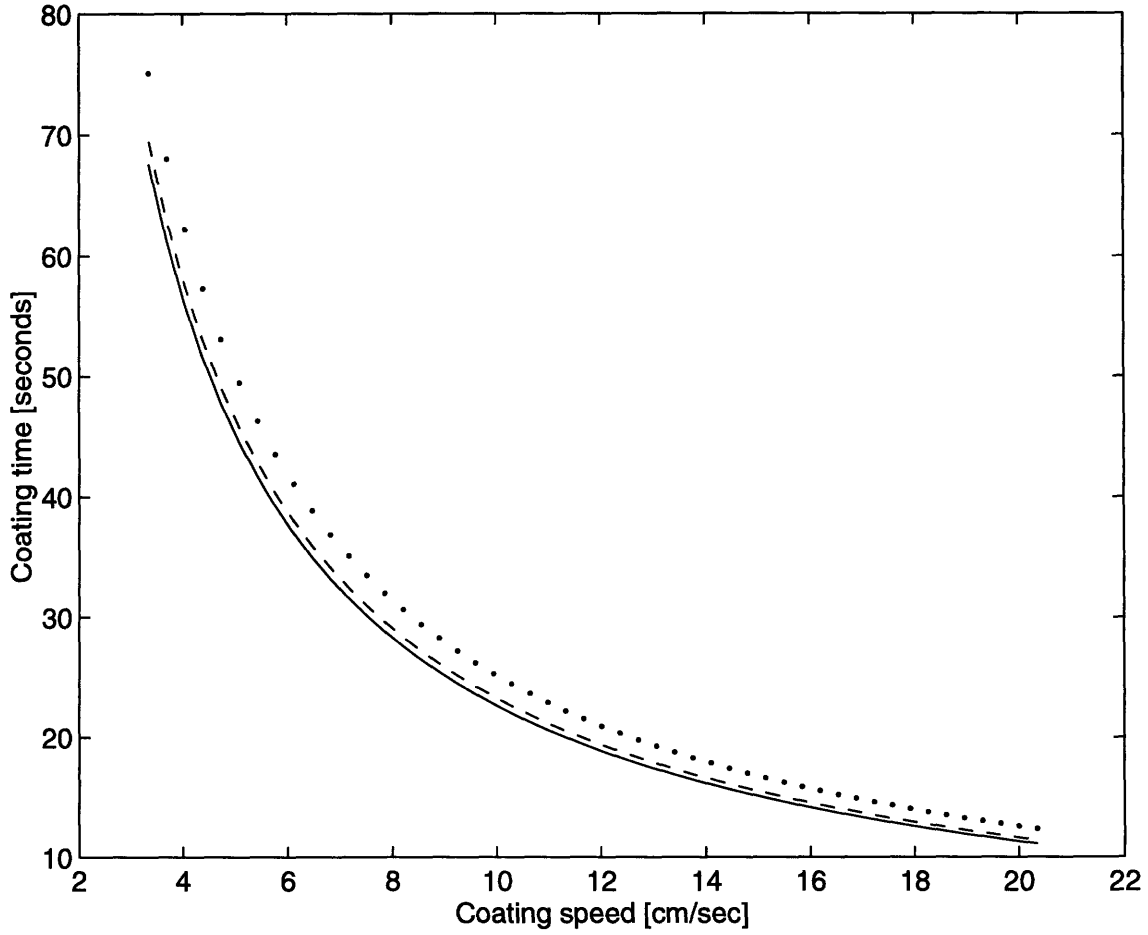

Figure 4-4: Coating time for extrusion-spin coating. Exact spiral (—), modified spiral when $r_c = w$ (– –), modified spiral when $r_c = 2w$ ($\cdots$). $v = 10$ cm/sec, $w = 2$ cm.

Adding this excess time required to complete the modified spiral to the total coating time for the normal spiral gives the total coating time for the modified spiral as:

$$T_{mod} = \frac{\pi r_0^2}{wv} + \frac{\pi r_c^2}{wv} \tag{4.17}$$

Figure 4-4 shows the coating time as a function of coating velocity for a 20-cm diameter disk ($r_0 = 12$ cm).

4.3 Thickness and Thickness Uniformity

In extrusion-spin coating, the spiral shape of the initial wet coating creates thickness variations, overlap bumps, and an excess pool of fluid in the center of the disk.

4.3.1 Wet Coating Thickness

As discussed in Chapter 3, the wet thickness, h, of an extruded film is:

$$h = \frac{Q}{vw} \tag{4.18}$$

where Q is the fluid dispense rate, w is the width of the extruded film, and v is the relative tangential velocity of the extrusion head with respect to the coating surface. Because of the spiral motion in extrusion-spin coating, however, the relative velocity between the substrate and the extrusion head is not uniform across the extrusion head. Substituting Equation 4.18 into Equation 4.1, the thickness at any point along the radius can be found:

$$h = \frac{Q}{\Omega r w} \tag{4.19}$$

The thickness difference, Δh, between the inner and outer edges of the extrusion head is then:

$$\Delta h = \frac{Q}{\Omega(r-w)w} - \frac{Q}{\Omega r w} = \frac{Qw}{\Omega(r-w)r} \tag{4.20}$$

Two factors should make the actual thickness difference less than that of the value value predicted by Equation 4.20. First, higher fluid velocities at the outer edge of the extrusion head create a lower pressure which directs more of the fluid to the outer edge. Second, surface tension will tend to even out the coating surface after it is applied.

4.3.2 Fluid Overlap Between Extrusion Rings

Two spiral rings extruded during subsequent revolutions of a disk being coated can be deposited next to each other in three ways: separated by a gap, exactly matched, or overlapped. For each of these conditions, the desired result is a continuous, uniform photoresist coating.

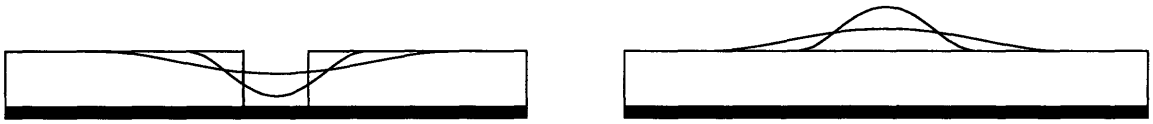

(a) (b)

Figure 4-5: Fluid cross section for (a) a valley created when a gap is left between extruded rings and (b) a bump created when two extruded rings overlap. Surface shape changes show how surface tension might spread the valley or bump over a larger area.

When a small gap separates two rings, fluid must flow into the gap to join the rings into a continuous fluid layer. There are three potential forces which might force the fluid into the gap. First, gravity forces could cause a flow into the gap. Since the coatings are extremely thin, it is unlikely that gravity would overcome the more dominant surface tension forces. Second, when the fluid wets the substrate, surface tension forces could cause the edges of the fluid to be drawn across the substrate until the spiral rings are joined. Such processes are highly dependent on surface characteristics which vary greatly with surface material, temperature, vapor prime, cleanliness, etc. Once two rings join together, surface tension forces will tend to make the resulting "valley" become shallower and wider as shown in Figure 4-5(a). As a result, the thickness of the coating tends to become more uniform. The third force which could cause the fluid to flow into the gaps is the inertial force on the fluid during high-speed rotation of the substrate. Such flows are difficult to model because of their unsteady dynamics. If the gap is not completely closed, pin holes can form.

If the edges of the spiral rings matched each other exactly, the fluid layer would be theoretically uniform. In practice, however, extruded layers have thickness variations near their edges which lead to "bumps" or "valleys" in the photoresist film at the intersection of the two rings. In addition, the edges of a spiral ring are not exactly straight because of minute variations in process parameters such as resist flow rate, wafer to extrusion die gap, coating speed, temperature, and surface properties. These variations can lead to alternating gaps and overlaps of the spiral rings.

When the spiral rings are overlapped, a "bump" in the fluid is created. These bumps spread into the surrounding fluid by the same three phenomena which bridges gaps between spiral rings. To attain the desired coating thickness uniformities, these

bumps must be spread out before a final high-speed spin. Figure 4-5(b) shows a polynomial bump profile as it spreads.

Creating Overlap Between Extrusion Rings

A nominal overlap, Δw, between spiral rings can be created by using a width, w', smaller than the actual width, w, to calculate the motion of the extrusion die. The result is that the extrusion die moves more slowly across the diameter of the disk, creating a nominal overlap which is less than the actual overlap when neck-in occurs. The new effective width, w', which must be used in Equations 4.2 to 4.20 to obtain an overlap is:

$$w' = w - \Delta w \tag{4.21}$$

4.3.3 Fluid Deposition at the Spiral Center

The fluid profile at the center of a disk before a high-speed spin greatly affects the final coating. During the high-speed spin, any excess fluid flows over the fluid on the rest of the disk. Similarly, any thin areas in the center can remain due to a lack of fluid. Therefore, it is important to characterize the fluid profile produced by spiral coating at the center of the disk.

Spiral Center Fluid Overlap

Because the extrusion head has a constant width, the inner ring of a spiral-coated disk overlaps the previous ring as shown in Figure 4-2. The volume of extra fluid in this overlap, V_{center}, is approximately:

$$\Delta V_{center} = \frac{\pi w^2 h}{6} = \frac{\pi w^2}{6}\left(\frac{Q}{wv}\right) = \frac{\pi w Q}{6v} \tag{4.22}$$

When the spiral is completed, the overlapped fluid is off-center and can cause uniformity problems.

Excess Fluid in Center of Modified Spiral

When a modified coating spiral is used, as discussed in Sections 4.1.2 and 4.2, the coating time is increased for the center portion of the spiral. This increase in coating time results in a corresponding increase in the volume of resist deposited:

$$\Delta V_{mod} = Q\Delta T_{center,excess} = \frac{Q\pi r_c^2}{wv} \tag{4.23}$$

This extra fluid adds to the excess already created by the center overlap.

4.3.4 Extrusion-Spin Coating Thickness Uniformity

Calculating the thickness uniformity of extrusion-spin coats requires three steps. First, the thickness of the wet coating produced by extrusion coating must be determined over the entire coating surface. Second, the spreading of the wet coat before the final high-speed spin must be calculated. Third, the change in thickness during the high-speed spin much be characterized.

Wet Thickness Uniformity

The wet thickness of the extruded coating depends on the fluid deposition parameters discussed above: spiral ring thickness variation, spiral overlap, center fluid deposition, and possibly gap variation. According to Choinski[14], however, the gap variation is not critical to extrusion slot coating as long as the gap remains below a certain critical value. Therefore, variation in the gap is not considered in this analysis.

Figure 4-6 shows a typical fluid thickness distribution across the diameter of an extrusion-coated disk. The thickness variation is greatest toward the center where the coating velocity across the length of the extrusion die is the highest. Spiral overlaps would introduce even more fluid at the intersection of the extrusion rings.

Wet Coating Uniformity Improvement

It is important to understand how the wet coating thickness evolves over time to see if uniformities improve. Surface tension forces cause areas on the fluid surface with high curvature to spread out. Since this problem requires more detailed analysis, it is discussed separately in Chapter 5.

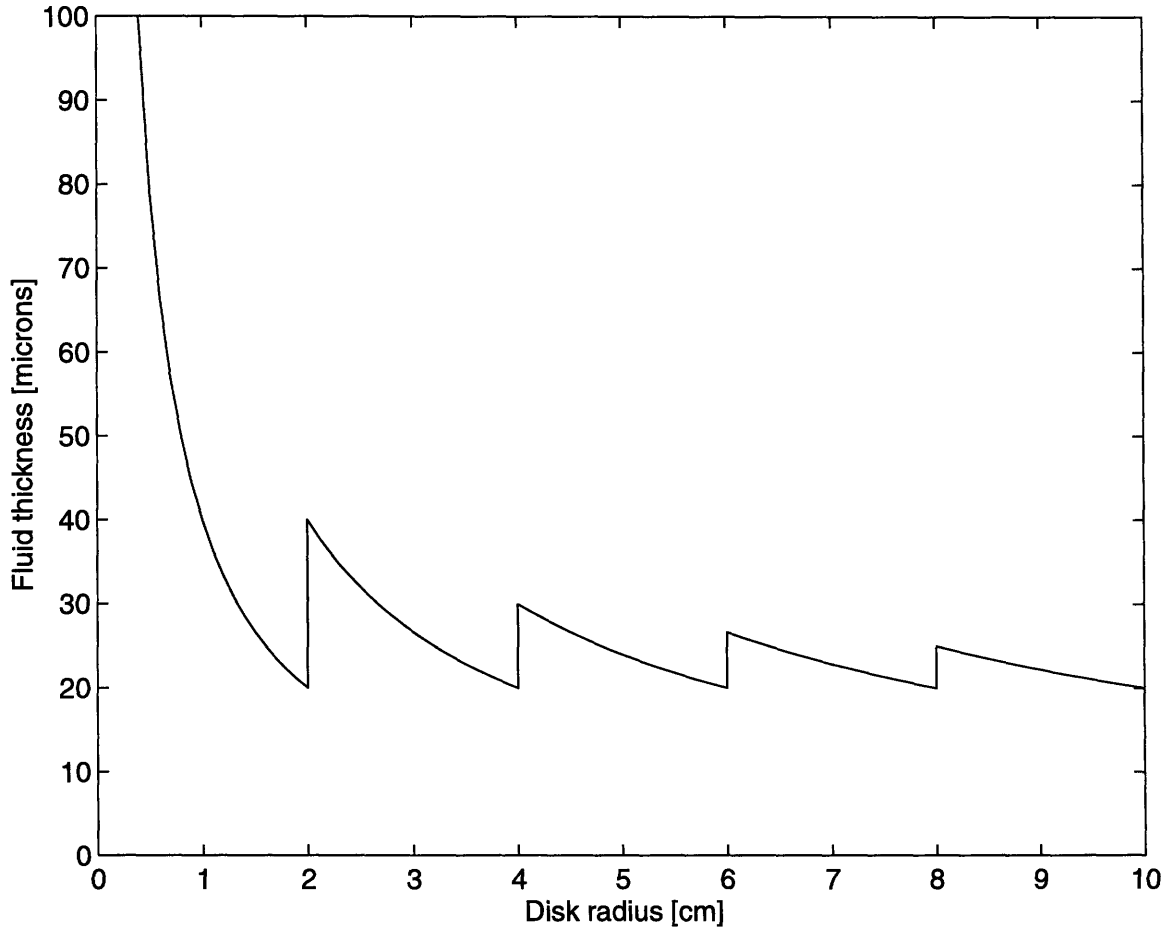

Figure 4-6: Fluid thickness along the diameter of a disk with a 20-μm nominal coating thickness.

Evaporation Effects on Final (Dry) Thickness Uniformity

During the high-speed spin fluid accelerates radially outward as described in Section 2.1. During this phase the coating becomes thinner and variations in the coating thickness become less and less. Because of the spiral coating technique, however, evaporation has a much more pronounced effect than for spin coating. As the solvent evaporates, the viscosity of the fluid increases according to Equation 1.1, leading to thicker films after the final high-speed spin. Therefore, if evaporation is not uniform across the substrate, non-uniformities in the final film thickness will also be present. Appendix B shows the derivation of the mass transfer rate per unit area for evaporation from a spinning disk:

$$\dot{m}'' = \frac{0.585\rho D_{as}}{0.6/\mathrm{Sc} + 0.95/\mathrm{Sc}^{1/3}} \left(\frac{\Omega}{\nu_{as}}\right) \ln\left(\frac{1}{1 - m_{s,s}}\right) \tag{4.24}$$

where D_{as} is the air-solvent diffusion coefficient, Sc ($= \nu_{as}/D_{as}$) is the Schmidt number, Ω is the rotational speed of the disk, ν_{as} is the viscosity of the solvent-air mixture over the disk, and $m_{s,s}$ is the mass fraction of the solvent at the surface of the fluid film on the disk (determined by the partial pressure of the solvent at the surface). To obtain an upper bound on solvent evaporation, a fluid layer of 100% solvent will be assumed. This assumption neglects any liquid-phase resistance to solvent diffusion. Because the mass transfer coefficient is independent of radial position, the evaporation rate is uniform over the entire surface of the disk.

The total solvent evaporation at any point on the disk can be calculated by using Equation 4.12 to substitute for Ω in Equation 4.24. The mass of evaporated fluid per unit area is:

$$\Delta m'' = \int_{t_0(r)}^{T} \dot{m}'' dt \tag{4.25}$$

where T is the total coating time and $t_0(r)$ is the time at which fluid is first deposited at radius r on the disk. The fraction of solvent evaporated from the fluid surface is:

$$e = \frac{\Delta m''}{\rho h} \tag{4.26}$$

where ρ is the fluid density and h is the fluid thickness.

Figure 4-7 shows solvent evaporation for a 25-μm spiral coated from the edge of the disk to the center. Evaporation is nearly an order of magnitude higher at the edge

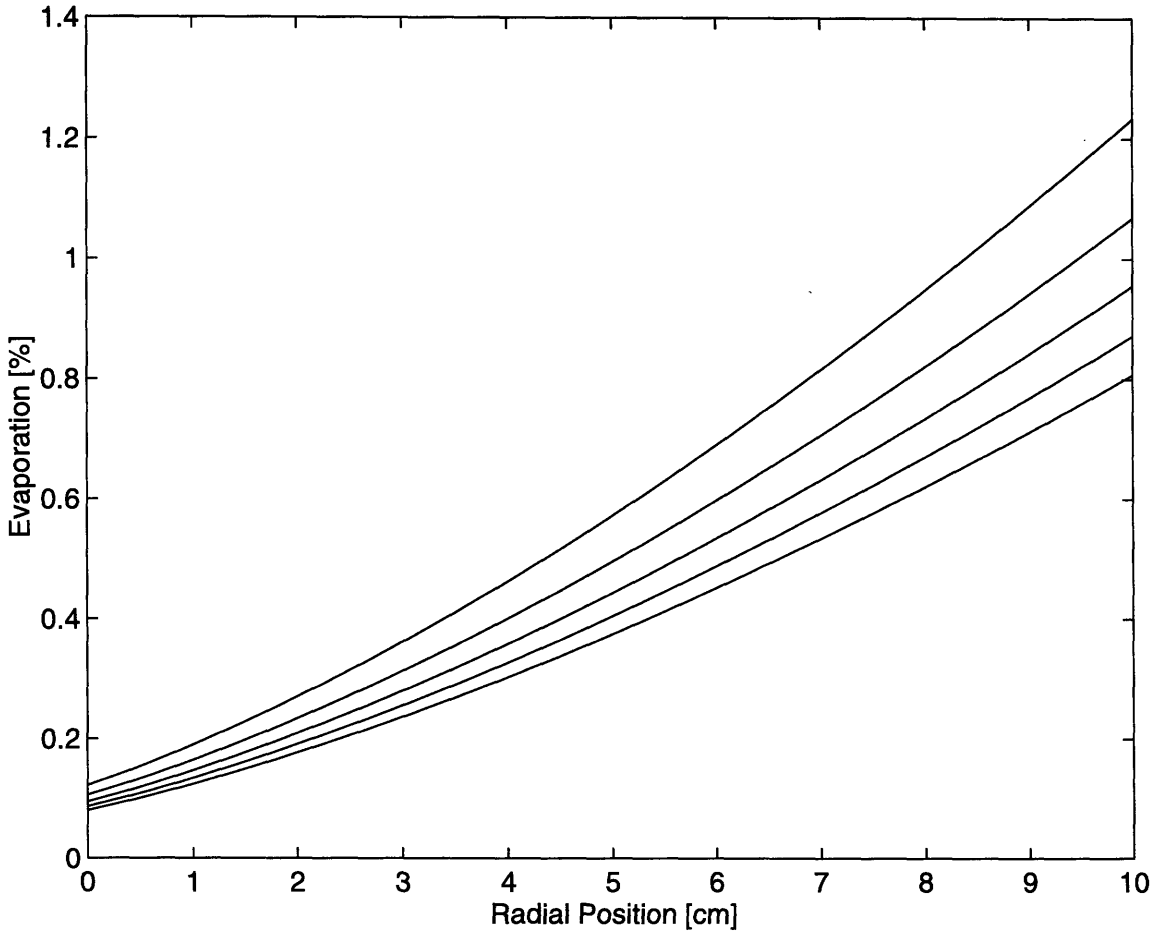

Figure 4-7: Solvent evaporation for a 25-μm thick wet coating for coating velocities of 6, 8, 10, 12, and 14 cm/sec (top to bottom).

of the disk than at the center. Higher coating speeds actually lower the evaporation because coating takes less time. We can thus expect that higher evaporation rates at the edge of the disk will cause the edge of the disk to have higher viscosities and greater film thicknesses than those at the center of the disk.

Figure 4-8 shows the total evaporation effects at the edge of a 20-cm diameter disk. Thinner films have a greater fraction of fluid evaporated because they have less fluid to begin with. Therefore, evaporation has a greater effect on thinner coating films. The results of this model predict that the edges of extrusion-spin coated disks will be thicker than the center, unless solvent evaporation is inhibited significantly.

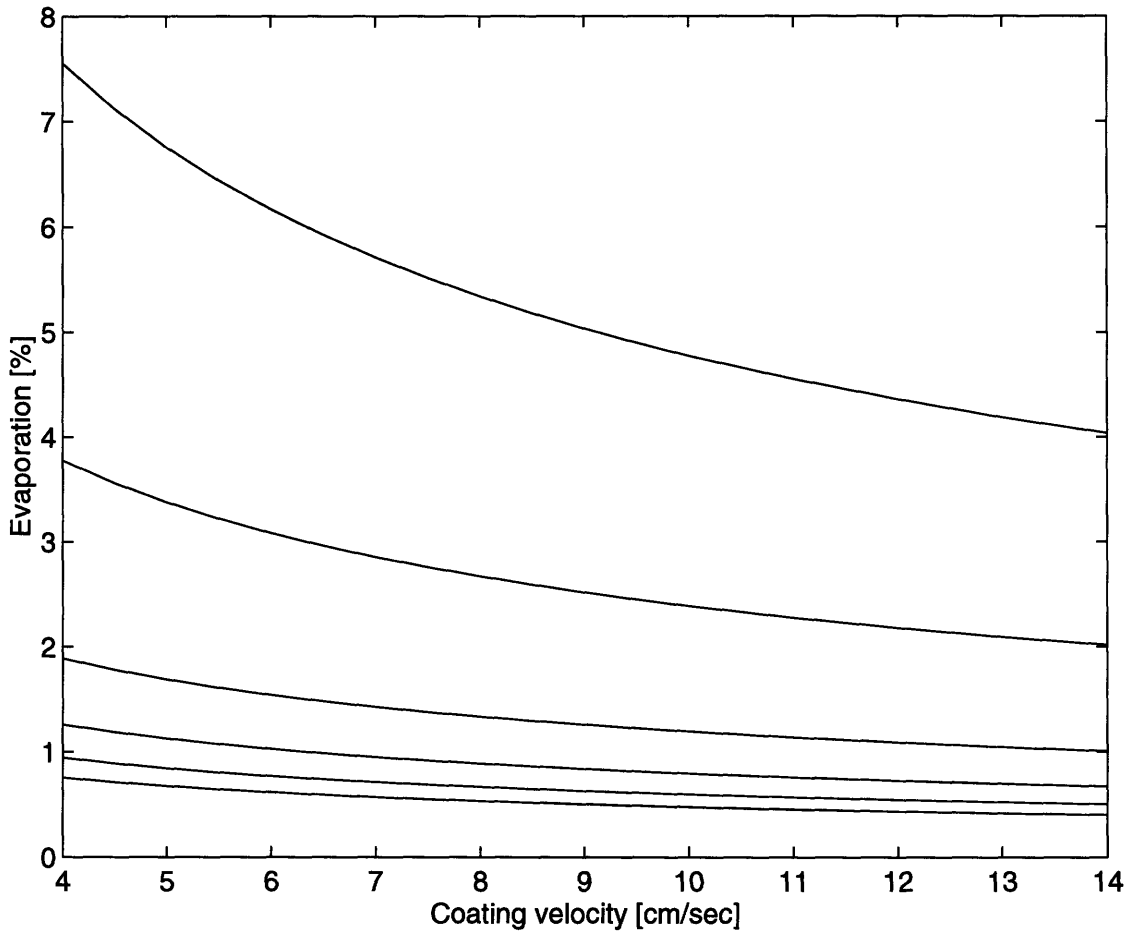

Figure 4-8: Total olvent evaporation at the edge of a disk after coating with wet thicknesses of 5, 10, 20, 30, 40, and 50 μm (top to bottom).

4.4 Extrusion-Spin Coating Efficiency

The extrusion coating process wastes fluid in several ways: lost fluid at the wafer edge, a double layer of fluid at the center, overlap of spiral rings, and fluid thickness in excess of the minimum required thickness. Waste calculations in this section are based on a spiral coating geometry. Figure 4-2 shows the waste that occurs at the outer edge of a disk when a spiral shape starts off the edge of the disk. The volume of fluid wasted in this outer region is approximately half a ring of fluid:

$$\Delta V_{edge} = \pi R w h \tag{4.27}$$

where R is the disk radius, w is the width of one spiral ring, and h is the thickness of the extruded fluid. A second fluid waste is the double layer created by the spiral pattern at the center of the wafer, also shown in Figure 4-2. The excess volume of fluid in the double layer is approximately:

$$\Delta V_{center} = \frac{\pi w^2 h}{6} \tag{4.28}$$

Thirdly, each spiral ring is overlapped with the rings next to it, creating an extra "bump" of fluid (see Figure 4-5(b)) that has an approximate volume of:

$$\Delta V_{overlap} = \pi R^2 h \left(\frac{\Delta w}{w}\right) \tag{4.29}$$

where Δw is the overlap. Fourthly, the uniformity requirements discussed in Section 2.4 require the wet fluid thickness, h, after the initial coating to be thicker than the minimum required wet thickness, h_{min}. This allows for uniformity improvement during a high-speed spin. The excess fluid is the difference between the actual volume used and the minimum theoretical volume of fluid needed to coat a wafer:

$$\Delta V_{thickness} = \pi R^2 (h - h_{min}) \tag{4.30}$$

where $h_{min} (= h_{dry}/c)$ is the minimum theoretical fluid thickness. (See Section 1.2.6.) Fifthly, the excess fluid that is deposited in the center due to the modified spiral shape is:

$$\Delta V_{mod} = \pi r_c^2 h \tag{4.31}$$

Using these wasted volumes, it is evident that the overall efficiency, defined as the fraction of the fluid consumed which actually remains on the wafer after the coating is complete, is:

$$\varepsilon = \frac{\pi R^2 h_{min}}{\pi R w h + \pi R^2 h \left(\frac{\Delta w}{w}\right) + \frac{\pi w^2 h}{6} + \pi R^2 (h - h_{min}) + \pi R^2 h_{min} + \pi r_c^2 h} \tag{4.32}$$

The second, third, and fifth waste volume terms are negligible when there is a small overlap, spiral ring width is less than half the radius of the wafer, and $r_c \leq w$. Figure 4-9 shows the efficiency when these term are ignored and the efficiency reduces to:

$$\varepsilon = \frac{h_{dry}}{hc}\left(\frac{R}{w+R}\right) \tag{4.33}$$

4.5 Defects in Extrusion-Spin Coating

A number of defects can arise when using extrusion-spin coating. Some of these are the same as those which are encountered in extrusion slot coating, while others develop because of the spiral shape of extrusion-spin coating. Only those defects which arise because of the unique features of extrusion-spin coating are discussed below.

4.5.1 Gap Variations Due to Misalignments

Coating defects may arise when the coating gap does not remain constant. In practice, misalignments in extrusion-spin coaters introduce two kinds of errors in the coating gap. First, there is an absolute gap error, ΔG. Second, there is an angle, ϕ, between the extrusion die lips and the substrate, which causes a difference in gap, $\Delta G_\phi (= w \sin\phi)$, between the ends of the extrusion die lips.

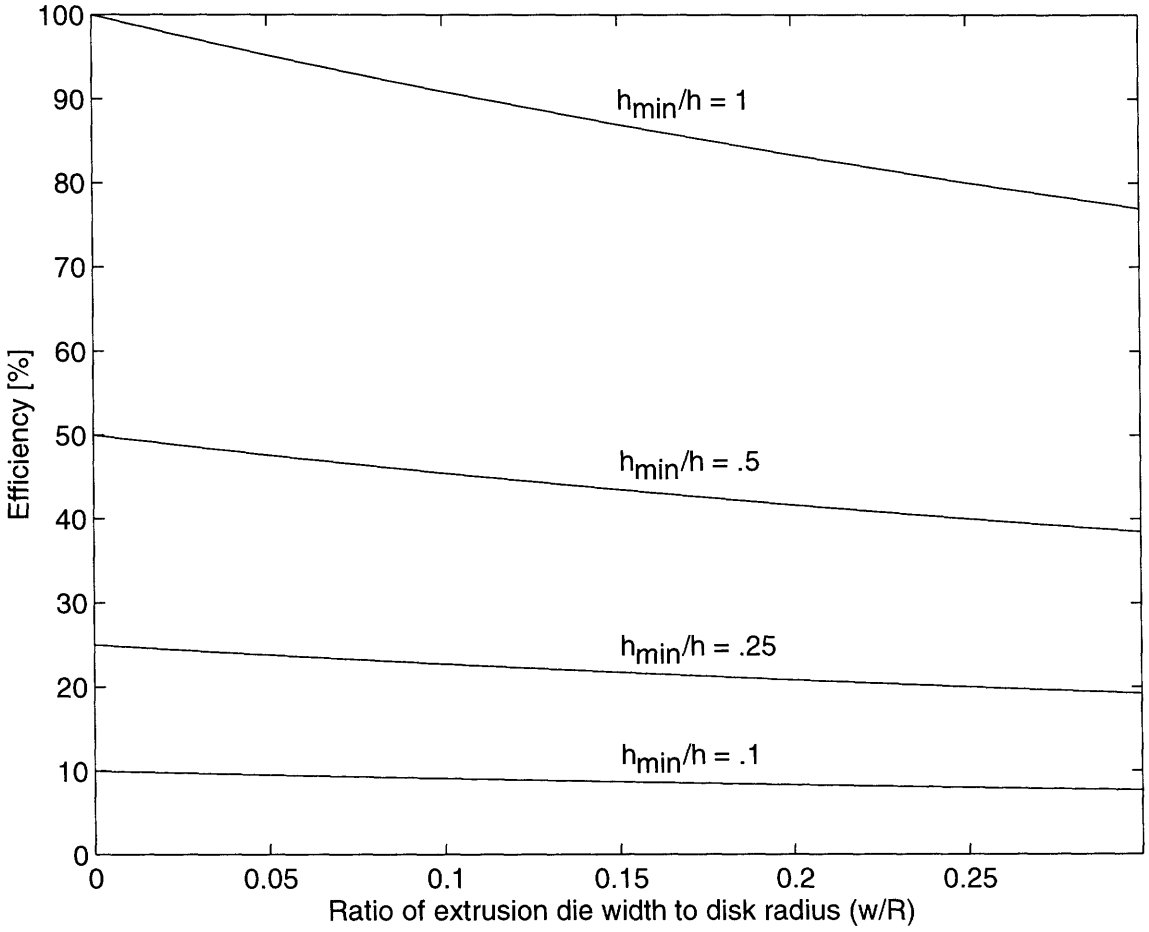

Figure 4-9: Photoresist use efficiency for extrusion-spin coating.

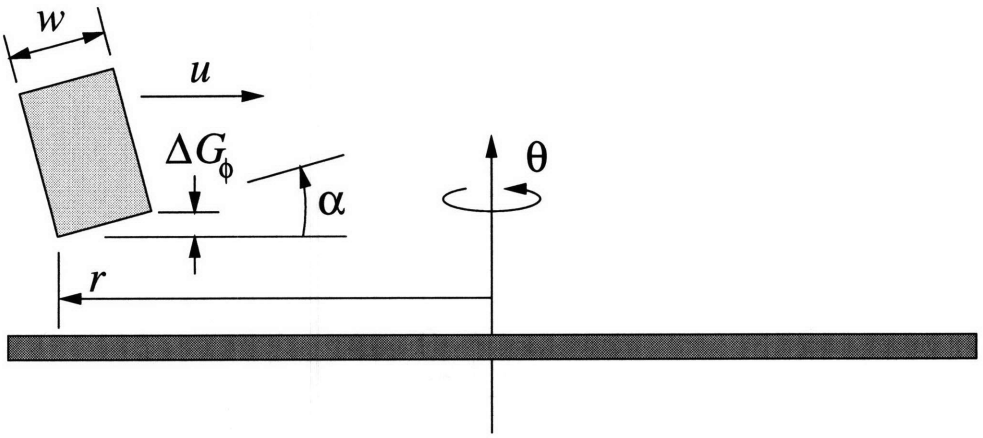

Figure 4-10: Gap error when extrusion die lips are not parallel to the substrate.

Extrusion Head Misalignment with Horizontal Motion Axis

When the extrusion die lips are not parallel to the direction of the motion of the extrusion die, the gap between the extrusion die and the substrate is inconstant. Figure 4-10 shows that the difference in gap from one end of the extrusion slot to the other will be:

$$\Delta G_\phi = \alpha w \tag{4.34}$$

where α is the angle between the extrusion die lips and the substrate.

Spinner Chuck Runout

When the axis of rotation of the disk being coated is not perpendicular to the extrusion die lips, the gap from the extrusion die to the disk varies periodically as shown in Figure 4-11. The magnitude of the gap variation, $\Delta G(\theta)$, is:

$$\Delta G(\theta) = -r \tan(\beta) \cos(2\pi\theta) \tag{4.35}$$

where β is the misalignment angle. The angle between the disk and extrusion die will also vary periodically, causing the gap to vary from one end to the other by a distance:

$$\Delta G_\phi = w \tan(\beta) \cos(2\pi\theta) \tag{4.36}$$

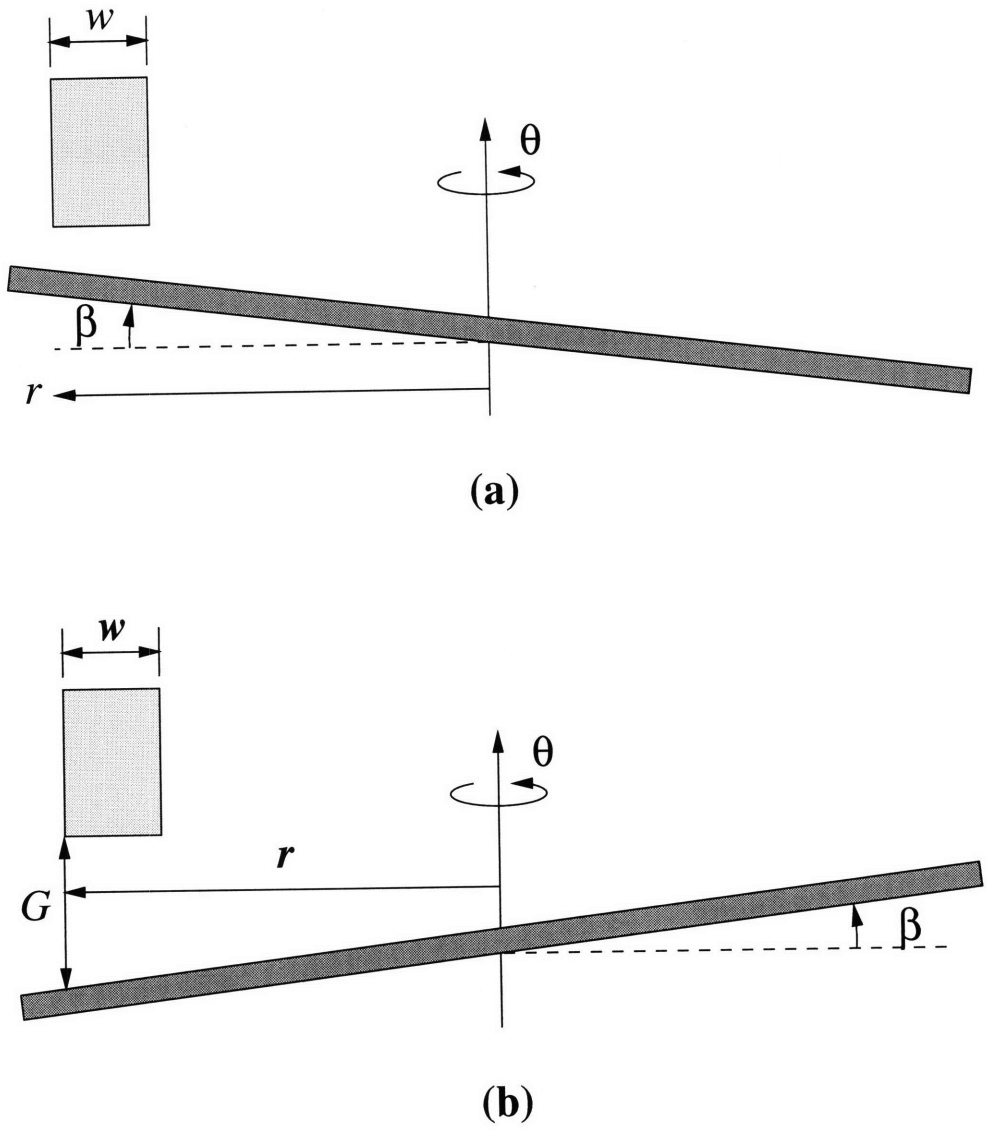

Figure 4-11: Gap error when the coating surface is not perpendicular to the axis of rotation. (a) $\theta = 0°$, (b) $\theta = 180°$.

If a sensor is used to actively control the disk-extrusion die gap, the angle variation will still remain, but the absolute gap error becomes much smaller. The remaining gap error, $\Delta G(\theta)$, is Abbe error which causes periodic gap variation as shown in Figure 4-12:

$$\Delta G(\theta) = -(b + w)\tan(\beta)\cos(2\pi\theta) \tag{4.37}$$

where b is the distance between the sensor measurement point and the inner edge of the extrusion die lips.

Spinner Chuck Axis Misalignment with Horizontal Motion Axis

When the disk rotational axis is not perpendicular to the axis of motion of the extrusion head by an angle, γ, the gap increases linearly with the extrusion head position only when no sensing is used, as shown in Figure 4-13:

$$\Delta G = (r_0 - r)\tan(\gamma) \tag{4.38}$$

Total Misalignment Error

When there is no active control of the gap, the gap error at any radius r is:

$$\Delta G_r(\theta) = -r\tan(\beta)\cos(\theta) + (r_0 - r)\tan\gamma \tag{4.39}$$

where r_0 is the initial radial position of the extrusion die and the angles α, β, and γ are defined in the figures in Section 4.5.1. When a sensor is present, the gap error is:

$$\Delta G_r(\theta) = -(d + w)\tan(\beta)\cos(\theta) \tag{4.40}$$

where w is the extrusion die width and d (=1.5cm) is the distance from the sensor position to the inner edge of the extrusion die. There is also a component of gap change due to the angle of the wafer, which is the same with or without a sensor:

$$\Delta G_\phi(\theta) = w\tan(\alpha) + w\tan(\beta)\cos(\theta) + w\tan(\gamma) \tag{4.41}$$

The angle of the extrusion die with respect to the wafer (for small angles) is then

$$\phi = \frac{\Delta G_\phi}{w} = \alpha + \beta\cos(\theta) + \gamma \tag{4.42}$$

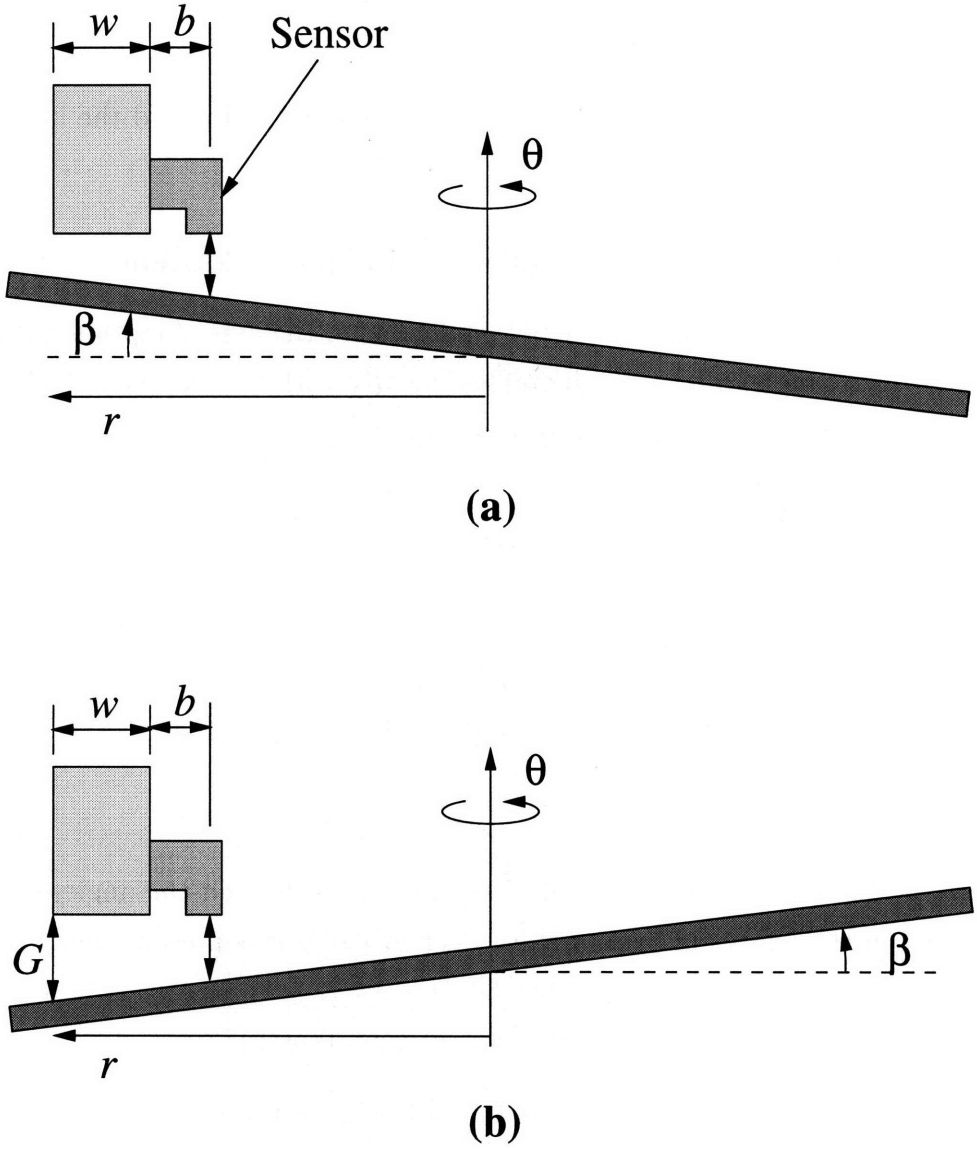

Figure 4-12: Gap error when the coating surface is not perpendicular to the axis of rotation, and a sensor is used to track the coating surface. (a) $\theta = 0°$, (b) $\theta = 180°$.

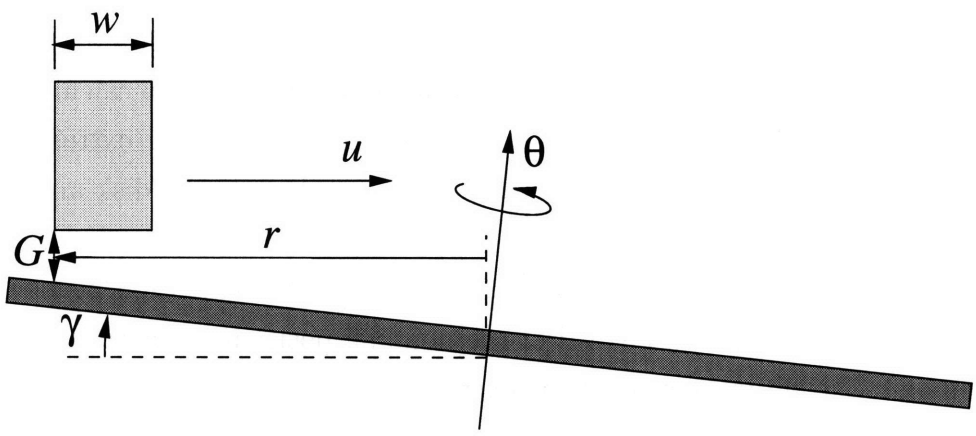

Figure 4-13: Gap error when the axis of rotation is not perpendicular to the axis of extrusion die motion.

From this we can calculate the gap error at the leading edge of the extrusion die, $\Delta G_{r-w}(\theta)$, (when a sensor is used) as:

$$\Delta G_{r-w}(\theta) = \Delta G_r + \Delta G_\phi = -d\tan(\beta)cos(\theta) + w(\tan(\gamma) + \tan(\alpha)) \tag{4.43}$$

4.5.2 Center Defects Due to Misalignment

To get a complete coating, the path of the extrusion slot must pass directly over the axis of rotation of the disk. When the extrusion slot misses the axis of rotation, a round area which has a radius equal to the misalignment is left uncoated. This spot can cause severe defects over the whole surface of the disk during the final high-speed spin.

4.5.3 Overlap Errors

In practice, there are two problems which cause the spiral overlaps to increase or decrease as the spiral develops. First, the overlap changes when the ratio between the extrusion head speed and the chuck rotation rate is inconstant. As the ratio changes, so the overlap changes proportionally according to Equations 4.6 and 4.7.

The second source of overlap changes is a misalignment of the extrusion head with the axis of rotation of the disk. This problem arises because the extrusion

head velocity and the disk spin speed must both be inversely proportional to the radial position, r, of the extrusion head in order to produce a perfect spiral. (See Equations 4.1 and 4.3.) In practice, however, a controller is used to calculate the disk and extrusion head positions. If the actual radial position of the extrusion head is greater than the position used by the controller to calculate the disk and extrusion head speeds, the overlap will increase. If the actual radial position is less than the controller's position, the overlap will decrease. When the extrusion head begins its motion at position $r_0 + \Delta r_0$ instead of the nominal position, r_0, away from the disk rotation axis, the actual motion of the extrusion head will no longer be described by Equation 4.5. Different initial conditions ($r = r_0 + \Delta r_0$ instead of $r = r_0$ at time $t = 0$), cause the actual position of the extrusion head to be:

$$r' = \sqrt{(r_0 + \Delta r_0)^2 - \frac{wv}{\pi}t} \tag{4.44}$$

where r' is the actual position of the extrusion head. Because the angular position of the disk is calculated by the controller based on the nominal position r_0, however, the chuck angular position is still described by Equation 4.8. By inverting Equation 4.8, the time, $t(\theta)$, for any radial position of the chuck can be found as:

$$t(\theta) = \frac{\pi r_0^2}{wv}\left[1 - \left(1 - \frac{w\theta}{2\pi r}\right)^2\right] \tag{4.45}$$

The overlap, $\Delta w(\theta)$, at any angular position along the spiral can then be calculated by taking the difference between two spiral positions one revolution apart and subtracting the extrusion width:

$$\Delta w(\theta) = r'(\theta) - [r'(\theta - 2\pi) - w] \tag{4.46}$$

where θ is measured in revolutions. Figure 4-14 shows the growth in the overlap error for several misalignment values. The final overlap error can be significant even for small initial errors. Figure 4-15 shows the final overlap errors once the leading edge of a 2-cm extrusion head reaches the center of a 20-cm disk. The overlap errors are independent of coating velocity.

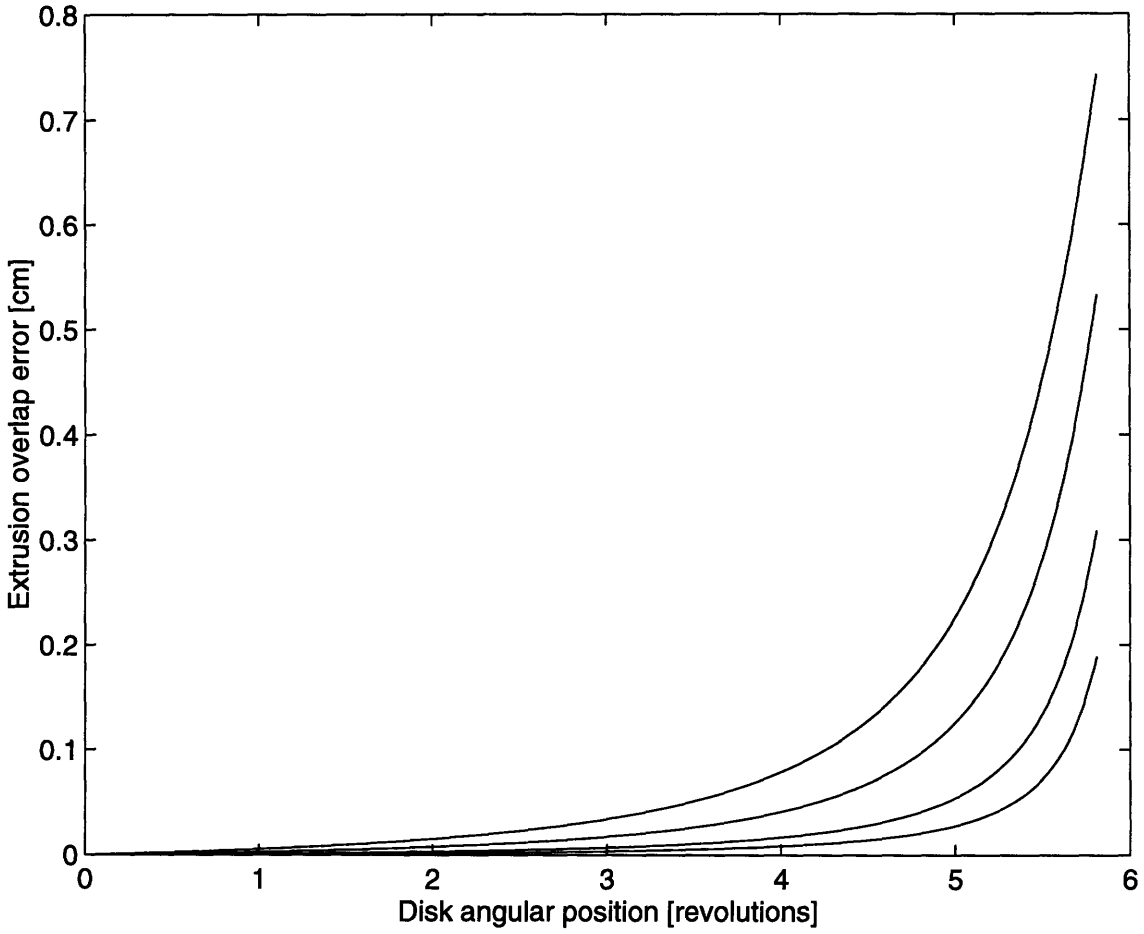

Figure 4-14: Extrusion overlap error for extrusion die misalignments of 0.01, 0.02 0.05, and 0.1 cm (bottom to top).

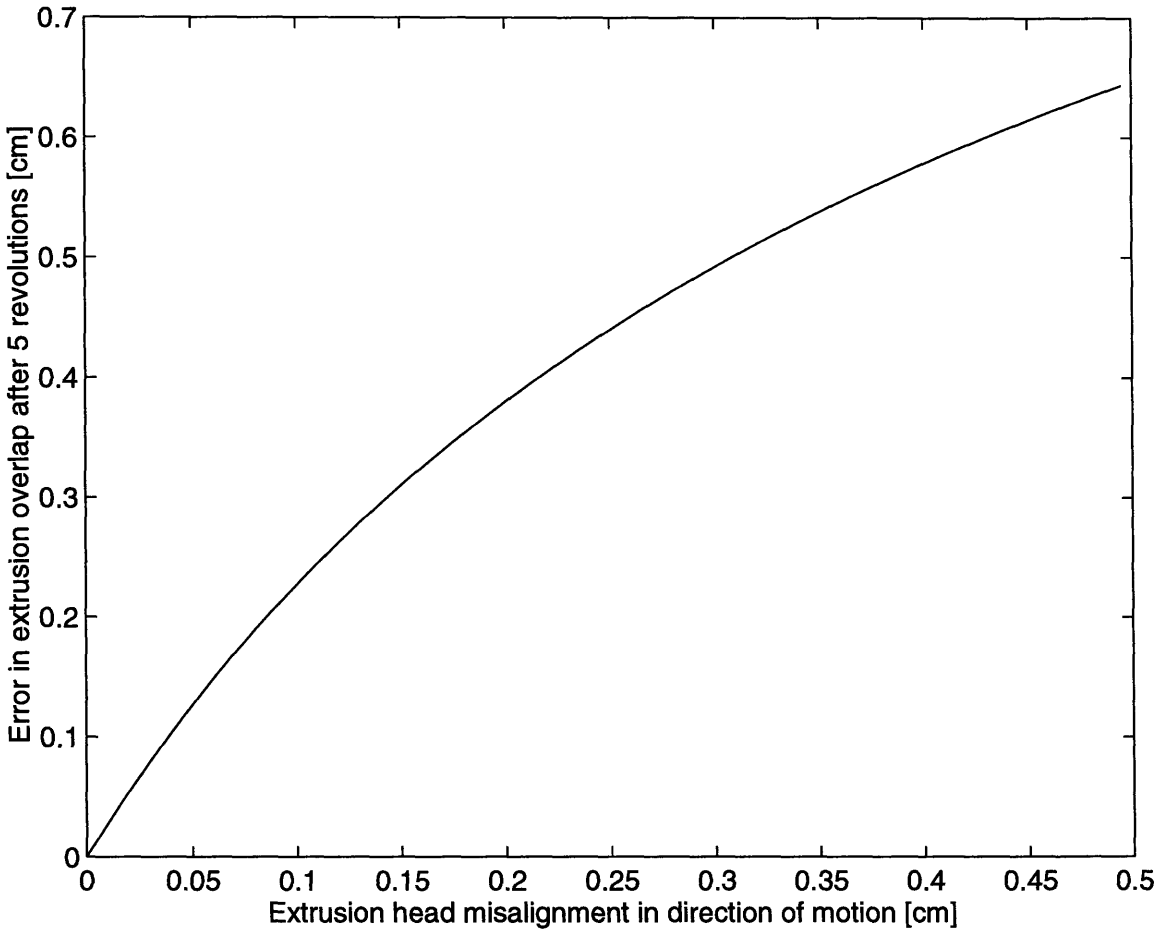

Figure 4-15: Extrusion overlap errors after 5 revolutions (i.e., when the leading edge of the extrusion die reaches the center of the disk). $w = 2$.

4.6 Evaluation of Extrusion-Spin Coating

Using many of the analyses in this chapter and Chapter 3, a coating window for extrusion-spin coating can be developed, as shown in Figure 4-16. Efficiency requires the coating thickness be less than the maximum allowed by Equation 4.33. The maximum time requirement mandates a minimum coating speed, as discussed in Section 4.2. Evaporation is also decreased at higher coating speeds, as discussed in Section 4.3.4. The low-flow limit of coatability puts a limit on the maximum coating speeds and minimum coating thicknesses, as discussed in Chapter 3. Within these limits acceptable extrusion-spin coatings can be made.

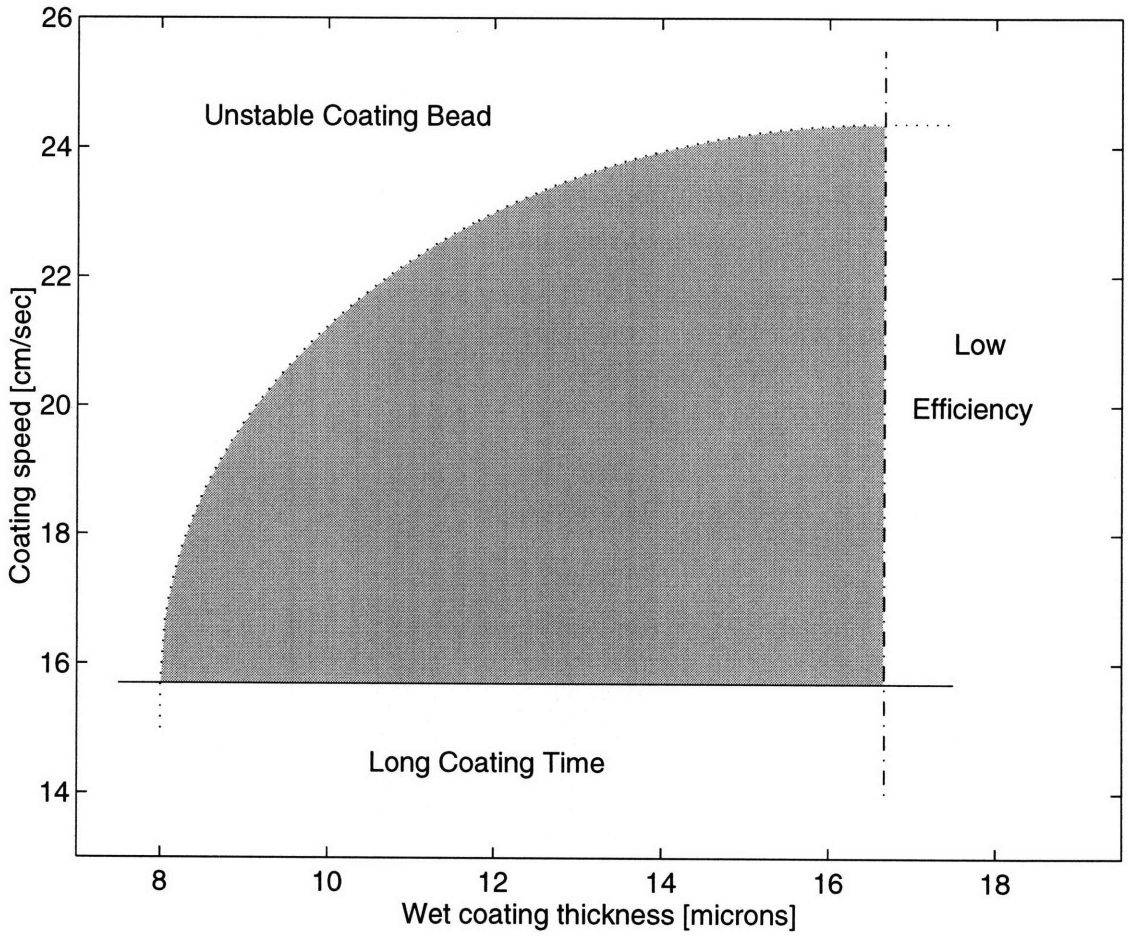

Figure 4-16: Coating window for extrusion-spin coating. 20-second coating time (—), 25% efficiency (– · – ·), bead stability limits (· · ·) which are dependent on the viscosity and other properties of the coating fluid.

Chapter 5

Fluid Spreading Models

Because the fluid thickness is not uniform after extrusion spiral coating, a simple model is needed to describe the spreading of "bumps" or "valleys" created during coating. The overlaps between spiral rings will be investigated in particular. To determine which physical phenomena should be included in the model, the dimensionless groups which show the relative importance of each phenomenon can be compared. The Bond number represents the ratio of gravitational forces to surface tension forces:

$$Bo = \frac{\rho g a^2}{\sigma} \tag{5.1}$$

where ρ is the density, g is the acceleration due to gravity, a is the characteristic length, and σ is the surface tension. The Weber number is the ratio of inertia to surface tension forces:

$$We = \frac{\rho U^2 a}{\sigma} \tag{5.2}$$

where U is the characteristic velocity. The Capillary number is the ratio of viscous to surface tension forces:

$$Ca = \frac{\mu U}{\sigma} \tag{5.3}$$

where μ is viscosity.

Both the Weber and Capillary numbers depend on the unknown characteristic fluid velocity in the bump. To determine the relative importance of the three parameters, their magnitude can be plotted as a function of the velocity. Figure 5-1 shows that the Weber number (i.e., inertial force) dominates at high velocities, the

Capillary number (i.e., viscous force) dominates at medium velocities, and the Bond number (i.e., gravitational force) dominates at very low velocities.

During spreading, a bump progresses through each of these three spreading regimes. When first created, a bump or valley has a high radius of curvature, and thus a large pressure gradient from surface tension forces. The initially large pressure gradient leads to large fluid velocities dominated by inertial forces. As the bump or valley spreads, the curvature of the fluid decreases dramatically, and the viscous forces slow down the fluid. At lower velocities the viscous retarding forces become more significant than the inertial forces. Eventually as the spreading velocity decreases to near zero, the gravitational forces become significant. Since dominance of the inertial forces occurs only at high velocities, the inertial spreading time should be much smaller than the spreading time under the dominance of viscous forces. Thus we can approximate bump spreading by using a model which balances the spreading force due to surface tension with the retarding viscous force.

5.1 Two-Dimensional Spreading Model

To develop a model for spreading due to surface tension, locally fully-developed viscous flow was assumed for the case when two fluid layers overlap. Other assumptions were made as follows:

- no air is trapped beneath the two layers
- the two layers join to form an isotropic fluid bump
- far from the bump the fluid has uniform thickness, h
- the fluid does not evaporate
- surface tension is uniform across the surface of the fluid

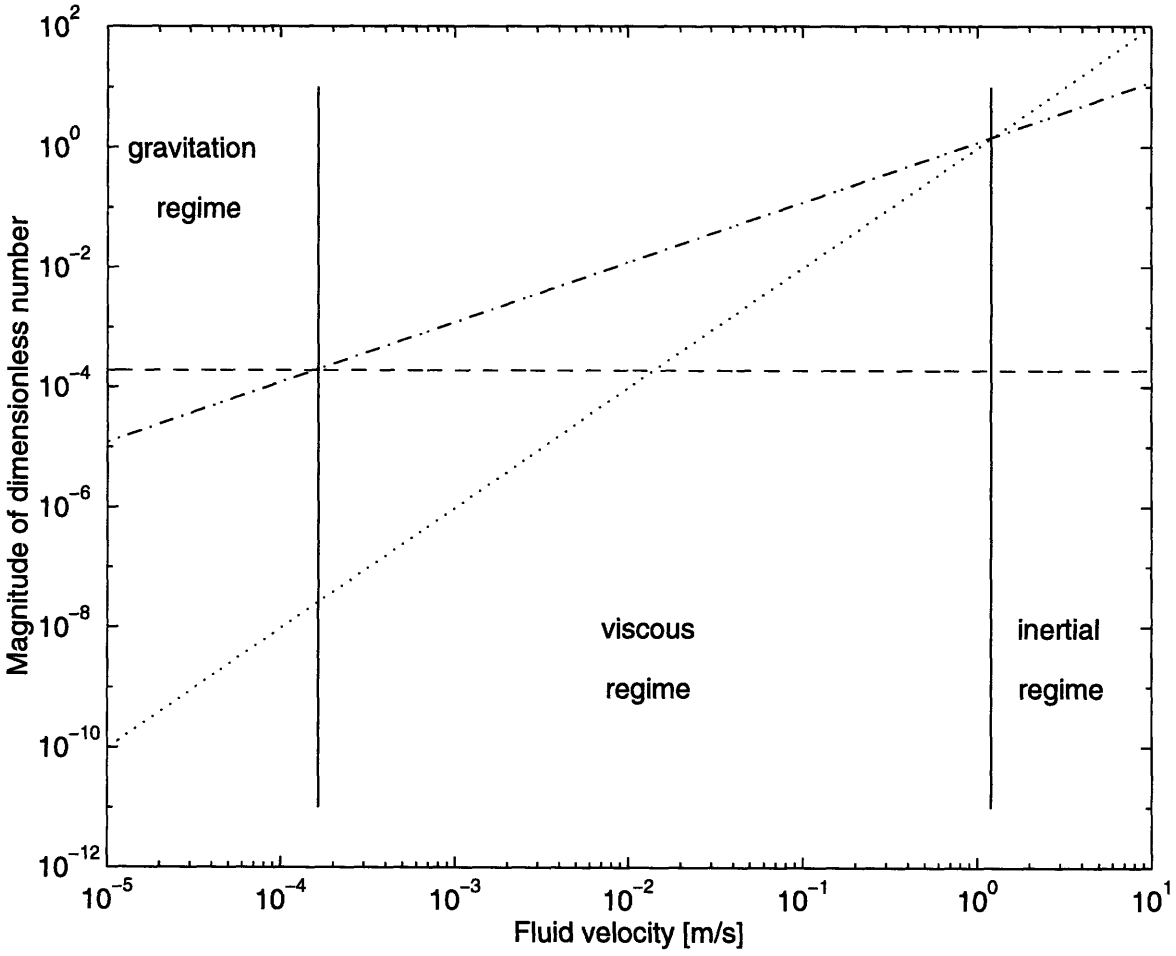

Figure 5-1: Regime map for photoresist bump spreading. Dimensionless numbers plotted are Bond number (– –), Weber number ($\cdots$), and Capillary number (– $\cdot$ – $\cdot$). $a = 10\mu$m, $g = 9.8$ m/s, $\rho = 1.06$ g/cm, $\sigma = 0.022$ N/m, $\mu = 0.0265$ Pa-sec.

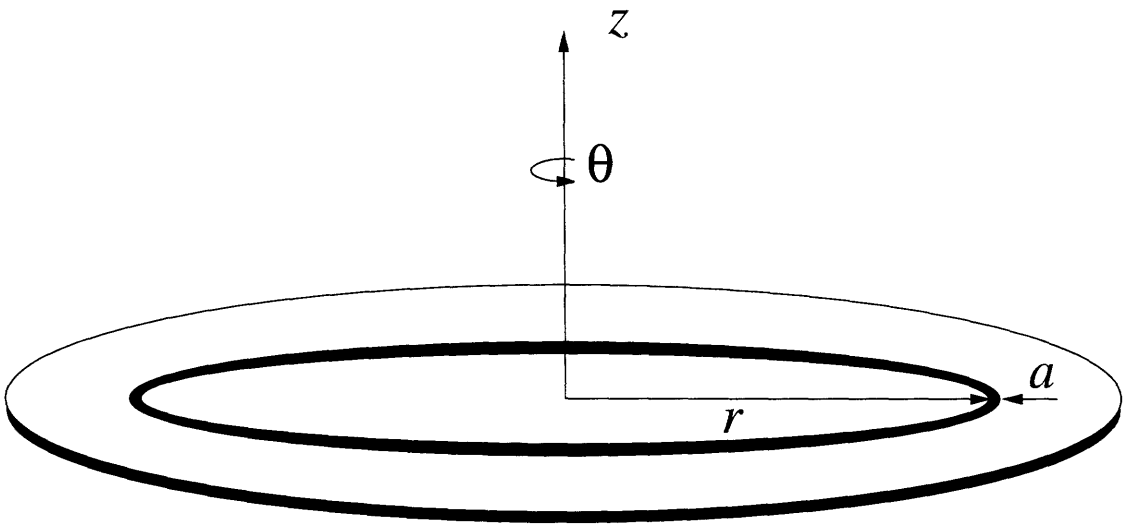

Figure 5-2: Coordinates for bump spreading model.

If the spiral is approximated as circular, cylindrical coordinates can be used for the spinning disk shown in Figure 5-2 and the flow can be approximated as axisymmetric. Most of the inertial terms and the viscous terms can be eliminated from the Navier-Stokes equations in the θ and z directions to obtain:

$$-\rho\dot{\theta}^2 r = -\frac{\partial p}{\partial r} + \mu\frac{\partial^2 u}{\partial z^2} \tag{5.4}$$

and:

$$0 = -\frac{\partial p}{\partial z} - \rho z \tag{5.5}$$

where u is the fluid velocity in the r direction, p is the pressure, μ is the fluid viscosity, ρ is the density, and g is the acceleration due to gravity. Assuming small changes in fluid thickness, h, at the fluid surface ($z = h$), the boundary condition is:

$$p_{atm} - p_{in} = \sigma\frac{\partial^2 h}{\partial r^2} \tag{5.6}$$

where p_{atm} is the atmospheric pressure outside the fluid layer and p_{in} is the pressure just inside the fluid surface. Equation 5.5 can be integrated to obtain:

$$p = p_{atm} + \rho g(h - z) - \sigma\frac{\partial^2 h}{\partial r^2} \tag{5.7}$$

Differentiating Equation 5.7 with respect to r, substituting into Equation 5.4, and integrating twice with respect to z give an equation for the fluid velocity:

$$u = \frac{1}{\mu}\left(\rho g\frac{\partial h}{\partial r} - \rho\dot{\theta}^2 r - \sigma\frac{\partial^3 h}{\partial r^3}\right)\left(\frac{z^2}{2} + hz\right) \tag{5.8}$$

Then integrating from $z = 0$ to h leads to an expression for the fluid flow rate:

$$Q = \frac{2\pi r h^3}{3\mu}\left(\rho g\frac{\partial h}{\partial r} - \rho\dot{\theta}^2 r - \sigma\frac{\partial^3 h}{\partial r^3}\right) \tag{5.9}$$

Satisfying the continuity of a fluid element of width Δr and height h requires:

$$\frac{\partial}{\partial t}(2\pi r\Delta r h) + \frac{\partial Q}{\partial r}\Delta r = 0 \tag{5.10}$$

Canceling Δr and substituting for Q, a differential equation is obtained for the fluid height as a function of time:

$$\frac{\partial h}{\partial t} + \frac{1}{3\mu r}\frac{\partial}{\partial r}\left[rh^3\left(\rho g\frac{\partial h}{\partial r} - \rho\dot{\theta}^2 r\right)\right] = \frac{\sigma}{3\mu r}\frac{\partial}{\partial r}\left[rh^3\frac{\partial^3 h}{\partial r^3}\right] \tag{5.11}$$

This equation is only valid for thin fluid layers with small changes in fluid height that satisfy the following requirements:

$$\frac{h^2}{\nu\tau} << 1 \tag{5.12}$$

$$\frac{uh^2}{\nu a} << 1 \tag{5.13}$$

$$\left(\frac{h}{a}\right)^2 << 1 \tag{5.14}$$

where ν is the kinematic viscosity, τ is the timescale of fluid motion, and a is the length scale in the r direction over which the fluid motion occurs.

The order of magnitude of the timescale for spreading due to surface tension can be calculated by equating the first term in Equation 5.11 to the surface tension term (on the right side). This yields:

$$\tau \sim \frac{\mu a^4}{\sigma h^3} \tag{5.15}$$

	$h = 10\mu$m	$h = 5\mu$m	$h = 1\mu$m	$h = .2\mu$m
$a = 200\ \mu$m	1.93	15.4	1.93×10^{3}	2.41×10^{5}
$a = 100\ \mu$m	0.12	0.964	120	1.51×10^{4}
$a = 50\ \mu$m	7.53×10^{-3}	6.02×10^{-2}	7.53	941
$a = 20\ \mu$m	1.93×10^{-4}	1.54×10^{-3}	0.193	24.1
$a = 10\ \mu$m	1.2×10^{-5}	9.64×10^{-5}	1.2×10^{-2}	1.51

Table 5.1: Order of magnitude values of bump spreading time constant, τ [seconds].

where τ is the timescale of spreading for a bump. From this time constant it is apparent that spreading is faster when bumps are narrower, when the fluid thickness is greater, when surface tension is greater, and when viscosity is smaller. Since r increases and h decreases as the bump spreads, it is expected that the bump spreading speed will decrease even faster as the bump spreads.

Table 5.1 lists values of the time constant for a photoresist having a viscosity of 26.5 mPa-sec and a surface tension of 22 dyne/cm. For an initial bump half-width, a, of 10 μm and a coating thickness, h, of 10 μm, the time constant is very small, and spreading is very fast. As the bump spreads to a 100 μm half-width, the height of the bump decreases to approximately 1 μm, and the spreading time constant increases by a factor of 10^7. Thus it is evident that the rate of bump spreading changes dramatically as the height of the bump changes.

5.2 Average Flow and Pressure Model

In the region where viscous forces are dominant in balancing the surface tension forces, the bump spreading flow can be modeled in the following manner:

- assume a reasonable shape for the bump
- calculate the surface tension forces which arise from the curvature of the fluid surface
- calculate the pressure gradient created by the surface tension forces
- calculate the flow rate which would occur in a thin layer of fluid with an equivalent pressure gradient and thickness

- using the flow rate, calculate a new bump profile with a similar shape
- repeat the above process in small time steps to determine bump profile evolution
- use several profile shapes to determine how much the assumed shape affects the outcome

5.2.1 Polynomial Shape

Figure 5-3 shows a forth-order polynomial bump on a thin layer of fluid. To get a reasonable shape, it is assumed that the bump is symmetric and has zero slope at its edges. The equation which describes its shape is:

$$z = l\left[\left(\frac{x}{a}\right)^4 - 2\left(\frac{x}{a}\right)^2 + 1\right] \tag{5.16}$$

where l is bump thickness, a is the half-width of the bump, and h is the thickness of the film on which the bump is located. Integrating the profile yields the area of the bump:

$$A = \frac{8}{15}la \tag{5.17}$$

The curvature of the bump surface at a distance, x, from the center is:

$$\kappa = \frac{d^2z/dx^2}{[1+(dz/dx)^2]^{3/2}} = \frac{l\left(\frac{12x^2}{a^4} - \frac{4}{a^2}\right)}{\left[1 + l^2\left(\frac{4x^3}{a^4} - 4\frac{x}{a^2}\right)^2\right]^{3/2}} \tag{5.18}$$

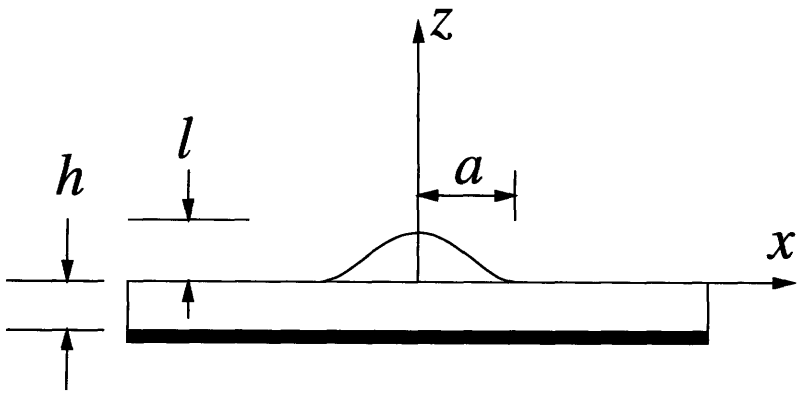

Figure 5-3: Coordinates for bump evolution of a polynomial shaped profile.

The pressure drop across the fluid surface due to surface tension forces is then:

$$\Delta p = p - p_0 = -\sigma\kappa \tag{5.19}$$

By taking the derivative of the pressure drop with respect to x and integrating from x=0 to x=a, the average pressure gradient along the profile can be found:

$$\left(\frac{\partial p}{\partial x}\right)_{avg} = \frac{1}{a}\left(\int_0^r \frac{\partial p}{\partial x}\right) = \frac{1}{a}\left(\Delta p\,|_{x=0}^{x=a}\right) = -\frac{12\sigma l}{a^3} \tag{5.20}$$

Assuming constant density, conservation of mass for the photoresist in the bump results in:

$$\frac{dQ_x}{dx} = -\frac{dz}{dt} \tag{5.21}$$

where Q_x is the flow rate of photoresist in the x-direction. By integrating $\frac{dQ_x}{dx}$ twice from x=0 to x=a and dividing by a, the average flow rate for a change in bump thickness can be found. Using Equation 5.17 to simplify the result yields:

$$\bar{Q}_x = -\frac{a}{6}\frac{dl}{dt} \tag{5.22}$$

The average thickness of the bump can be found by integrating z from x=0 to x=a and dividing by a:

$$\bar{z} = -\frac{8}{15}l \tag{5.23}$$

Using the average pressure, flow rate and bump thickness, the evolution of the bump thickness can be calculated by using the viscous flow approximation:

$$\bar{Q}_x = \frac{-(\bar{z}+h)^3}{6\mu}\left(\frac{\partial p}{\partial x}\right)_{avg} \tag{5.24}$$

Substituting Equations 5.20, 5.22, and 5.23 into Equation 5.24 yields a first order differential equation for the bump thickness:

$$\frac{dl}{dt} = -\frac{16,384}{16,875}\frac{\sigma l^5}{\mu A^4}\left(\frac{8}{15}l + h\right)^3 \tag{5.25}$$

Using fourth-order Runge-Kutta numerical integration, the bump thickness was calculated as a function of time. Figure 5-4 shows that bumps which are initially thicker take longer to spread, but the differences in spreading time are small compared

to the overall spreading time. Figure 5-5 shows that the photoresist overlap has a significant effect on the spreading time. The time needed to reduce a 10-μm bump to a thickness of 0.2 μm is only 2 seconds if the overlap is 20 μm, but it takes 37 seconds if the overlap is 40 μm. Thus the overlap must be as small as possible.

5.2.2 Sinusoidal Shape

Using a sinusoidally-shaped bump with the same coordinates as in Figure 5-3, the equation which describes the bump is:

$$z = \frac{l}{2}\left[\cos\left(\frac{\pi x}{a}\right) + 1\right] \tag{5.26}$$

where l is bump thickness, a is the half-width of the bump, and h is the thickness of the film on which the bump is located. Integrating the profile, the area of the bump can be found to be:

$$A = \frac{1}{2}la \tag{5.27}$$

By the same method as the polynomial bump, the average pressure gradient along the profile can be determined:

$$\left(\frac{\partial p}{\partial x}\right)_{avg} = -\frac{\pi^2 \sigma l}{a^3} \tag{5.28}$$

Assuming constant density, conservation of mass for the photoresist in the bump results in:

$$\frac{dQ_x}{dx} = -\frac{dz}{dt} \tag{5.29}$$

where Q_x is the flow rate of photoresist in the x-direction. By integrating $\frac{dQ_x}{dx}$ twice from x=0 to x=a and dividing by a, the average flow rate for a change in bump thickness can be found. To do this, Equation 5.17 is used to simplify the result:

$$\bar{Q}_x = -\frac{\pi^2 - 4}{4\pi^2} a \frac{dl}{dt} \tag{5.30}$$

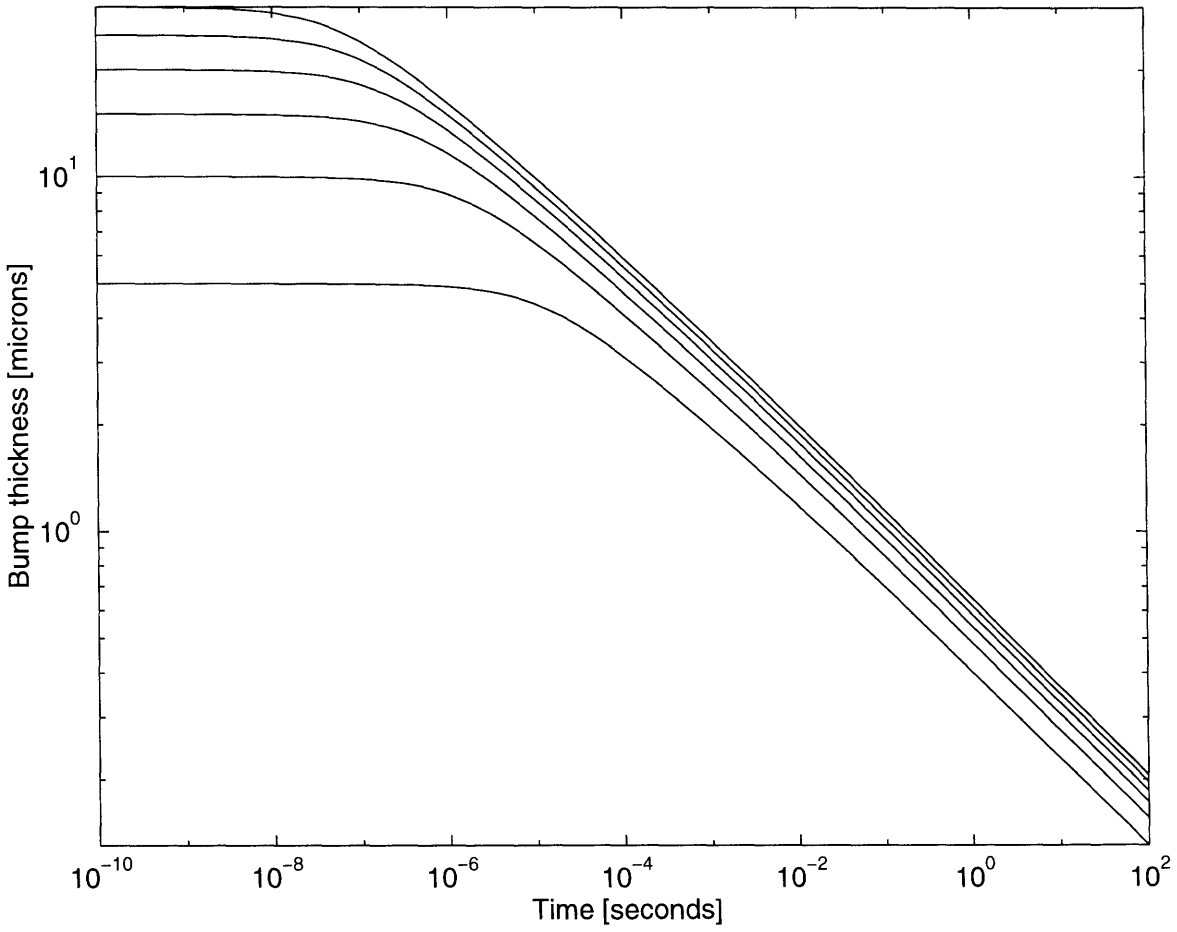

Figure 5-4: Bump thickness evolution. Fluid thickness, h = initial bump thickness, l_0 = 5, 10, 15, 20, 25, 30 μm (bottom to top). a_0 = 20 μm, σ = 0.022 N/m, μ = 0.0265 Pa-sec.

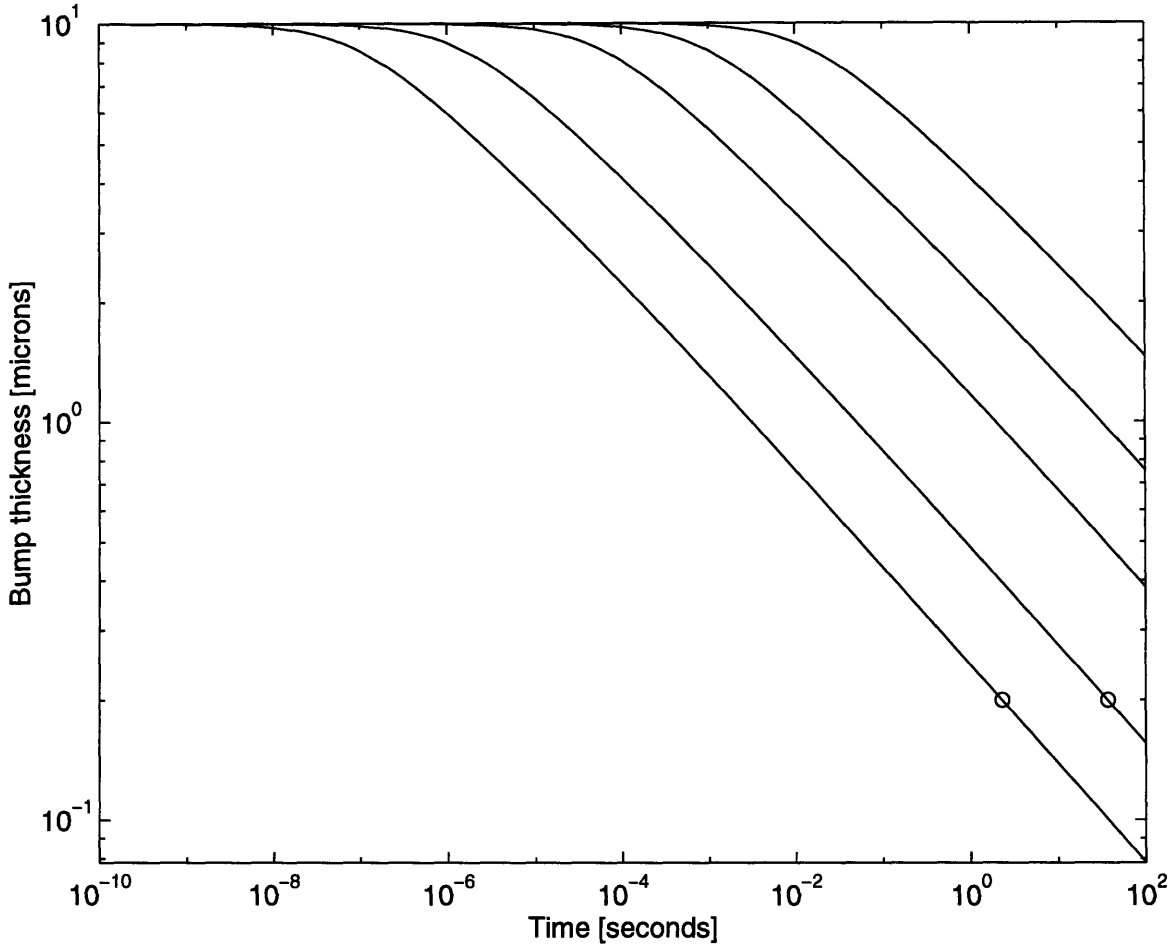

Figure 5-5: Bump thickness evolution. Fluid layer half-overlaps, a_0, = 10, 20, 50, 100, 200 μm (bottom to top). $h = l_0 = 10$ μm, $\sigma = 0.022$ N/m, $\mu = 0.0265$ Pa-sec.

The average thickness of the bump can be found by integrating z from x=0 to x=a and dividing by a:

$$\bar{z} = -\frac{1}{2}l \tag{5.31}$$

Using the average pressure, flow rate and bump thickness, the evolution of the bump thickness can be calculated by using the viscous flow approximation:

$$\bar{Q}_x = \frac{-(\bar{z}+h)^3}{6\mu}\left(\frac{\partial p}{\partial x}\right)_{avg} \tag{5.32}$$

Substituting Equations 5.28, 5.30, and 5.31 into Equation 5.32 yields a first order differential equation for the bump thickness:

$$\frac{dl}{dt} = -\frac{\pi^2}{24(\pi^2-4)}\frac{\sigma l^5}{\mu A^4}\left(\frac{1}{2}l+h\right)^3 \tag{5.33}$$

Figure 5-6 compares the polynomial and sinusoidal models. Since both models produce similar bump spreading rates, it appears as if the assumed shape of the bump does not significantly affect the results.

5.3 Summary of Fluid Spreading Results

The bump spreading models indicate that fluid bumps will spread rapidly during the initial stages after they are created, but that the spreading will slow significantly after several seconds. More experimental investigation must be done to determine the actual rates at which these bumps spread out and their effect on the coating thickness after the final high-speed spin.

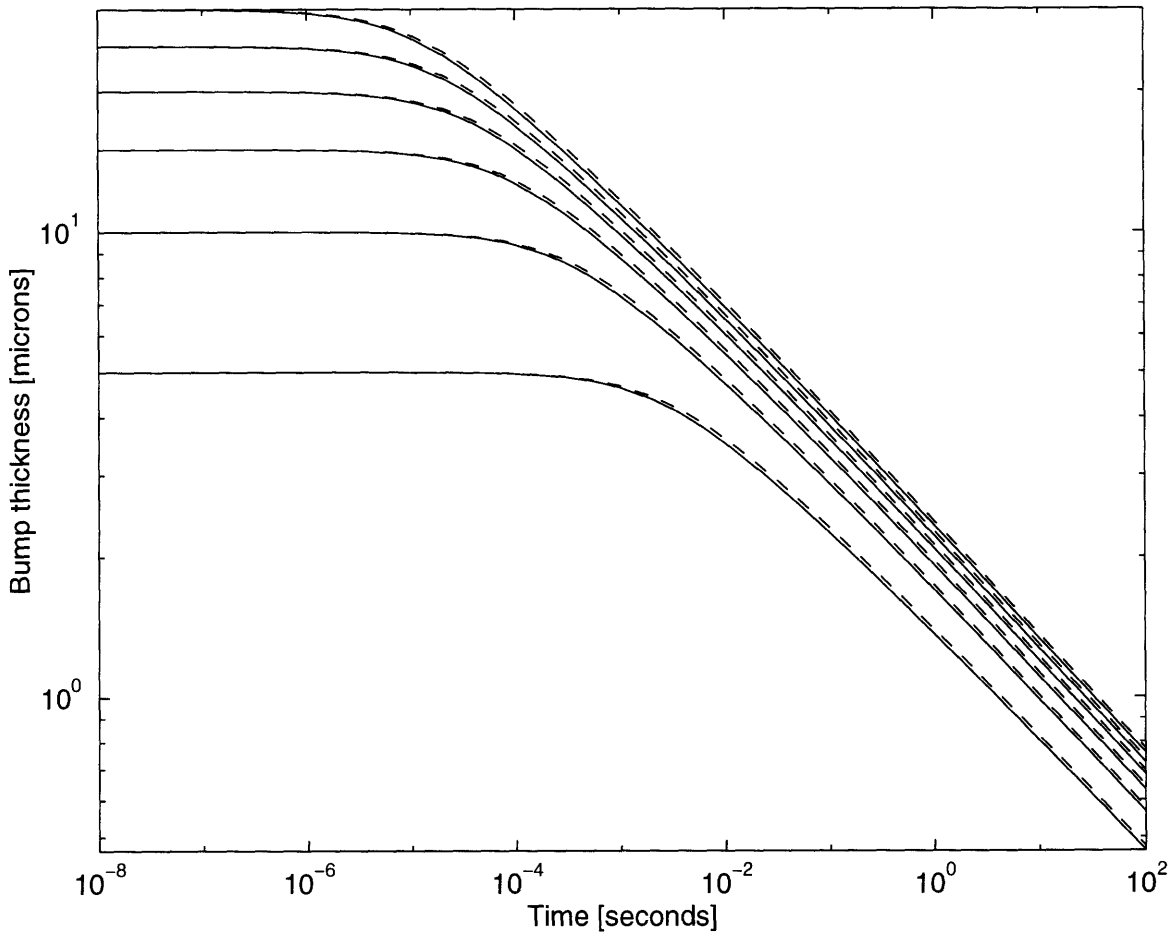

Figure 5-6: Comparison of polynomial (—) and sinusoidal (- -) bump thickness evolution. Fluid thickness, h = initial bump thickness, l_0 = 5, 10, 15, 20, 25, 30 μm (bottom to top). $a_0 = 100$ μm, $\sigma = 0.030$ N/m, $\mu = 0.011$ Pa-sec.

Chapter 6

Extrusion-Spin Coater Prototype

The experimental coater developed for testing the extrusion-spin coating process consists of many components linked together by control equipment. The coater consists of an x-z positioning system mounted on top of a spin coating module. The x-z positioning system positions an extrusion die relative to the spinner while photoresist is dispensed through the die from a pump. Each system is described below.

6.1 Spinner Module

The spinner for the extrusion-spin coater is an SVG 90SE coater module (one component of an SVG 90SE Wafer Processing Track). The heart of the coater module is a spinner assembly consisting of the spinner servomotor connected to a long, vertical shaft which supports a Teflon vacuum chuck. The entire spinner assembly can be moved vertically using another servomotor (chuck elevator motor). The chuck is surrounded by a catch cup at the lowest position of the spinner assembly. The catch cup serves three purposes: it catches and drains waste photoresist flung off the wafer; it has an exhaust vent through which evaporated solvent is removed; and it directs the flow of air over the wafer to avoid turbulence. (See Figure 6-2.) A centering device at the top of the coater module has eight Teflon pins for centering wafers on the chuck and three vertical pins for supporting loose wafers before and after processing. Sensors on the coater module indicate chuck vertical home position, vacuum state (on/off), and centering pin position.

6.2 Positioning System

On top of the coater module is an aluminum base plate 50 cm deep by 81 cm wide which supports the positioning system shown in Figures 6-1, 6-2, and 6-3. Two vertical aluminum plates 38 cm high on top of the base support a cross-support 81 cm long on which a two-axis positioning system is mounted. The positioning system consists of two Parker Daedal Motion Tables capable of 25 cm of motion driven by 5-pitch ball screws. The "z-axis" positioning table is mounted on the carriage of the "x-axis" positioning table. The x-axis table moves in a horizontal direction parallel to the surface of the wafer, and the z-axis table moves in a vertical direction perpendicular to the surface of the wafer. The extrusion head is mounted at the bottom of an aluminum support mounted on the z-axis table. The extrusion head can be positioned above the base plate or moved down into the spinner area of the coater module through a 25 cm-by-25 cm hole in the base plate.

6.3 Control System

6.3.1 Control Hardware

Control of the experimental extrusion-spin coater is divided into two systems: the positioning controller and the spinner controller. The main controller is a Parker Compumotor AT6450 Controller, a Pentium-based card which has four channels of servomotor control, an analog to digital converter, and digital inputs and outputs. Two servomotor outputs control the x and z-axis positioning table motion using Parker Compumotor SM232 brushless servomotors and Parker Compumotor TQ10 torque (current) amplifiers. A third servomotor output controls the spinner elevator motor. The optically isolated digital inputs of the controller allow input of vacuum on/off status, centering pin in/out position, manual positioning commands, and start/stop and error communication with the spinner controller. The digital outputs of the controller send signals to the spinner controller, dispense pump, vacuum solenoid, centering solenoid, z-axis motor brake, spinner elevator motor brake, and photoresist on/off valve. A 14-bit AD converter records the voltage from a Philtec RC140L optical sensor which measures the gap between the extrusion head and the wafer. The sensor voltage is updated in the controller every 3.5 ms. Programs downloaded from a PC to the controller produce the desired coating motion.

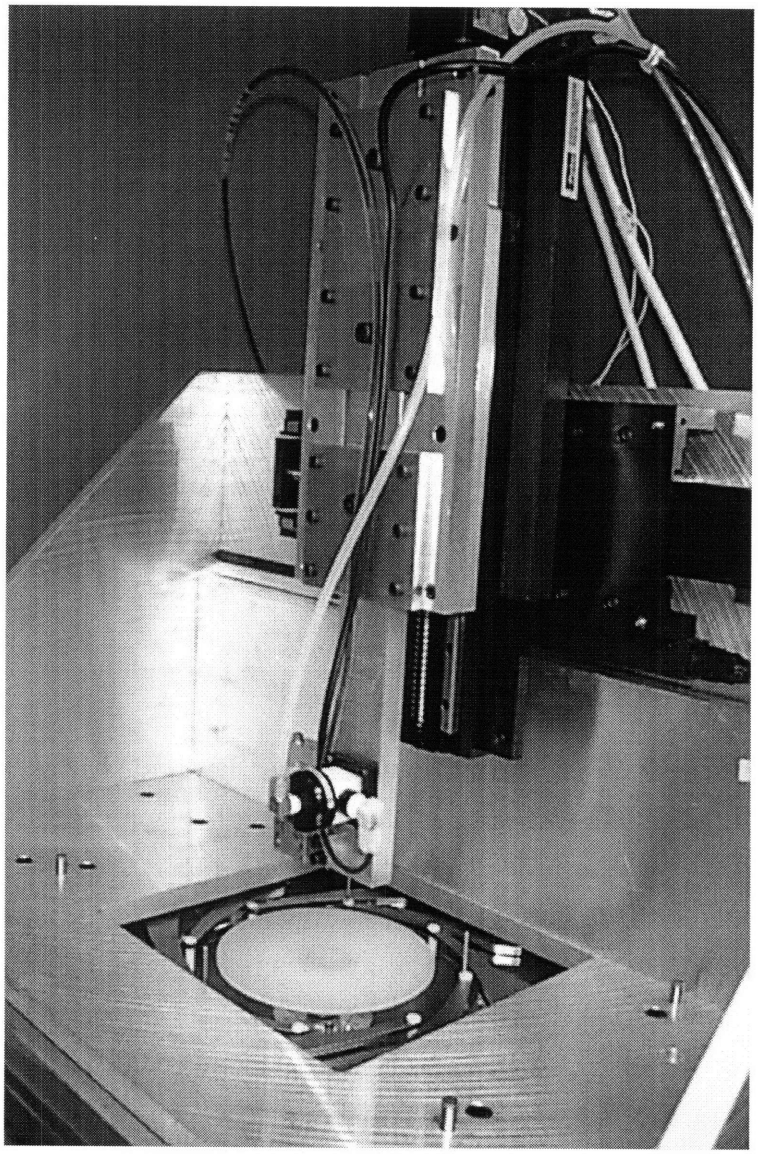

Figure 6-1: Photograph of Extrusion Coater. Scale: 1 cm = 7.25 cm.

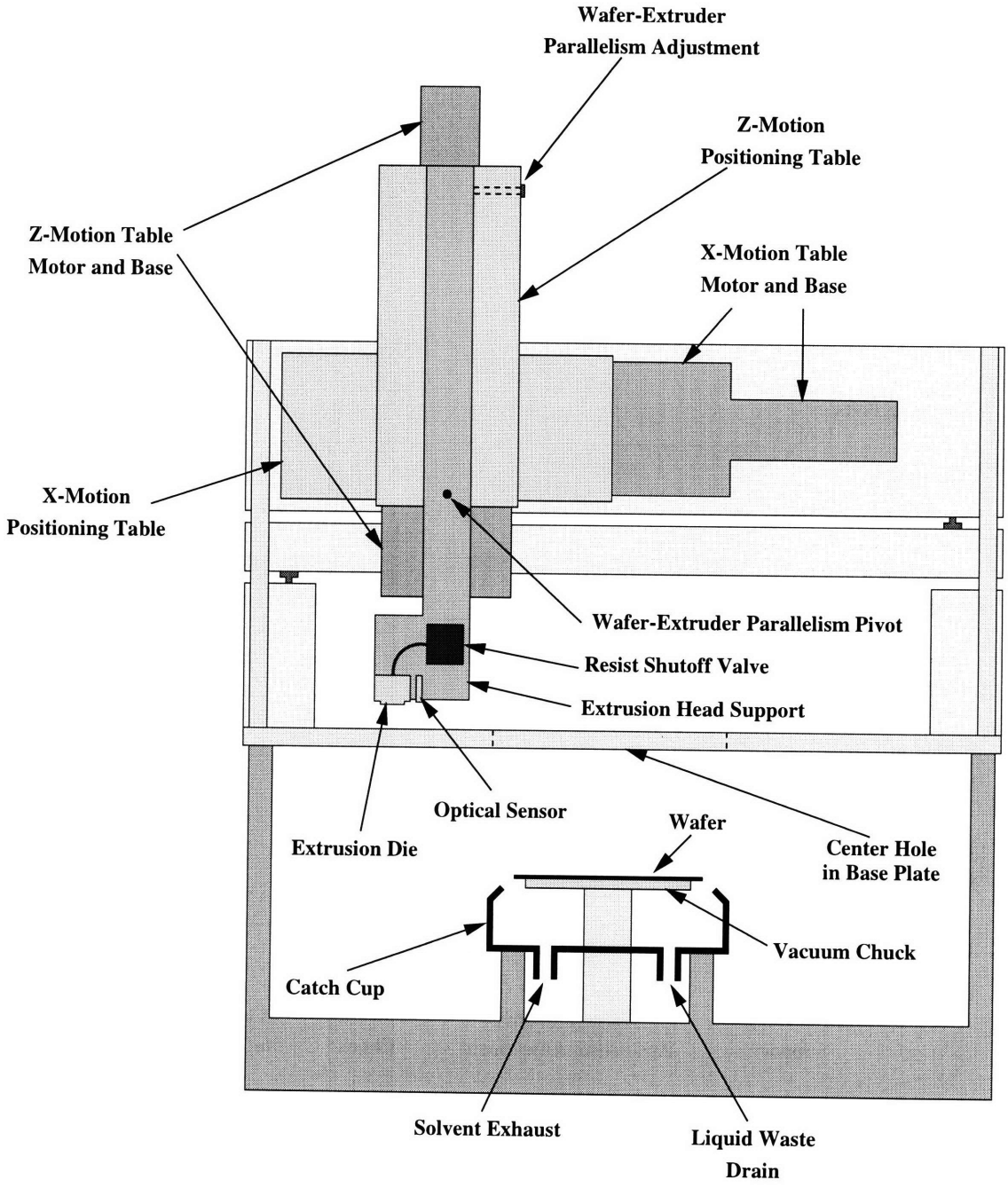

Figure 6-2: Front view of extrusion coater.

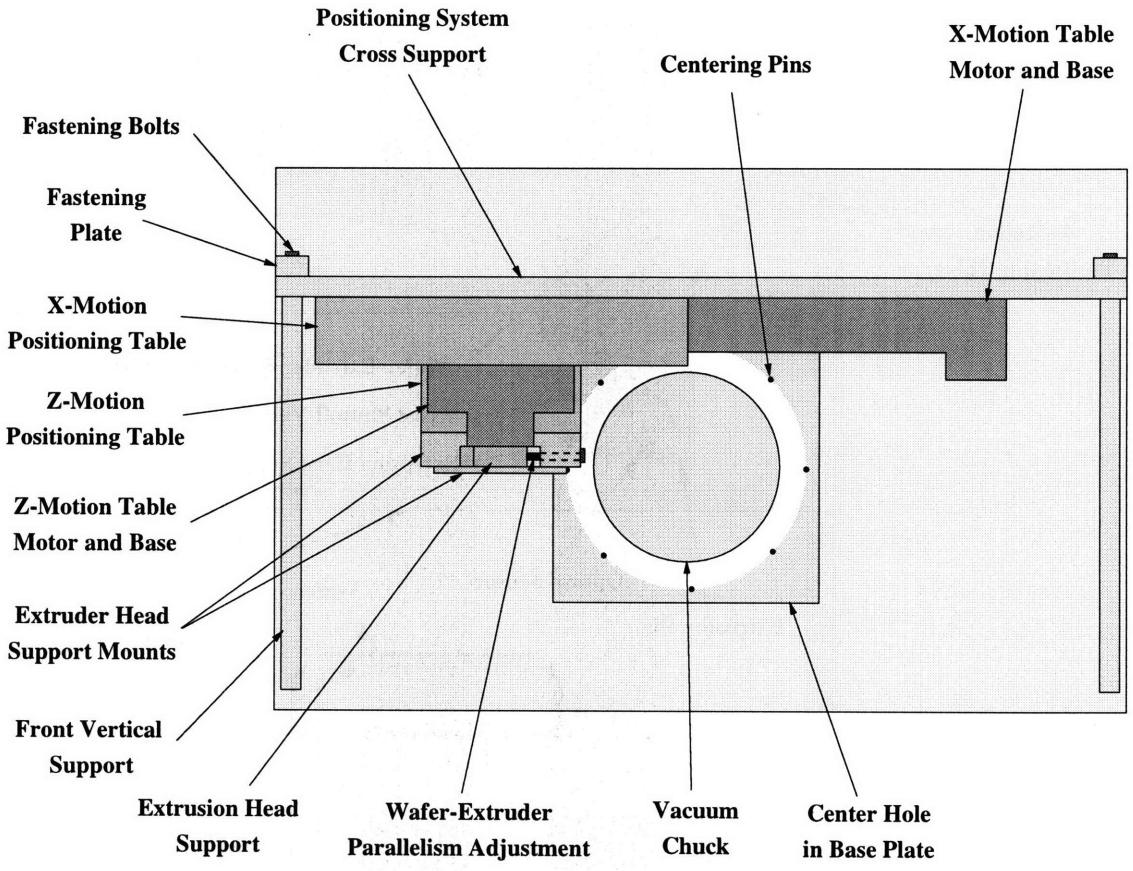

Figure 6-3: Top view of extrusion coater.

A Pacific Scientific SC 755 is the secondary controller used to set the spinner angular speed and position. Appendix A shows that the uncertainty in spinner speed was 8.2% (1 σ), and the uncertainty in spinner position was 0.026 radians (1 σ). This controller runs coating and spin cycles in response to digital inputs and outputs connected to the main controller. A simulated encoder signal generated by this controller allows electronic gearing of the spinner speed with the x-axis of the main controller. Programs written for the Pacific Scientific controller are also downloaded from the PC.

The Philtec RC140L sensor is a reflectance compensated optical displacement sensor. It shines a light on the surface of the wafer, measures the reflected light, and generates a voltage proportional to the intensity of the measured light. The spot size of the sensor is 6 mm and it has a DC-100 Hz bandwidth. Although the voltage-distance curve of the sensor is non-linear, it has a linear region when the sensor-wafer distance is between 5.51 and 6.17 mm. The sensor is positioned so that all measurements fall within the linear range.

6.3.2 Gap Control

During the coating motion, the gap between the extrusion die and the wafer is maintained at a constant distance by a simple control loop. The gap is measured using the sensor input and compared with the desired gap to obtain the gap error. The z-axis positioning table is commanded to move the distance required to correct the gap error. After the motion is complete the loop is repeated. Appendix A shows that there was an absolute gap error of -2.6 μm with an uncertainty of 7.2 μm (1 σ), with an additional periodic amplitude variation of 3.6 μm $\pm$ 0.42 μm (1 σ).

6.4 Photoresist Dispense System

The photoresist flow rate is mainly controlled by a Millipore Gen 2 displacement pump with a Gen 2 plus controller. Photoresist in a high-density polypropylene bottle flows through the pump, through 3.2-mm ID Teflon tubing, and into a Teflon shutoff valve. A 1.6-mm ID Teflon tube leads from the shutoff valve to a tee. One branch of the tee leads directly to the extrusion die while the other leads to a shutoff valve and a needle valve in series before going to the waste bottle. The needle valve is used to precisely drain off part of the flow from the pump in order to get lower flow rates

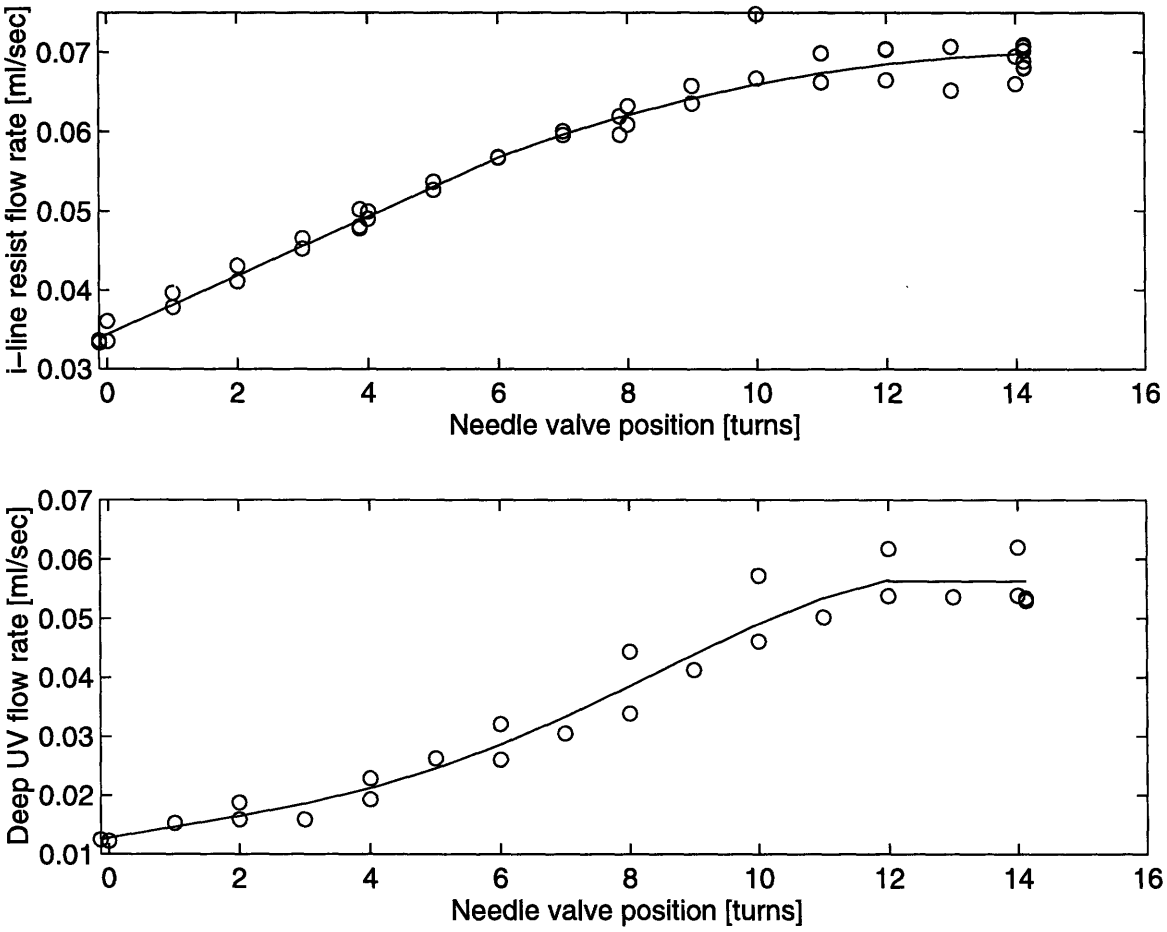

Figure 6-4: Photoresist dispense rate calibration data with calibration curves (—).

than the minimum flow rate of the pump.

To calibrate the flow rate, 1–2 ml of photoresist was dispensed and weighed at known positions of the needle valve for each type of photoresist. A negligible percentage of the photoresist evaporated between dispense and weighing. Figure 6-4 shows the calibration curves for the two photoresists. The uncertainty in the flow rate is was 2.5–4% for the i-line photoresist and 11.5–16.9% for the deep UV photoresist.

The extrusion die (described in Section 3.1) had a nominal coating width, w, of 2 cm. This size was chosen because it was large enough so that the coating time was not too long, yet small enough that the thickness variation across the width of each extruded ring was not too large.

6.5 Alignment System

The extrusion head and motion tables must be aligned with respect to the wafer to obtain uniform coatings. Three alignments are needed. The first alignment adjusts the path of the extrusion slot so that it passes directly over the center of the chuck. This is necessary for a complete coating in the center of the wafer. The extrusion head is positioned over the center of the wafer by sliding the vertical supports forward or backward over the base. The motion of the vertical supports is constrained by a guide on the base. Adjustment bolts at the back of each of the vertical supports allow fine-tuning of their position before they are fastened in place. The uncertainty of this alignment was within approximately 0.5 mm.

The second alignment adjusts the angle of the x-axis until it is parallel to the wafer surface. This alignment is necessary to maintain a constant gap between the wafer and the extrusion head as the x-positioning table changes position. The angle of the x-axis with respect to the wafer surface can be changed by rotating the motion system support about the pivot at one end. (See Figure 6-5.) Fine and coarse adjustment bolts allow adjustments of the angle between the x-axis and the wafer surface of 1.64×10^{-5} radians per turn of the fine adjustment bolt. The angle of the x-axis with respect to the wafer surface can be determined by scanning across the wafer with the optical sensor close to the wafer surface. During the scan, with the z-axis fixed, measurements of the sensor output and the x-position are recorded. A linear regression of these data pairs gives the angle between the wafer and the x-axis. Appendix A shows that during experiments this angle was 2.4×10^{-4} radians with an uncertainty of 2.8×10^{-4} radians ($1\ \sigma$).

The third alignment adjusts the bottom edge of the extrusion head until it is parallel with the x-axis and the wafer surface. This alignment is crucial for maintaining a constant gap across the width of the extrusion head. The angle between the bottom edge of the extrusion head and the x-axis can be adjusted using the wafer-extruder parallelism adjustment bolt shown in Figure 6-5. This bolt pivots the extrusion head support about a pivot at the base of the z-motion table. The angle between the x-axis and the bottom of the extrusion head can be measured using an LVDT sensor. The LVDT sensor is secured to the wafer surface with the measurement tip pointing vertically up. Next, the extrusion head is lowered until the lips of the extrusion slot move the LVDT sensor to a reference position. After the x and z-table positions are recorded the procedure is repeated for several other positions along the extrusion head

lips. The slope of the extrusion head with respect to the x-axis is determined using a linear regression of these data pairs. Appendix A shows that during experiments this angle was less than 1 $\times 10^{-4}$ radians from parallel.

6.6 Calibrations

Two steps are required to calibrate the optical sensor input voltage with the gap distance between the wafer and the extrusion head. First, the zero-gap voltage is determined by measuring the sensor voltage at many small gap distances using precision shims. A linear regression analysis of the gap distance and sensor voltage data calculates the sensor voltage at a zero gap. Second, the constant of proportionality of the sensor voltage versus the movement of the z-positioning table is determined by moving the z-positioning table away from the wafer in 12.7-μm increments and recording the sensor voltage at each position. A linear regression of the data pairs provides the voltage versus z-position slope. It is important that the wafer be aligned parallel with the extrusion head before the sensor is calibrated so that errors will not arise from the angle between the extrusion head lips and the wafer surface. Appendix A shows that the uncertainty in this calibration was 5.7 μm (1 σ).

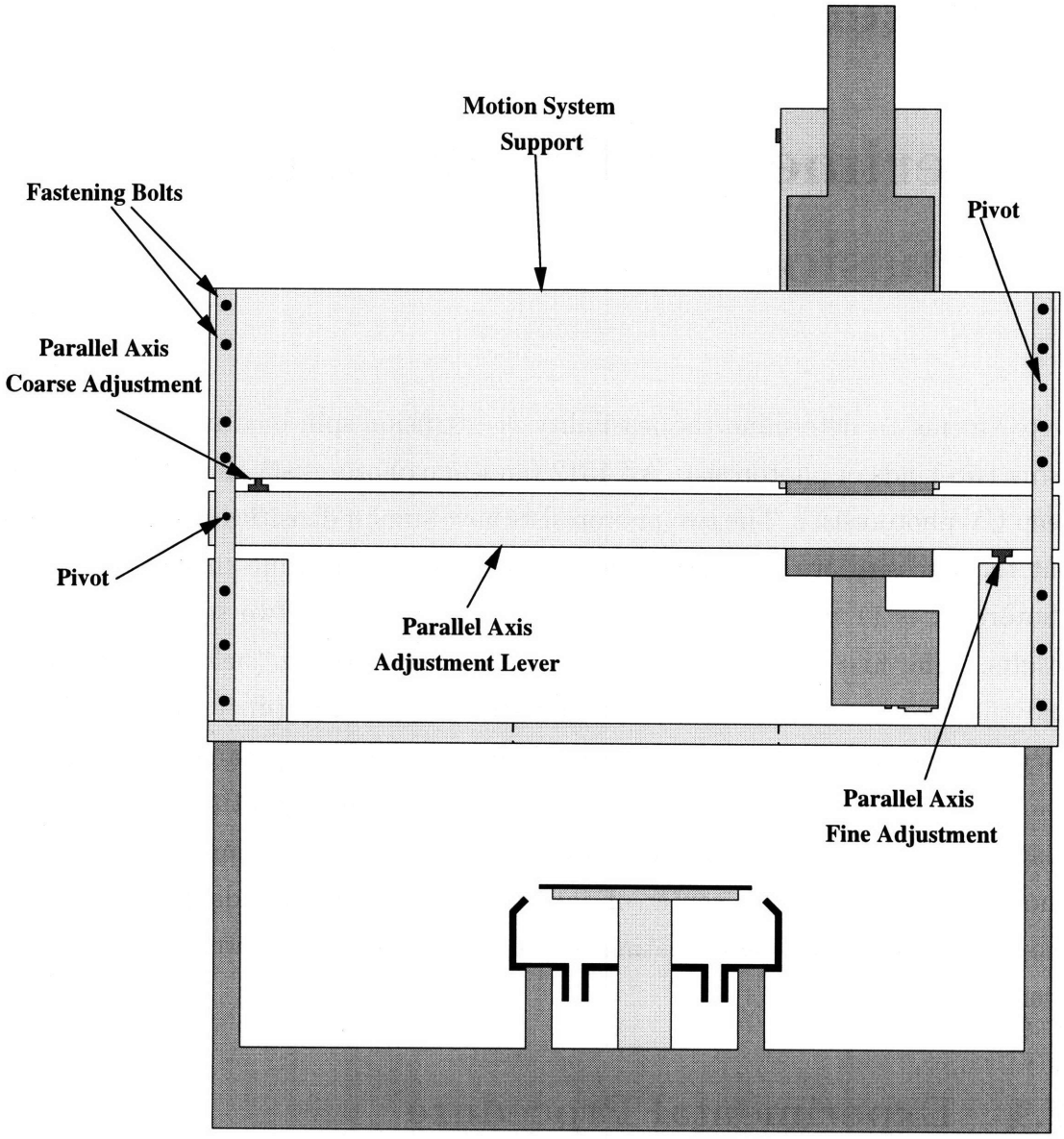

Figure 6-5: Back view of extrusion coater.

Chapter 7

Experimental Results and Discussion

Experiments to determine the feasibility of extrusion-spin coating were carried out using two kinds of photoresist: AZ 1512 (an i-line photoresist) and AZ DX 1200 P (a deep UV photoresist). The two photoresists have similar densities and surface tension, but the viscosity of the i-line photoresist is 19 mPa-sec while that of the deep UV photoresist is 11 mPa-sec. For each photoresist there are two sets of experimental results. The first set shows the limits on the wet coating (before the final spin), and the second set shows the characteristics of the final (dry) coating. No bead vacuum was used for these experiments. The experimental parameters evaluated for the wet coating were the coating gap, neck-in, maximum coating speed, minimum coating thickness, extrusion ring overlap, and the effect of coating parameters on the photoresist profile in the center of the wafer. For the final (dry) coating, each of the requirements for a new coating method was examined as well as extrusion ring overlap effects.

7.1 Experimental Procedure

Before each set of extrusion-spin coating experiments, the alignment was checked, the sensor was calibrated, the extrusion die was cleaned, and the photoresist pump was primed. Each individual coating was produced by the following procedure:

- The chuck was raised through the base plate, and the wafer was placed on the chuck, as shown in Figure 7-1(a)

- The wafer was centered on the chuck using the coater module's centering pins
- The chuck vacuum was turned on to secure the wafer to the chuck
- The wafer was lowered into coating position
- The extrusion die was positioned at the edge of the wafer with the inner edge of the extrusion slot exactly above the outer edge of the wafer, as shown in Figure 7-1(b)
- The gap between the wafer and the extrusion die lips was adjusted to a specified distance
- The spinner began rotating at an initial rotational speed corresponding to the specified coating speed
- The photoresist shutoff valve was opened
- The pump began dispensing photoresist at the specified flow rate
- Photoresist was dispensed for several seconds to remove bubbles from the extrusion slot opening
- During all subsequent motion of the extrusion die along the surface of the wafer, sensor feedback was used to maintain a constant gap by controlling the position of the z-axis positioning table
- The extrusion die moved inward along the diameter of the wafer at a speed proportional to the spinner speed (This was accomplished by electronically gearing the x-axis position as a slave of the spinner angular position.)
- The coating speed (the relative tangential speed between the extrusion die and the wafer) was kept constant by increasing the spinner rotational speed and extrusion die speed
- When the leading edge of the extrusion die lips reached the center of the wafer, the spinner stopped accelerating and remained at a constant speed for the rest of the coating process
- The extrusion die continued moving across the wafer at a constant speed until it reached a specified position (Figure 7-1(c) shows the trailing edge of the extrusion die lips reaching the center of the wafer.)

- The photoresist pump stopped dispensing and the shutoff valve was closed (either before or after the extrusion die stopped moving)
- The spinner stopped rotating
- The wafer was lowered into the catch cup and the extrusion die was removed from the coating area, as shown in Figure 7-1(d)
- The wafer was accelerated very rapidly to a high-speed spin which was maintained for an extended period of time
- After the wafer stopped spinning, it was raised up through the base plate and the vacuum was turned off

7.2 Experimental Conditions

During all experiments the extrusion-spin coater was located in a clean hood which constantly forced filtered air to flow downward over the extrusion-spin coater. The temperature in the room was unregulated and ranged from 19 to 27°C. The relative humidity was also unregulated between 24 and 49%.

7.3 Pre-Spin (Wet Coating) Results

To understand the extrusion-spin coating process, the maximum coating gap, the minimum coating thickness, and the maximum coating speed were investigated using a number of experiments which characterized the important process parameters of the extrusion part of extrusion-slot coating.

7.3.1 Gap and Neck-in

The maximum coating gap was measured by maintaining a constant coating speed and constant dispense rate while increasing the coating gap until it became unstable. Near the limits of stability, neck-in increased dramatically and scalloped edges developed, as described in Section 3.8. Finally as the gap was increased even more, rivulets developed, leaving two or more paths of photoresist separated by dry regions. At even larger gaps, the coating bead remained together, but its width grew and shrunk

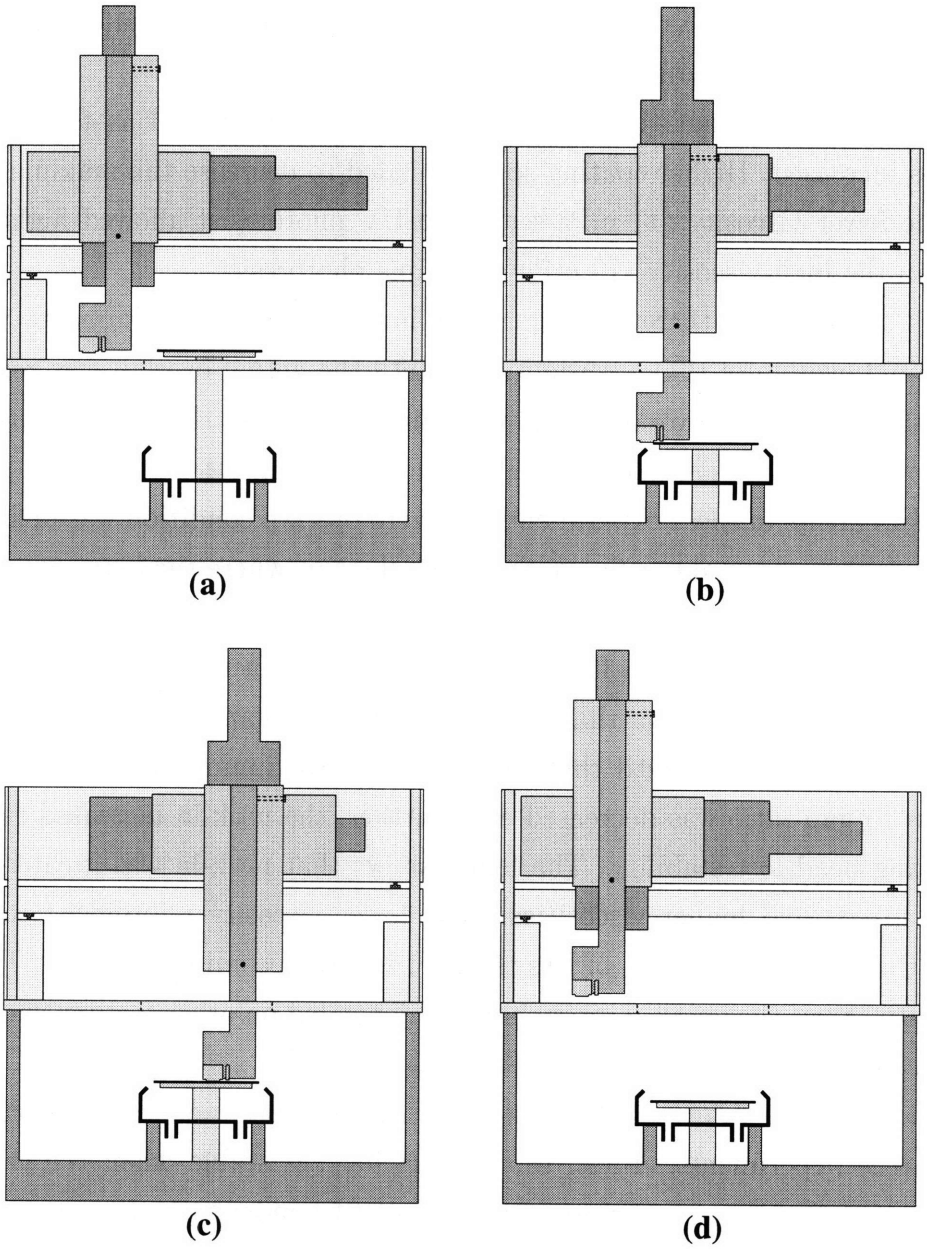

Figure 7-1: Extrusion-spin coating process. (a) Wafer is placed on vacuum chuck. (b) Wafer is lowered into coating position and extrusion die is positioned at the outer edge of the wafer. (c) Wafer is rotated as the extrusion die moves along the diameter of the wafer until the extrusion die completely crosses the center of the wafer. (d) Extrusion die is removed, and wafer is lowered into the catch cup and rotated at high speed.

with large, periodic oscillations. It was observed that the coating bead could remain stable at larger gaps if the extrusion-ring overlap was increased sufficiently to make up for the lack of photoresist in the coating bead.

Figure 7-2 shows that the maximum coating gap increased as the wet coating thickness increased. Higher coating speeds tended to decrease the maximum coating gap. The lower viscosity (11 mPa-sec) deep UV photoresist allowed higher coating gaps than the high-viscosity (19 mPa-sec) i-line photoresist.

At all coating gaps there was some neck-in. Neck-in was measured by increasing the nominal overlap of the extrusion rings until the actual overlap was zero. Determining the actual zero overlap point was difficult because the extrusion rings often joined together along some of their edges but not along others. For the purpose of the measurements in these experiments, the zero overlap condition was defined as the point when there were about five or fewer small strips where the extrusion rings were not joined together.

In Figure 7-3, the neck-in for the experiments is plotted versus the thickness to gap ratio. The figure shows that as the thickness to gap ratio was decreased, the neck-in increased slowly until the gap neared its maximum stability limit. As the thickness to gap ratio was decreased even further, the neck-in increased rapidly and the coating bead lost stability. The figure shows that neck-in was greater at higher coating speeds and higher viscosities. The lower viscosity photoresist was able to reach a thickness to gap ratio of less than 0.1 before becoming unstable. The scatter in the data shows that neck-in probably also depended on other factors, such as wafer surface conditions, which are not as easily controlled.

Several generalizations can be drawn for coating conditions which correspond to those in the experiments. First, the coating bead is stable when the thickness to gap ratio remains above a certain critical limit (dependent on viscosity and coating speed). This is consistent with the work of Choinski[14]. Second, for a constant gap, lower viscosity fluids and slower coating speeds produce lower minimum wet thicknesses. Third, the trend in the maximum gap data seems to indicate that as the coating thickness is decreased,the maximum coating gap would reach zero before the minimum wet thickness reached zero. This indicates that there is probably a minimum thickness below which no coatings can be made.

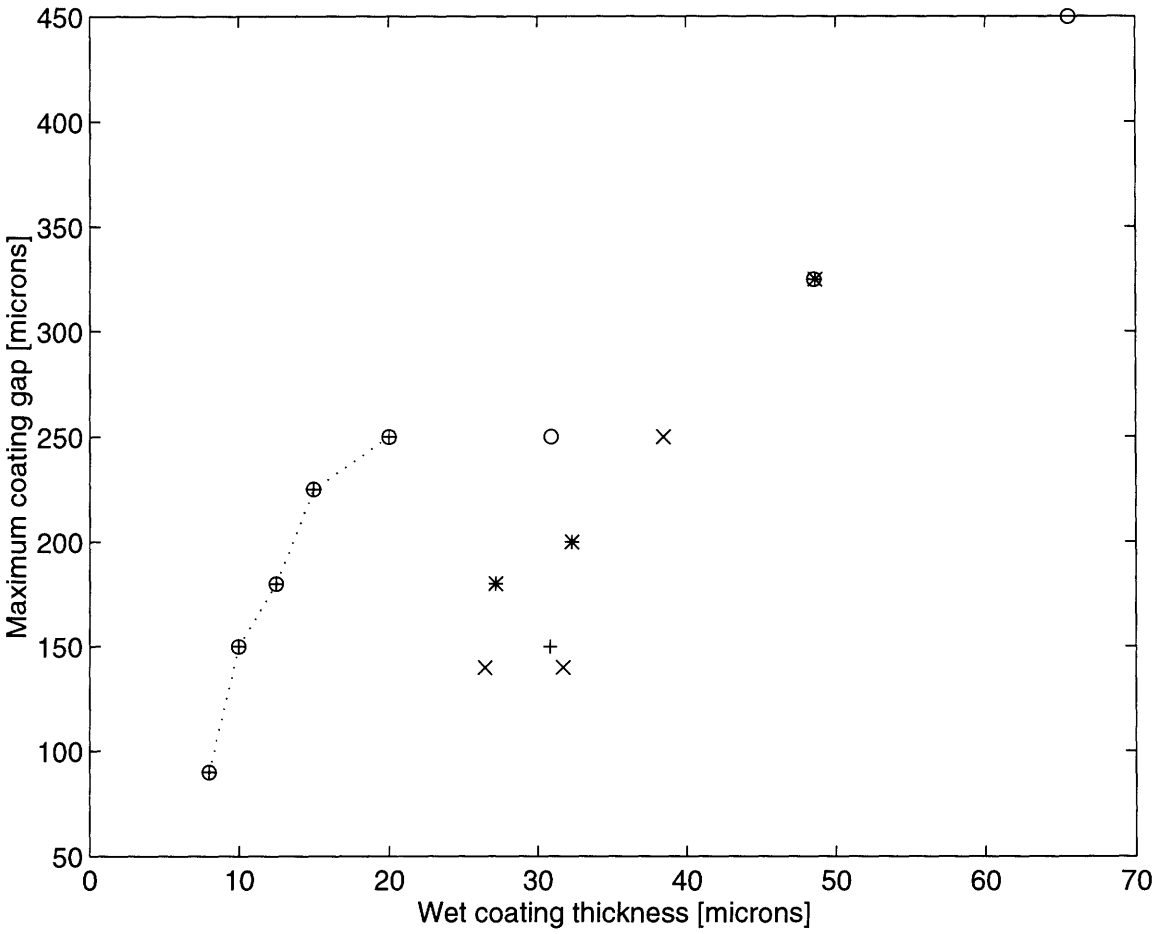

Figure 7-2: Maximum coating gap. i-line photoresist coating speeds: 6 cm/sec (o), 8 cm/sec (*), 10 cm/sec ($\times$), and 12 cm/sec (+). Deep UV coating speed: 8 cm/sec ($\cdots \oplus \cdots$).

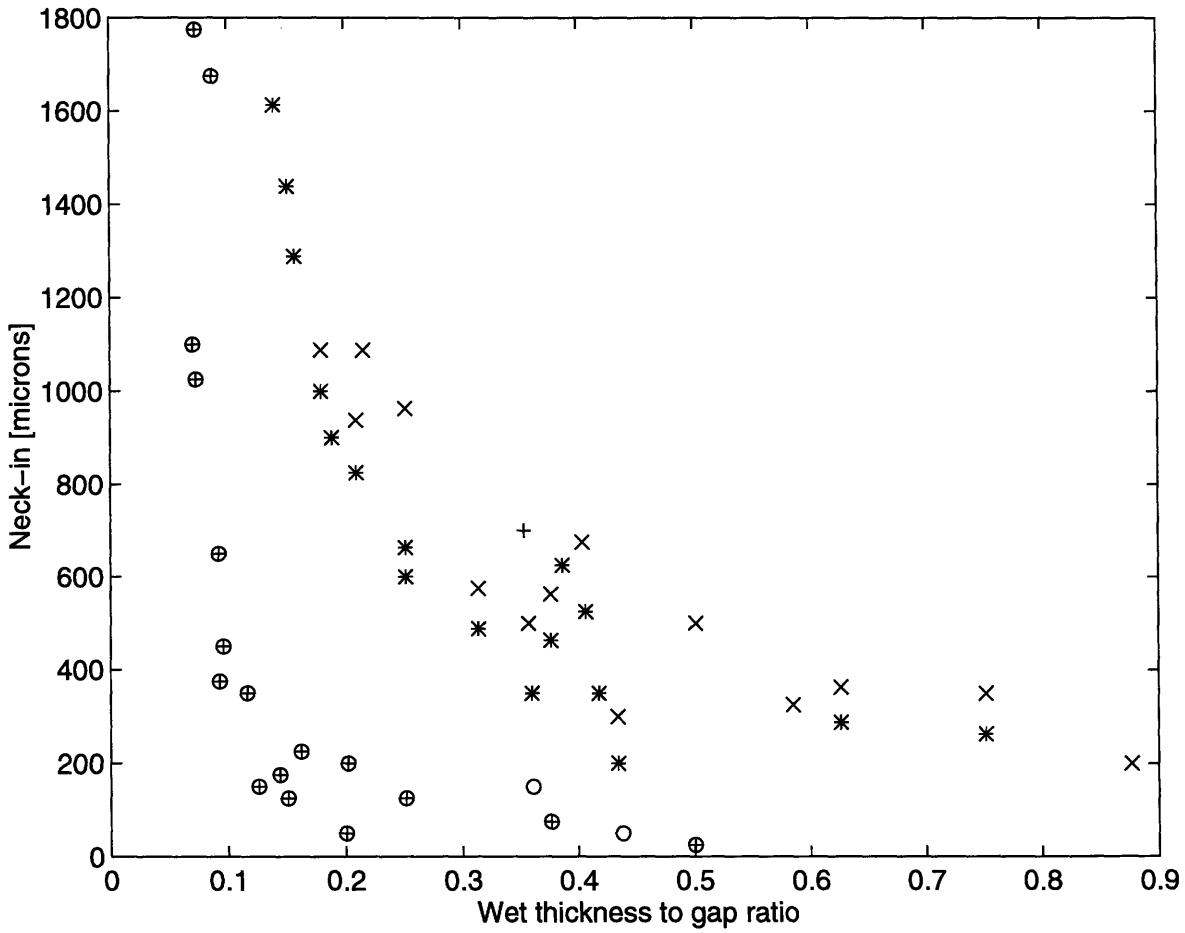

Figure 7-3: Neck-in of coating bead. i-line photoresist coating speeds: 6 cm/sec (o), 8 cm/sec (*), 10 cm/sec ($\times$), and 12 cm/sec (+). Deep UV coating speed: 8 cm/sec ($\oplus$).

7.3.2 Maximum Coating Speed and Minimum Wet Thickness

As discussed in Chapter 3, the maximum coating speed and the minimum coating thickness are limited by the same phenomenon. This limit was measured by maintaining a constant fluid flow rate while increasing the coating speed until coating defects developed. Figure 7-4 shows the maximum coating speed for both photoresists. Above the maximum coating speeds, streaks of uncoated wafer appeared. Usually these streaks developed at the outer edge of the extruded rings where the tangential speed between the wafer and the coating die was highest. The thickness of the coating at the maximum speed was computed using Equation 4.18. The extruded width, w, used in the equation was calculated by subtracting the neck-in from the extrusion die width. The figure shows that the lower viscosity of the deep UV photoresist allowed much higher coating speeds and thinner coatings than the speeds and thicknesses attained by the i-line photoresist. As the coating thickness increased, the maximum coating speed also increased. The dotted lines in the figure indicate the lowest flow rate the pump could deliver for each photoresist. The only coating speeds and thicknesses which could be produced by the experimental equipment were those below the maximum coating speed and above the minimum flow rate of the pump. The experiments indicated in the figure were designed to examine the highest coating speeds and the lowest coating thicknesses in order to attain the minimum coating times and maximum coating efficiencies possible with the experimental equipment.

7.3.3 Wet Thickness Uniformity

The uniformity of the wet coating was not measured directly, but a number of observations were made. First, color variation across each extruded ring indicated that the extruded rings were thinner toward the outer edge and thicker on the inner edge, as described in Section 4.3. There was a large bead of photoresist around the outer edge of the wafer which was two or more times the thickness of the rest of the coating. For thin coatings, this edge bead spread toward the center of the wafer when there was a time delay between the initial coating and the final high-speed spin. In the center of the wafer, there was a pool of photoresist which had a shape dependent on the coating speed and photoresist dispense rate.

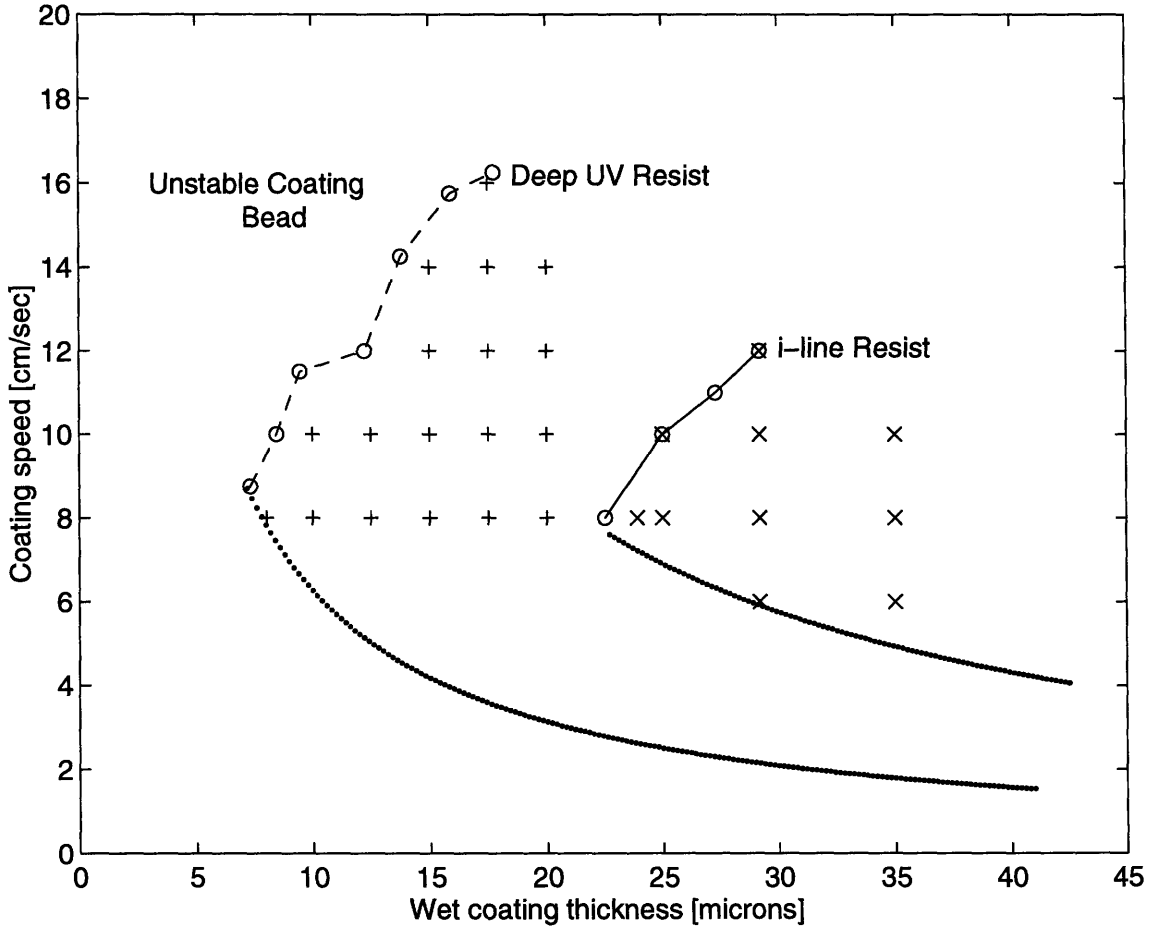

Figure 7-4: Experimental limitations on maximum coating speed and minimum wet thickness. Maximum coating speed for the i-line photoresist (–⊖–), maximum coating speed for the deep UV photoresist (– – ⊖ – –), minimum flow rate (· · ·), experimental conditions for i-line experiments (×), experimental conditions for deep UV experiments (+).

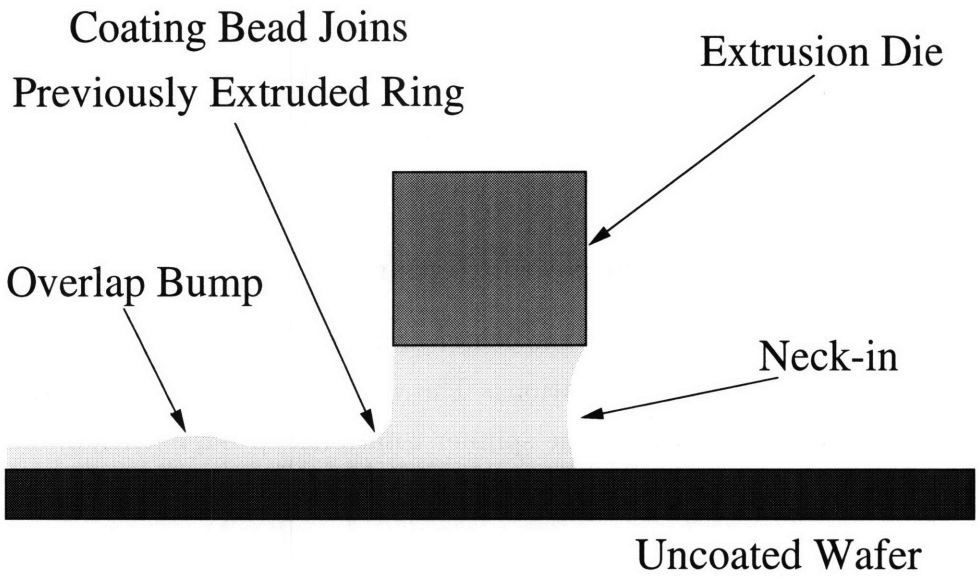

Figure 7-5: Coating bead merging with previously extruded ring.

7.3.4 Overlap of Spiral Rings

The overlap of the spiral rings was set by using Equation 4.21. The actual extrusion width, w, was determined by subtracting the neck-in from the length of the extrusion die lips. It was observed that the thickness of the bumps created by extrusion ring overlap was much thinner than the coating thickness. Although it is possible that the surface tension forces spread out the overlaps, a more likely explanation is that the coating bead joined with the edge of the spiral ring deposited during the previous revolution of the wafer, as shown in Figure 7-5, spreading any excess fluid over a much wider area than had been expected.

7.3.5 Wet Coating Defects

Two kinds of defects were observed in the wet extrusion-spin coating. The first type were general defects associated with the extrusion coating process. The second type of defects were those in the center of the wafer, created by the spiral adaptation to extrusion coating.

General Defects

Of the coating defects described in Section 3.8, neck-in, scalloped edges, rivulets, and edge beads were observed as described in the sections above. A small amount

of chatter was present but the visible thickness variations disappeared quickly after coating. It is likely that the chatter was created by the coating velocity fluctuations described in Appendix A. Pin holes in the coating were observable when air bubbles were present in the dispense line.

Defects Associated with the Spiral Center

An excess or deficiency of fluid in the center of a wafer during extrusion-spin coating created defects and thickness variations. The volume and distribution of photoresist in the wafer center depended on the spinner rotational speed, extrusion die position, dispense rate, and gap while the center part of the spiral is coated.

Center Defect Mechanisms There are three mechanisms in the center pool of fluid which caused defects in the final coating. First, bubbles often remained in the pool of photoresist after the coating bead was broken by removal of the extrusion die. It was likely that one bubble was formed when the final point of the extrusion spiral was coated. If the extrusion die passed over this point too quickly, air was trapped beneath the coating layer. Another possible source of bubbles was suckback from the pump at the end of the dispense. (Suckback is the small reversal of flow at the end of a dispense to keep the extrusion die from dripping after it is lifted from the substrate surface.)

Second, a small indentation was left in the wet film when the extrusion die was lifted from the substrate. This indentation may have arisen because the extrusion die lips were below the surface of the center photoresist pool before the die was lifted. Changing the speed at which the die was lifted from the surface did not noticeably affect the indentation.

Third, the photoresist pool was not centered on the wafer when the extrusion die was moving during the final rotation of the wafer. Because the photoresist was pulled along by the extrusion die, the spinner had to rotate a full revolution after the extrusion die had stopped moving to center the photoresist pool.

Center Defect Elimination Two categories of solutions were used to address the problems associated with the center. In the first category the amount of photoresist was reduced to decrease the effect of the center photoresist pool. One way this was accomplished was by ending the photoresist dispense before the end of the coating motion, allowing the photoresist left in the bead to spread over the remaining

uncoated wafer surface. This method effectively reduced the amount of photoresist in the center, but when the dispense was ended too soon, there were areas of the center left uncoated. Another method was to reduce the flow rate of photoresist as the extrusion die approached the center. This method was attempted using manual dispense control without much improvement. Low-flow, variable-rate pumps must be developed before this method can be used effectively.

In the second category, the shape of the photoresist pool was changed so that it caused fewer problems during the high-speed spin. One method was to stop the extrusion die motion slightly before the end of the spiral. This technique caused the center overlap to be more centered on the wafer and led to fewer visible thickness variations. Another method was to turn the wafer an extra rotation after the extrusion die stopped moving, spreading the photoresist over a greater area in the center. Although this technique spread the photoresist effectively, it also left circular streaks when the extra rotation occurred at high speed. A third method was to raise the extrusion die slowly during the final rotation of the wafer so that the surface in the center of the wafer was smoother. This method effectively eliminated most of the rough spots left behind when the extrusion die was raised while the wafer was stationary.

7.4 Final (Dry) Coating Results

A set of experiments were done with each of the two photoresists to test the effectiveness of extrusion-spin coating. The wet coating thicknesses and the coating speeds for all of these experiments are found in Figure 7-4. After the wet coating was applied, each wafer was accelerated at 5000 RPM/sec to a rotational speed of 3000 RPM. Next, after spinning for 40 seconds, each wafer was baked at 110°C for 30 minutes.

7.4.1 Coating Thickness

For each experiment, the final (dry) coating thickness was measured using a Prometrix spectral interferometer. A typical 49-point map of the photoresist thickness is shown in Figure 7-6. The thickness maps for most of the wafers had a low center region with increasing thickness towards the edges. A significant number of the wafers coated with i-line photoresist had a bump or indentation at the center of the wafer (probably due to the center problems discussed above). Most of the large center non-

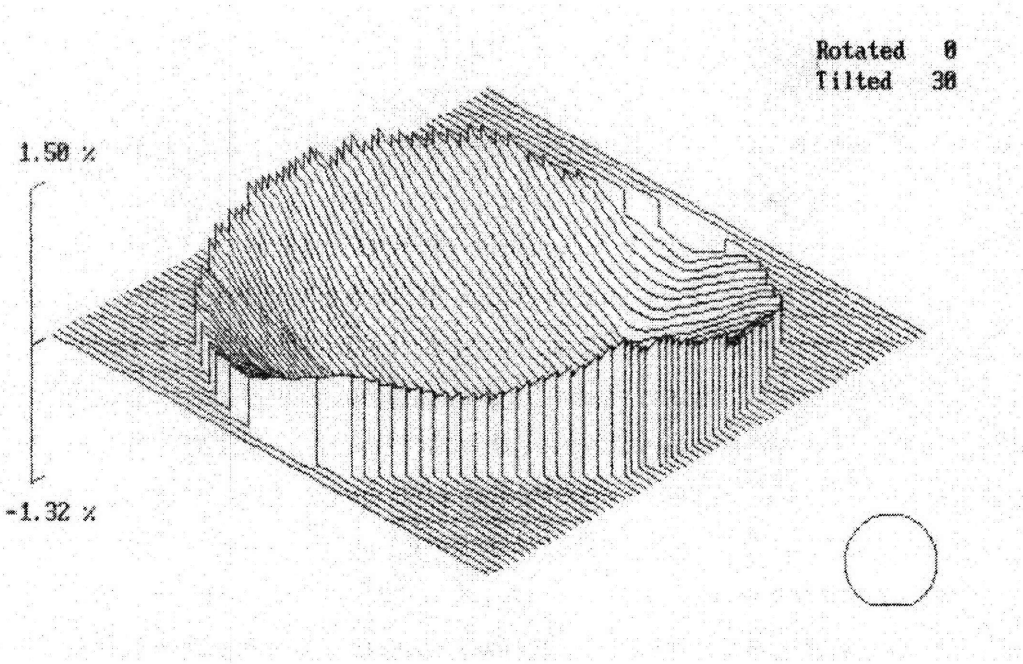

Figure 7-6: Map of final (dry) coating thickness.

uniformities were eliminated for the wafers coated with deep UV photoresist. The average coating thickness for the experimental conditions in Figure 7-4 are shown in Figures 7-7 and 7-8. These figures show that for both types of photoresist, slower coating speeds and thinner wet coatings tended to produce thicker dry films. These results agree with the model in Section 4.3.4 which indicates that evaporation effects are greatest for thinner films and slower coating speeds. More evaporation makes the photoresist viscosity increase and leads to a thicker film after the final high-speed spin. A 9.5-second delay between coating and the final high-speed spin for one i-line photoresist coating resulted in a much higher final coating thickness, indicating again that evaporation is the cause of thicker films.

To compare extrusion-spin coating with spin coating, one wafer was coated for each photoresist using a center dispense and traditional spin coating. The same acceleration, spin speed, and spin time were used as those in the extrusion-spin coating experiments. The mean photoresist thicknesses on these spin-coated wafers are shown

in Figures 7-7 and 7-8 for comparison. The mean thickness for all coating experiments with i-line photoresist was 1.44 μm with a standard deviation of 0.024 μm. This is slightly below the spin-coating comparison test (1.46 μm) and slightly above the thickness predicted by AZ photoresist (1.42 μm) for a final spin speed of 3000 RPM[12]. The mean thickness of the deep UV photoresist extrusion-spin coatings was 0.735 μm with a standard deviation of 0.020 μm. This mean was slightly above the spin-coating comparison test (0.728 μm). The thickness map for traditional spin-coating looked very similar to most of the extrusion-spin coating maps (low center with upward-sloping edges). This indicates that evaporation effects are also present in traditional spin coating but are more pronounced in extrusion-spin coating, especially for thin coatings and long coating times (corresponding to slow coating speeds).

7.4.2 Thickness Uniformity

Thickness uniformity of the final (dry) coating was calculated from the thickness map for each wafer. Uniformity, measured by the coefficient of variation of the thickness data[1], is shown in Figure 7-9. The figure shows that thickness variation increases (uniformity decreases) as the coating thickness decreases and as the coating speed decreases. Just as for coating thickness, the variation in thickness increases when evaporation effects are greater. The results concur with the discussion in Section 4.3.4 which predicted poorer uniformities at lower coating speeds and thinner films. Coating uniformities were between 0.5 and 2% for i-line coatings with no delay and between 1 and 11.3% for deep UV coatings.

7.4.3 Coating Time

The total time required to process a wafer through a coating cycle depends on the wet coating time as well as the time required to load a wafer, move the extrusion die into position, remove the extrusion die after wet coating, complete the final high-speed spin, and unload the wafer. All these time requirements are constant for each of the experiments except the wet coating time. Figure 7-10 shows that the wet coating time depended mainly on the coating speed, decreasing as the coating speed increased. This is in agreement with Equation 4.13. Larger overlaps also increased the wet coating time slightly because part of the width of the extruded film was used

[1]The coefficient of variation equals the standard deviation as a percentage of the mean[25]

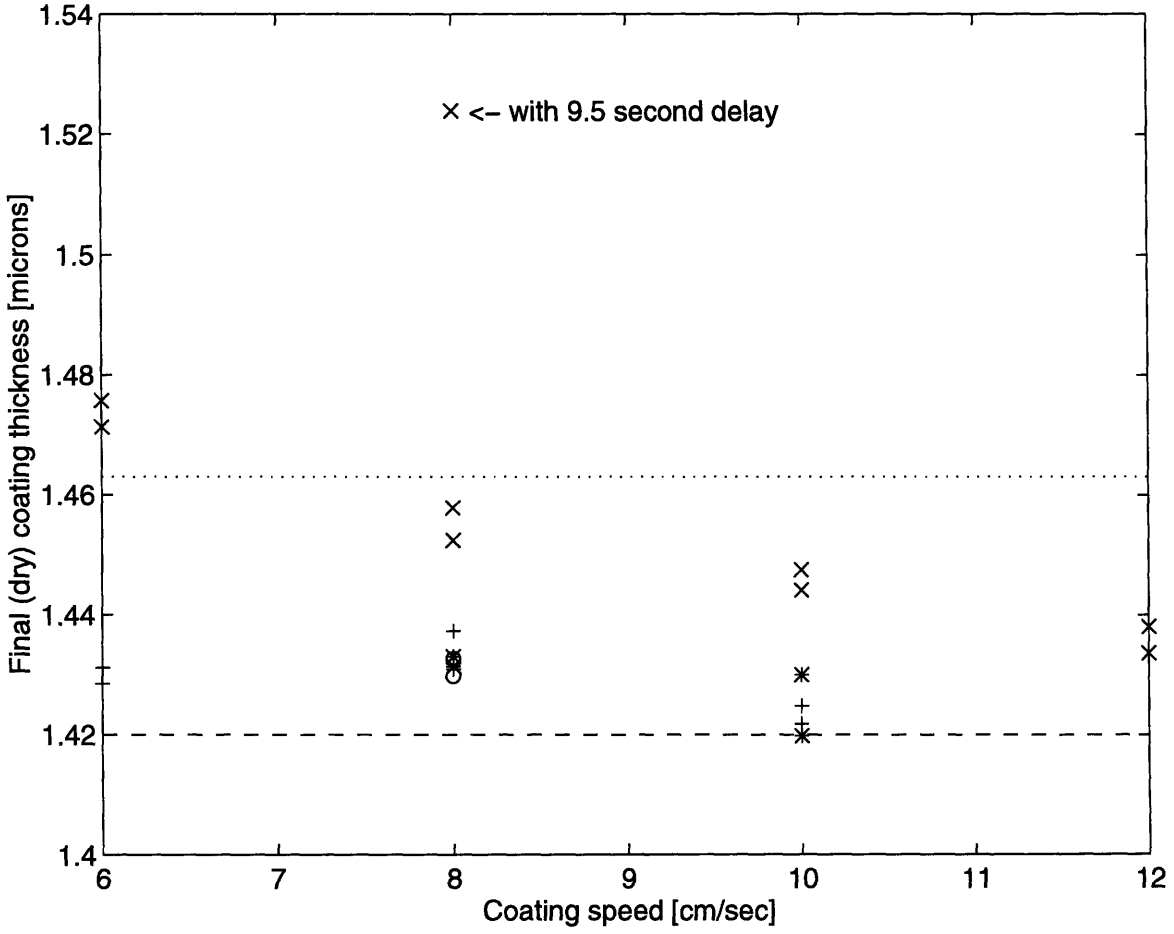

Figure 7-7: Final (dry) coating thickness for the i-line photoresist with coating thicknesses of 23.9 μm (o), 25 μm (*), 29.2 μm ($\times$), and 35 μm (+). Dashed line (– –) indicates AZ photoresist reported value. Dotted line ($\cdots$) indicates a traditional spin-coating comparison test.

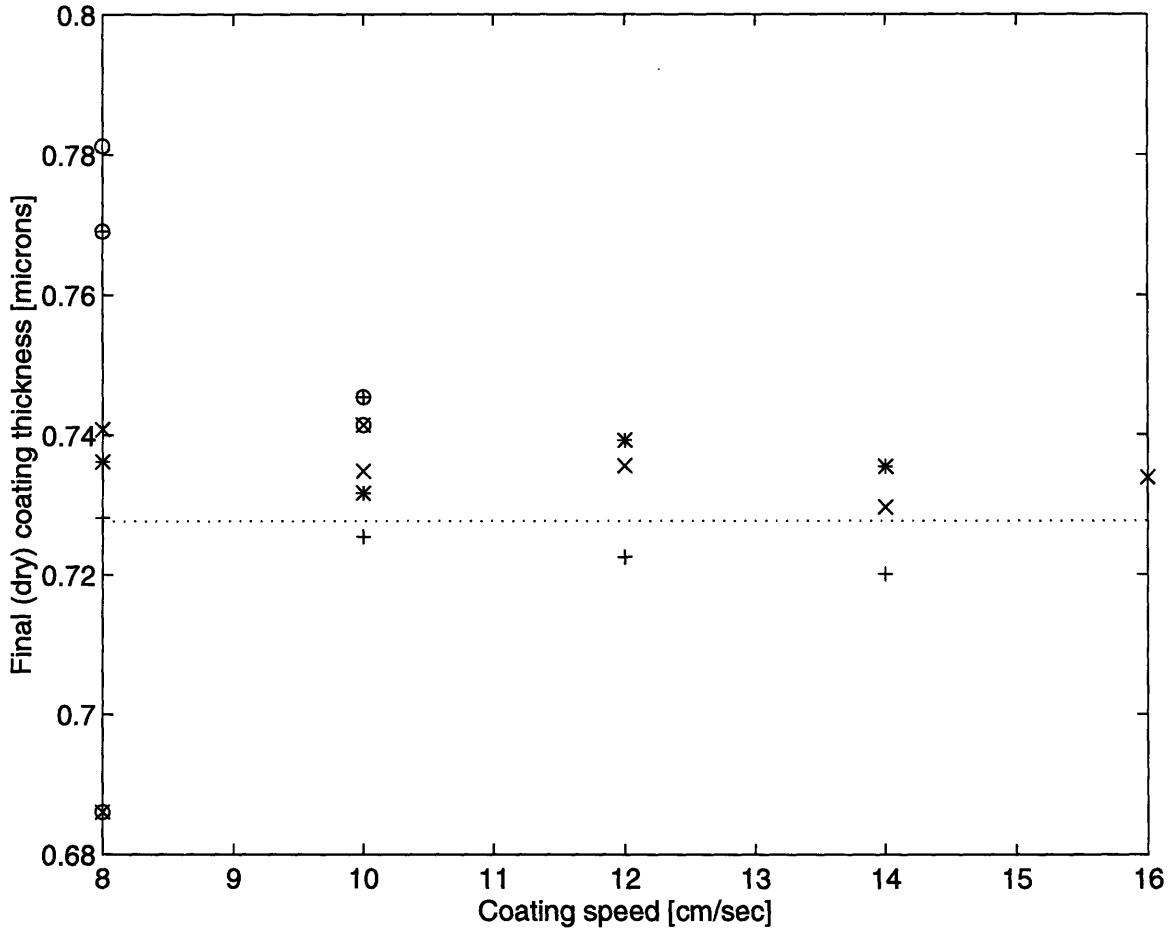

Figure 7-8: Final (dry) coating thickness for the deep UV photoresist with coating thicknesses of 20 μm (+), 17.5 μm ($\times$), 15 μm (*), 12.5 μm ($\otimes$), 10 μm ($\oplus$), and 8 μm (o). Dotted line ($\cdots$) indicates a traditional spin-coating comparison test.

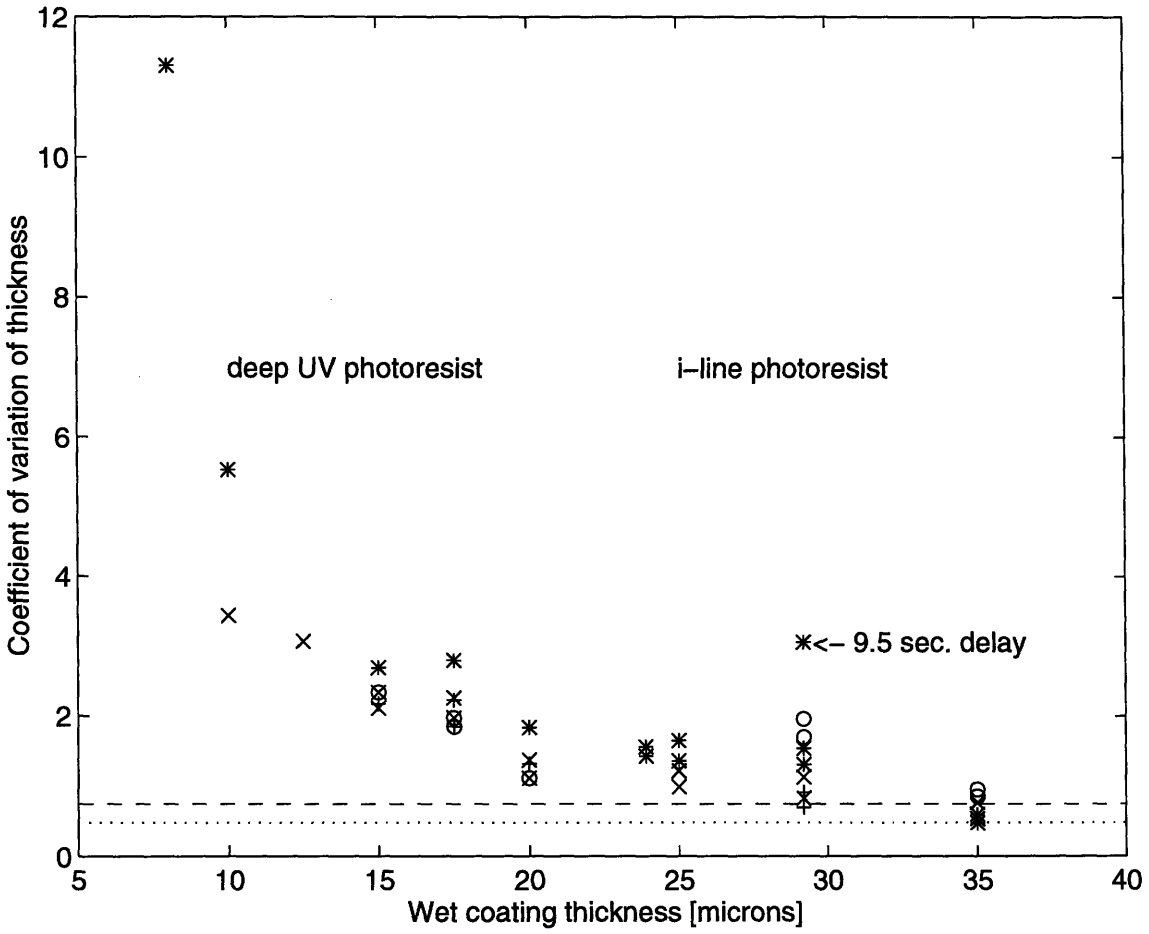

Figure 7-9: Final (dry) coating thickness uniformity. Coating speed = 6cm/sec (o), 8 cm/sec (*), 10 cm/sec (×), 12 cm/sec (+), 14 cm/sec (⊗), and 16 cm/sec (⊕). Traditional spin coating is indicated by (– –) for i-line photoresist and (· · ·) for deep UV photoresist.

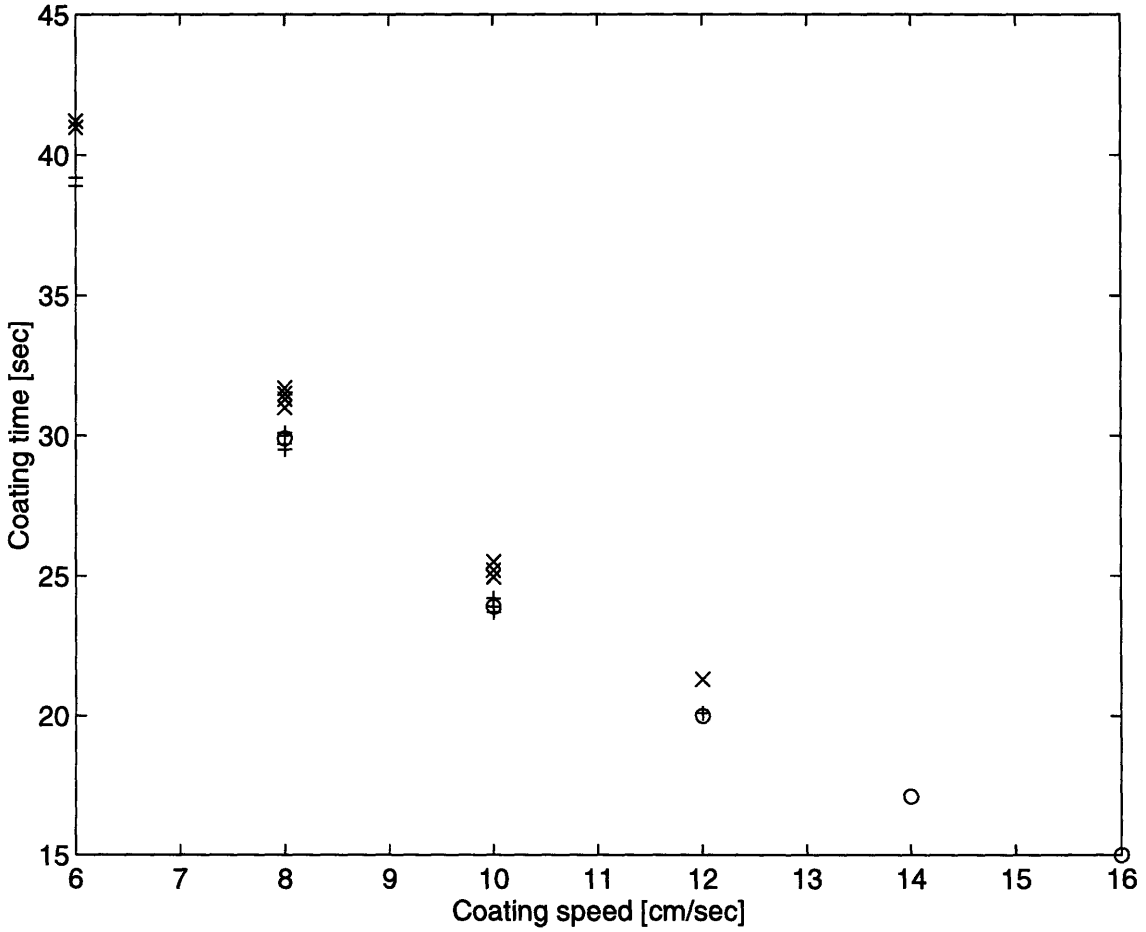

Figure 7-10: Coating time for deep UV photoresist (o), i-line photoresist with no extrusion ring overlap (+), and i-line photoresist with 1000μm overlap ($\times$).

to coat areas of the wafer that had already been coated, requiring more rotations to completely coat the wafer surface. The wet coating times for the experiments were from 15 to 41 seconds. Because the prototype coater was designed for experimental purposes, the positioning time was not a realistic measure of the actual time that would be required for a commercial extrusion-spin coater. Assuming 15 seconds are required for moving the wafer and the extrusion die in and out of position and 30 seconds are required for the final high-speed spin, the total coating times would have ranged from 60 to 86 seconds.

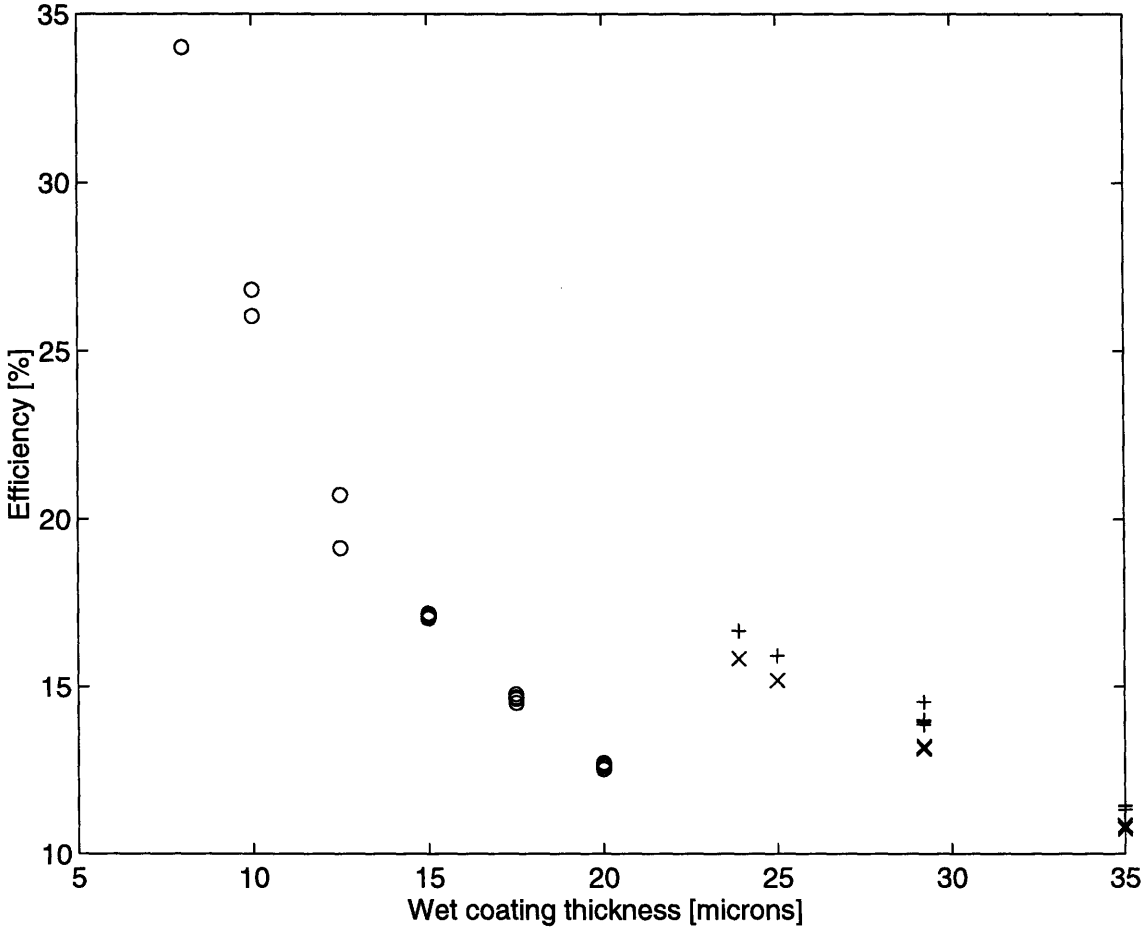

Figure 7-11: Photoresist use efficiency for deep UV photoresist (o), i-line photoresist with no extrusion ring overlap (+), and i-line photoresist with 1000-μm overlap ($\times$).

7.4.4 Coating Efficiency

Coating efficiency was calculated using Equation 1.4, dividing the volume of photoresist actually on the wafer (coated surface area times mean thickness) by the total volume of photoresist solids used to coat the wafer. Figure 7-11 shows that the efficiency increased as the thickness decreased. The discontinuity in efficiency between the i-line and deep UV photoresists was due to the difference in solids fraction. The efficiencies were between 10 and 16% for the i-line photoresist and between 12 and 34% for the deep UV photoresist.

7.4.5 Visible Coating Defects

Several types of coating defects were observed in the final dry film. The most frequent coating defect was streaks from the center of the wafer toward the edges. It is likely that these streaks were caused by excess photoresist from the center flowing across the wafer surface during the final high-speed spin. The centers of some wafers had thin regions which probably developed when the center pool of photoresist was off-center or when the spiral did not sufficiently cover part of the center. On some wafers, streaks from a particular radius outward developed when the spiral rings did not overlap, leaving thin lines of uncoated wafer.

7.5 Extrusion Overlap Effects

To determine whether the overlaps between spiral rings led to thickness non-uniformities, an ellipsometer was used to measure the thickness of several wafers at 635-μm intervals along their diameters. Figure 7-12 shows the thickness measurements for two wafers coated with a wet photoresist thickness of 9.9 μm—one with a 500-μm overlap and one with zero overlap. These tests were done at a very thin coating thickness where thickness variations from overlaps should have had the greatest effect. If the 500-μm overlap had spread to 1 μm thick, it would have spread to a width of approximately 5000 μm. Such an area would have resulted in thickness changes at in least 7 consecutive measurements. Since the thickness profiles of the two thickness measurements were essentially the same, apart from slope differences, they showed no evidence of thickness variations corresponding to extrusion ring overlap. Therefore, it appears that the extrusion ring overlaps had little if any effect on final coating uniformity. The overlaps did, however, affect overall coating thickness and thickness uniformity because of the increase in coating time required and the associated increase in evaporation, when the overlaps were present. The presence of overlaps also slightly decreased efficiency by applying more photoresist than necessary.

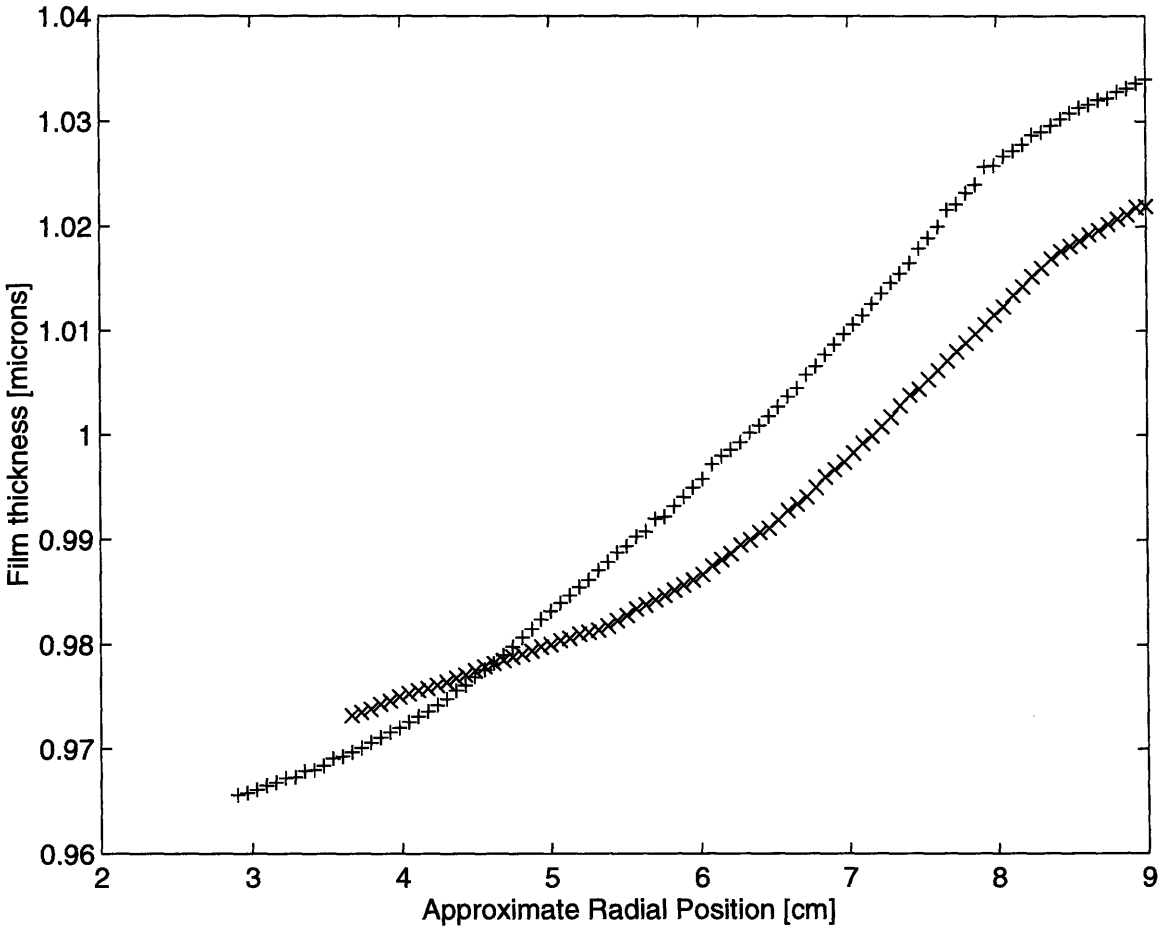

Figure 7-12: Film thickness of wafers coated with a 9.9-μm wet thickness. 500-μm overlap ($\times$), zero overlap ($+$).

Chapter 8

Conclusion

It has been shown that extrusion-spin coating is a viable method for coating round, flat substrates. To be an effective coating method to replace spin coating, however, extrusion-spin coating must meet each of the criteria established in Section 1.2. Each is discussed below.

8.1 Coating Materials

The experiments show that extrusion-spin coating produces good coatings using at least the two photoresists tested. Other fluids with similar properties could also be used. In particular, fluids with viscosities lower than 10 mPa-sec could be used to produce good coatings at speeds above 14 cm/sec and wet thicknesses less than 15 μm. Fluids with higher viscosities could be used for thicker wet films or at slower speeds. Higher speeds and thinner films could probably be obtained with higher viscosities if a bead vacuum were used.

8.2 Coating Thickness

The experiments demonstrated that final (dry) coating thickness was determined almost entirely by the viscosity of the photoresist, although other factors such as the final spin speed also have an effect (which was not tested in these experiments). Higher initial viscosities result in thicker final films. Because the viscosity of the photoresist is also a major determinant of the maximum coating speed and the minimum coating thickness, thicker final coatings can only be attained at longer coating times and

lower coating efficiencies. Adding a vacuum to the coating bead may reduce these limitations. From the data obtained in the experiments it appears that it would be difficult to meet the efficiency and coating time requirements for thicknesses above 1.5 μm when no coating bead vacuum is present.

8.3 Thickness Uniformity

The experiments showed that thickness uniformity is highly dependent on the amount of evaporation which occurs while the wet coating is being applied. Unless this evaporation can be inhibited, the extrusion-spin coating method does not meet the uniformity requirement. If, however, the evaporation which occurs while the wet coating is being applied can be significantly reduced or eliminated, extrusion-spin coating can meet the uniformity requirement.

8.4 Coating Time

The experiments indicated that wet coating time was determined almost entirely by the coating speed. The maximum coating speed is mainly determined by the photoresist viscosity but is also limited by the wet coating thickness. Therefore, to meet the coating time requirement while maintaining a thin wet coating thickness, a photoresist of sufficiently low viscosity must be used. The experiments indicate that viscosities of 10-20 mPa-sec or lower could be used to attain wet coating times of 20 seconds or less. Shorter coating times could be attained with higher-viscosity photoresists if a coating bead vacuum were used to increase the coating speed or if a wider extrusion die were used. Using a wider extrusion die, however, might lower the uniformity or efficiency.

8.5 Coating Efficiency

The experiments showed that photoresist use efficiency is limited mainly by the wet coating thickness. The minimum wet coating thickness is limited by the viscosity of the photoresist and the required coating speed. Therefore, the efficiency requirement has the same viscosity limitations as those for the coating time requirement. As the viscosity of the photoresist is decreased, the efficiency can be increased by

using thinner coatings. At some unknown point, probably above 50% efficiency, the thickness uniformity will begin to decrease because there is insufficient photoresist to improve the uniformity during the fluid spreading which takes place during the final high-speed spin. For photoresist viscosities between 10 and 20 mPa-sec, efficiencies between 10 and 35% can be expected. Optimal efficiencies are likely to occur with viscosities below 10 mPa-sec.

8.6 Coating Defects

The experiments showed that, except for the center region, very few defects developed when the coating speeds and wet coating thicknesses were within the limits of bead stability. The extrusion die does, however, have a tendency to leave an extra pool of photoresist at the center of the coating spiral. When the coated wafer is spun, the center photoresist pool can leave defects behind as described in Section 7.3.5. If this center pool of resist can be eliminated or spread out uniformly, the defect requirement will be met.

8.7 Extrusion Overlap

Because the extrusion overlap had no effect except a slight increase in coating time and a slight decrease in efficiency, it is recommended that the overlap be set to a small value (10–20 μm). This overlap avoids uncoated lines between extrusion rings which can cause defects.

8.8 Future Work

Extrusion-spin coating has been shown to be a viable alternative to spin coating if a few challenges can be overcome. It can be used to produce uniform coatings at thicknesses below 1.5 μm in approximately one minute at efficiencies of 25% or more.

There are two important aspects of extrusion-spin coating which must be solved before it can replace spin coating. There is also a third aspect which could improve the coating process even more. First, to attain sufficient uniformities, a method must be found to greatly reduce or eliminate solvent evaporation during the wet coating motion. Second, to attain a defect-free final coating, coating parameters must be

identified which produce a uniform fluid distribution in the center of the wafer. Third, to use photoresists with viscosities above 10–20 mPa-sec, a method for using a coating bead vacuum with extrusion-spin coating must be developed.

If these three challenges can be met, extrusion-spin coating will be an effective replacement for spin coating.

Appendix A

Uncertainty Analysis

A.1 Gap Errors

There are two components of the error in the coating gap: errors in the absolute gap distance and errors in the angle of the extrusion die lips with respect to the substrate. The sources of these errors are sensor inaccuracy, calibration errors, and machine misalignments (discussed in Section 4.5.1).

The sources of uncertainty in the coating gap, G, come from the uncertainties in all the machine misalignments listed in Section 4.5.1 as well as the uncertainties in calibration and in the sensor measurement itself.

The angle α can be determined from the alignment data. Alignments were done so that the uncertainty in parallelism alignment of the x-axis with the extrusion head was less than 2 μm over 2 cm. Therefore $\alpha < 1 \times 10^{-4}$.

Figure A-1 shows a typical plot of the z-axis position as a function of the x-axis position during an extrusion-spin coating spiral. The two dashed lines in the figure form angles with the horizontal from which we can determine the angles γ and β. The angle γ equals the average of the two angles formed by the dashed lines (i.e., γ equals the general slope of the data). The angle β equals half of the total angle formed by the two lines. The angle γ changed slowly during experimentation, probably due to thermal expansion of the supporting structure. For a series of 16 extrusion-spin coating experiments, the average values of these angles were γ = -1.3$\times 10^{-4}$ $\pm$ 1.2$\times 10^{-4}$ (1 σ) and $\beta = 2.4\times 10^{-4} \pm 2.8\times 10^{-5}$ (1 σ).

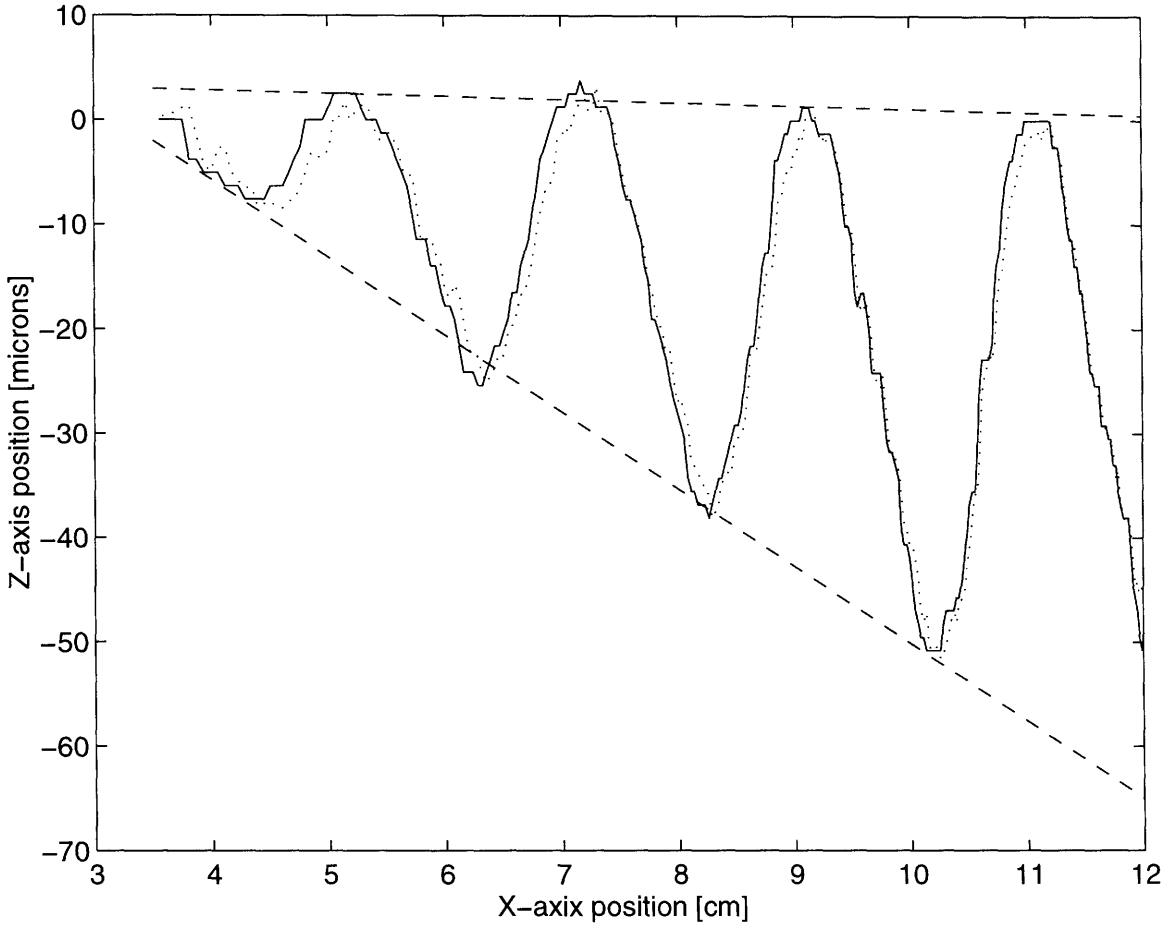

Figure A-1: Z-axis gap control. Z-axis position (—), desired z-axis position ($\cdots$), angle for calculation of β and γ ($-\,-$).

Since the component of the error due to β is oscillatory, it was quantified separately. The gap error due to machine misalignment (excluding β) was $\Delta G_{r-w} = -2.6$ μm with an uncertainty of 4.4 μm (1 σ). The angle β caused an additional periodic error in the gap of 3.6 μm $\pm$ 0.042 μm (1 σ). The maximum angle between the extrusion die and the substrate was $\phi_{max} = 4.7 \times 10^{-4}$ radians with an uncertainty of 1.5×10^{-4} radians (1 σ).

The uncertainty in gap due to calibration error was estimated to be 5.7 μm (1 σ), and the gap uncertainty due to sensor error was 0.472 μm (1 σ). The gap uncertainty due to z-positioning table errors is 0.015% and was considered negligible. When these errors are added up in the Pythagorean sense[4], the total increase in gap uncertainty due to calibration and sensor errors was is 5.7 μm (1 σ).

The total error in the gap was -2.6 μm with an uncertainty of 7.2 μm (1 σ), with an additional oscillatory component of 3.6 μm $\pm$ 0.042 μm (1 σ).

A.2 Spinner Speed Uncertainty

Figure A-2 shows a typical plot of the average rotational speed of the spinner. The extrusion die speed was proportional to the spinner speed. The uncertainty from the specified rotational speed was 8.2% (1 σ), and the uncertainty in the proportionality of the tracking of the extrusion die to the spinner speed was 0.19% (1 σ). The uncertainty in the spinner position was 0.026 radians (1 σ).

A.3 Pump Flow Rate Uncertainty

Uncertainties in flow rate were evaluated by computing the standard deviations of the calibration data from the calibration curves in Figure 6-4. The flow rate of the i-line resist had a standard deviation of 8.5 $\times 10^{-4}$ mL/sec (2.5%) at low flow rates and 0.0025 mL/sec (4%) at high flow rates. The standard deviation of the flow rate of deep UV resist was 0.0021 mL/sec (16.9%) at low flow rates and 0.0035 mL/sec (11.5%) with all flow rates considered.

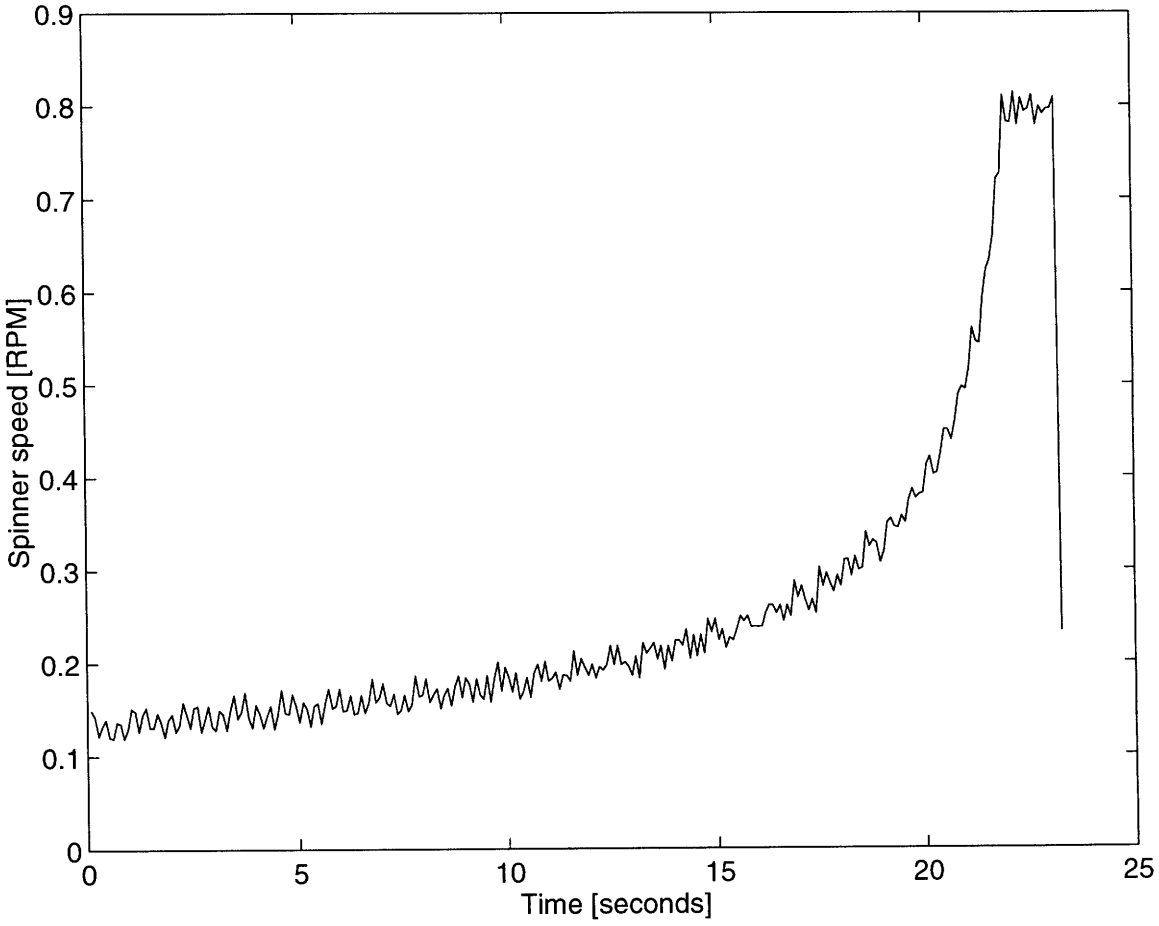

Figure A-2: Typical spinner speed during experiments.

A.4 Wet Thickness Uncertainty

The wet thickness uncertainty can be calculated by using Equation 4.18. Using a Pythagorean summation[4], we know that the error in thickness is:

$$\frac{\Delta h}{h} = \sqrt{\left(\frac{\Delta Q}{Q}\right)^2 + \left(\frac{\Delta v}{v}\right)^2 + \left(\frac{\Delta w}{w}\right)^2} \tag{A.1}$$

The error in w is equal to the error in establishing the neck-in value. This error was approximately 50 μm (0.25%). The uncertainty in wet coating thickness measurement was 9.1% (1 σ) for the i-line resist and 18.8% (1 σ) for the deep UV resist.

Appendix B

Evaporation from a Spinning Disk

Following Lienhard[32], we can calculate the mass transfer rate per unit area, $\dot{m}''$, from:

$$\dot{m}'' = g \ \ln(1 + B_s) \tag{B.1}$$

where g is the mass transfer coefficient at zero net mass transfer and B_s is the mass transfer driving force. (All liquid-phase resistance to solvent diffusion is neglected in this model.)

When solvent is the only species transferred (i.e. no air diffuses into the solvent):

$$B_s = \frac{m_{s,e} - m_{s,s}}{m_{s,s} - 1} \tag{B.2}$$

where $m_{s,e}$ is the mass fraction of solvent in the air far away from the fluid surface and $m_{s,s}$ is the mass fraction of solvent in the air just above the fluid surface. If we assume that any evaporated solvent gets carried away quickly, then $m_{s,e}$=0. If we assume that there is pure solvent at the liquid surface, we can find $m_{s,s}$ from the saturation pressure of the solvent. Then we can find the properties of the air-solvent mixture by using the procedure detailed by Lienhard.

The mass transfer coefficient, g, can be found by using an analogy between convective heat transfer and mass transfer which is only valid for low mass transfer rates. The heat transfer from a rotating disk in a laminar flow can be found from[17]:

$$\mathrm{Nu}_r = \frac{0.585\mathrm{Re}^{1/2}}{0.6/\mathrm{Pr} + 0.95/\mathrm{Pr}^{1/3}} \tag{B.3}$$

where Nu_r is the Nusselt number, Pr is the Pradtl number, and Re is the Reynolds number:

$$\mathrm{Re} = \frac{\Omega r^2}{\nu} \tag{B.4}$$

The transition to turbulence (when Equation B.3 becomes invalid) begins at $\mathrm{Re}_{tr} = 2.4 \times 10^5$.

Using this analogy we can replace the Nusselt number and Prandtl number with the Sherwood number and the Schmidt number[35]:

$$\mathrm{Sh}_r = \frac{gr}{\rho D_{as}} = \frac{0.585\mathrm{Re}^{1/2}}{0.6/\mathrm{Sc} + 0.95/\mathrm{Sc}^{1/3}} \qquad \text{(for any Sc)} \tag{B.5}$$

where $\mathrm{Sc} = \nu/D_{as}$, D_{as} is the diffusivity between air and the solvent on the disk surface, and g is the mass transfer coefficient. Solving for the mass transfer coefficient yields:

$$g = \frac{0.585\rho D_{as}}{0.6/\mathrm{Sc} + 0.95/\mathrm{Sc}^{1/3}} \left(\frac{\Omega}{\nu}\right)^{1/2} \tag{B.6}$$

This result is very similar to that of Kreith, Taylor, and Chong[29].

The air-solvent diffusion coefficient can be estimated using the Kinetic Theory of Gases by the methods of Chapman and Enskog[38].

Bibliography

[1] Photoresists for microlithography. *Solid State Technology*, June 1993.

[2] A. Acrivos, M.J. Shah, and E.E. Peterson. On the flow of a non-newtonian liquid on a rotating disk. *Journal of Applied Physics*, 31(6), June 1960.

[3] Susan Bagen and Carl Newquist. Extrusion coating of polymer films for low-cost flat panel display manufacturing. *1996 Display Manufacturing Technology Conference, Digest of Technical Papers*, 3, 1996.

[4] Thomas G. Beckwith, N. Lewis Buck, and Ray D. Marangoni. *Mechanical Measurements.* Addison-Wesley Publishing Company, Reading, Massachusetts, 1982.

[5] A. E. Beguin. Method of coating strip material. U.S. Patent 2,681,234, June 1954.

[6] N.E. Bixler. *Stability of a coating flow.* PhD thesis, University of Minnesota, 1982.

[7] Eric Bokelberg and William Venet. Effects of relative-humidity variation on photoresist processing. *SPIE: Advances in Resist Technology and Processing XII*, 2438, 1995.

[8] David E. Bornside and Robert A. Brown. The effects of gas phase convection on mass transfer in spin coating. *Journal of Applied Physics*, 73(2), January 1993.

[9] David E. Bornside and Robert A. Brown. Method for low pressure spin coating and low pressure spin coating apparatus. U.S. Patent 5,358,740, October 1994.

[10] D.E. Bornside, C.W. Macosko, and L.E. Scriven. On the modeling of spin coating. *Journal of Imaging Technology*, 13(4), August 1987.

[11] D.E. Bornside, C.W. Macosko, and L.E. Scriven. Spin coating: One-dimensional model. *Journal of Applied Physics*, 66(11), December 1989.

[12] AZ Product Bulletin. AZ 1500 series positive photoresists. Hoechst Celanese Corporation.

[13] B.T. Chen. Investigation of the solvent evaporation effect on spin coating of thin films. *Polymer Engineering and Science*, 23(7), May 1983.

[14] Edward J. Choinski. Patch coating: taking the spin out of thin. *Information Display*, 7(11), 1991.

[15] Edgar Cohen and Edward Gutoff. *Modern Coating and Drying Technology*, chapter 4. VCH Publishers, Inc., 1992.

[16] W.J. Daughton and F.L. Givens. An investigation of the thickness variation of spun-on thin films commonly associated with the semiconductor industry. *Journal of the Electrochemical Society*, 129(1), January 1982.

[17] D.K. Edwards, V.E. Denny, and A.F. Mills. *Transfer Processes.* Hemisphere, Washington, D.C., second edition, 1979.

[18] David J. Elliott. *Microlithography: Process Technology for IC Fabrication*, chapter 3. McGraw-Hill Book Company, New York, 1986.

[19] Alfred G. Emslie, Francis T. Bonner, and Leslie G. Peck. Flow of a viscous liquid on a rotating disk. *Journal of Applied Physics*, 29(5), May 1958.

[20] Mues et al. Observation of a dynamic wetting process using laser-doppler velocimetry. *AIChE Journal*, 35(9), 1989.

[21] F. Fahrni and A. Zimmermann. Coating device. U.S. Patent 4,109,611, April 1978.

[22] Warren W. Flack, David S. Soong, Alexis T. Bell, and Dennis W. Hess. A mathematical model for spin coating of polymer resists. *Journal of Applied Physics*, 56(4), August 1984.

[23] Nathalie Fraysse and George M. Homsey. An experimental study of rivulet instabilities in centrifugal spin coating of viscous newtonian and non-newtonian fluids. *Physics of Fluids*, 6(4), April 1994.

[24] Edgar B. Gutoff. Simplified design of coating die internals. *Journal of Imaging Science and Technology*, 37(6):615–627, 1993.

[25] Edward Gutoff and Edgar Cohen. *Coating and Drying Defects*, chapter 5. John Wiley and Sons, New York, 1992.

[26] J. Hens and W. Mues. Laser-dopler measurements in the vicinity of a moving contact line. AIChE Meeting, New Orleans, LA, 1988.

[27] L. E. Higgins and B. G. Scriven. Capillary pressure and viscous pressure drop set bounds on coating bead operability. *Chemical Engineering Science*, 35:673–682, 1980.

[28] P. Joos, M. Bracke, and P. Van Remoortere. The dynamics of wetting. Presented at AIChE Spring Meeting, Orlando, March 1990.

[29] F. Kreith, J. H. Taylor, and J. P. Chong. Heat and mass transfer from a rotating disk. *Journal of Heat Transfer*, 81:95–105, 1959.

[30] C.J. Lawrence. The mechanics of spin coating of polymer films. *Physics of Fluids*, 31(10), October 1988.

[31] Kwong-Yang Lee Lee, Li-Dah Liu, and Ta-Jo Liu. Minimum wet thickness in extrusion slot coating. *Chemical Engineering Science*, 47(7):1703–1713, 1992.

[32] John H. Lienhard. *A Heat Transfer Textbook*, chapter 12. Prentice Hall, Inc., Englewood Cliffs, New Jersy, second edition, 1987.

[33] Dietrich Meyerhofer. Characteristics of resist films produced by spinning. *Journal of Applied Physics*, 49(7), July 1978.

[34] Stanley Middleman and Arther K. Hochberg. *Process Engineering Analysis in Semiconductor Device Fabrication*, chapter 9. McGraw-Hill, Inc., New York, 1993.

[35] A.F. Mills. *Heat and Mass Transfer*. Richard D. Irwin, Inc., Chicago, 1995.

[36] W. Moreau, K. Cornett, J. Fahey, L. Linehan, M. Montgomery, R. Smith, and R. Wood. The shot size reduction of photoresist formulations. *SPIE: Advances in Resist Technology and Processing XII*, 2438, 1995.

[37] Wayne M. Moreau. *Semiconductor Lithography: Principles, Practices and Materials.* Plenum Press, New York, 1988.

[38] Robert C. Reid, John M. Prausnitz, and Bruce E. Poling. *The Properties of Gases and Liquids*, chapter 11. McGraw-Hill, Inc., New York, fourth edition, 1987.

[39] K. J. Ruschak. Limiting flow in a pre-metered coating device. *Chemical Engineering Science*, 31:1057–1064, 1976.

[40] Luigi Sartor. *Slot coating: Fluid mechanics and die design.* PhD thesis, University of Minnesota, 1990.

[41] L.E. Stillwagon and R.G. Larson. Leveling of thin films over uneven substrates during spin coating. *Physics of Fluids A*, 2(11), November 1990.

[42] Peter C. Sukanek. Spin coating. *Journal of Imaging Technology*, 11(4), August 1985.

[43] Chih-Ta Wang and Shi-Chern Yen. Theoretical analysis of film uniformity in spinning processes. *Chemical Engineering Science*, 50(6), 1995.

[44] S. Wolf and R.N. Tauber. *Silicon Processing for the VLSI Era: Volume 1 – Process Technology.* Lattice Press, Sunset Beach, CA, 1986.